Geophysics From Terrestrial Time-Variable Gravity Measurements

Michel van Camp, Olivier de Viron, Arnaud Watlet, Bruno Meurers, Olivier Francis, Corentin Caudron

AGU PUBLICATIONS

Reviews of Geophysics

REVIEW ARTICLE
10.1002/2017RG000566

Key Points:
- Review of the geophysical phenomena that can be addressed by terrestrial time-variable gravity
- The next challenges of terrestrial gravimetry are discussed
- Terrestrial gravimetry remains central in the Earth observation system

Correspondence to:
M. Van Camp,
mvc@oma.be

Citation:
Van Camp, M., de Viron, O., Watlet, A., Meurers, B., Francis, O. & Caudron, C. (2017). Geophysics from terrestrial time-variable gravity measurements. *Reviews of Geophysics*, *55*, 938–992. https://doi.org/10.1002/2017RG000566

Received 20 APR 2017
Accepted 18 SEP 2017
Accepted article online 23 SEP 2017
Published online 2 NOV 2017

Geophysics From Terrestrial Time-Variable Gravity Measurements

Michel Van Camp[1], Olivier de Viron[2], Arnaud Watlet[1,3], Bruno Meurers[4], Olivier Francis[5], and Corentin Caudron[6,1]

[1]Seismology-Gravimetry, Royal Observatory of Belgium, Uccle, Belgium, [2]Littoral, Environnement et Sociétés, Université de La Rochelle and CNRS (UMR7266), La Rochelle, France, [3]Geology and Applied Geology Unit, Faculty of Engineering, University of Mons, Mons, Belgium, [4]Department of Meteorology and Geophysics, University of Vienna, Vienna, Austria, [5]Faculty of Science, Technology and Communication, University of Luxembourg, Esch-sur-Alzette, Grand Duchy of Luxembourg, [6]Laboratoire de Volcanologie, G-time, Département Géosciences, Environnement et Société, Université Libre de Bruxelles, Brussels, Belgium

Abstract In a context of global change and increasing anthropic pressure on the environment, monitoring the Earth system and its evolution has become one of the key missions of geosciences. Geodesy is the geoscience that measures the geometric shape of the Earth, its orientation in space, and gravity field. Time-variable gravity, because of its high accuracy, can be used to build an enhanced picture and understanding of the changing Earth. Ground-based gravimetry can determine the change in gravity related to the Earth rotation fluctuation, to celestial body and Earth attractions, to the mass in the direct vicinity of the instruments, and to vertical displacement of the instrument itself on the ground. In this paper, we review the geophysical questions that can be addressed by ground gravimeters used to monitor time-variable gravity. This is done in relation to the instrumental characteristics, noise sources, and good practices. We also discuss the next challenges to be met by ground gravimetry, the place that terrestrial gravimetry should hold in the Earth observation system, and perspectives and recommendations about the future of ground gravity instrumentation.

Plain Language Summary In a context of global change and increased human vulnerability to terrestrial hazard, monitoring the Earth system is one of the key challenges of geoscience. In particular, terrestrial gravimetry, with its precision at the level of one part of a billion, allows the monitoring of many phenomena, from water resource availability to volcanic activity. This paper reviews the technique, its advantages and limitations, how it has been used in the Earth monitoring, and the next challenges to be met by ground gravimetry.

1. Introduction

Gravity is the magnitude of the gravity acceleration experienced by a body at the Earth surface resulting from the gravitational attraction of the Earth, the Sun, the Moon, and the planets and from the centrifugal effect associated with the Earth rotation. Gravity g is at the level of 9.8 m/s^2, though the exact value varies in both time and space, in response to any phenomena that affect the mass distribution around the sensor at all spatial scales, the Earth rotation, or the tides. The measure of time-variable gravity, because of its high accuracy, sensitivity, and sampling rate, allows the detection of signatures of elusive phenomena at the 10^{-9} level or smaller, which can be used to build an enhanced picture, and understanding, of the changing Earth. Gravity can either be measured directly, using a ground or space device measuring its action on a test mass, or inferred indirectly, from quantities directly linked to gravity, such as sea surface topography.

In a context of global change and increasing anthropic pressure on the environment, monitoring the Earth system and its evolution has become one of the key missions of the geosciences. Geodesy is the geoscience that measures the geometric shape of the Earth, its orientation in space, and its gravity field, as well as the changes of these properties with time. Gravimetry, that is, the measure of gravity, is an important part of the Global Geodetic Observing System (GGOS) (Plag & Pearlman, 2009), which aims at monitoring, mapping, and understanding changes in the Earth's shape, rotation, and mass distribution. Ground-based gravimetry can determine the change of gravity related to Earth rotation fluctuations, to celestial body and Earth attractions, to the mass variations in the direct vicinity of the instruments, and also to distant sources, and to

displacement of the instrument itself due to ground deformation. Gravity measurements contribute to risk assessment and mitigation, by improving our understanding of past and present ice mass changes (Kazama et al., 2013; Lambert et al., 2006; Larson & van Dam, 2000; Mazzotti et al., 2011; Mémin et al., 2011; Omang & Kierulf, 2011; Ophaug et al., 2016; van Dam et al., 2017), subsidence of low-lying areas (Van Camp et al., 2011; Zerbini et al., 2007), ground water resources (Creutzfeldt et al., 2010; Fores et al., 2017; Hector et al., 2015; Imanishi et al., 2013; Jacob et al., 2010; Kennedy et al., 2014; Lampitelli & Francis, 2010; Van Camp, de Viron, Pajot-Métivier, et al., 2016; Van Camp et al., 2006), and earthquakes (Imanishi, 2004; Montagner et al., 2016; Van Camp et al., 2011). Concurrently, terrestrial gravity measurements play a key role in the new definition of the kilogram (Stock, 2013), and our understanding of environmental effects affecting the gravity measurements will be useful to assess the Newtonian noise affecting gravitational wave detectors (Coughlin et al., 2016; Harms & Venkateswara, 2016).

Ground gravity measurements are also useful to map the gravity field, allowing to reveal small-scale ($<$100 km) geological structures (Mickus, 2003; Reynolds, 2011). Apart from measurements performed by classical gravimeters, airborne and seaborne gravimeters bring valuable information on static and dynamic geophysical phenomena and bridge the gap between terrestrial and satellite measurements of the static gravity field.

The precision of the best gravimeters has reached 0.1 nm/s^2 (10^{-11} g) at a period of 1 min, but retrieving the information at that level of precision is challenging. Indeed, the measured quantity integrates the gravity effect of many phenomena into one single number. Separation of the sources can only be achieved by one of the three following methods:

1. When one of the mixed signals is known precisely enough, it can be subtracted from the data; this is the case, for example, for Earth rotation changes.
2. When one of the mixed sources has a time/frequency behavior that is unique, it can be separated by signal processing techniques; this is the case, for example, for Earth tides.
3. When different measurement techniques or models, such as geophysical, geodetic, or seismic measurements and climate models (Valty et al., 2013), are available, with different transfer functions, combining the information can help to achieve source separation.

In addition to the source separation issue, interpreting the gravity signals should be considered with caution in view of the possible environmental and instrumental artifacts. Gravity measurements are cumulative observations and have a particular space-time transfer function. Hence, these measurements are extremely sensitive to local water storage changes, ocean loading, and atmospheric effects, which induce time-correlated signatures in the gravity time series (Van Camp, de Viron, & Avouac, 2016; Van Camp et al., 2010). Neglecting these signatures leads to underestimating the uncertainties on the computed gravity rates of change (Agnew, 1992; Van Camp et al., 2005; Williams, 2003). A better understanding and quantification of these effects is a prerequisite to any geophysical interpretation of gravity surveys.

This paper reviews the insights about the Earth system that can be gained from terrestrial measurements of time-varying gravity, considering the noise and artifacts affecting the measurements, as well as the geophysical phenomena that are best suited for investigation using this technique. A comparison with the review paper of Crossley et al. (2013) evidences the progress made in the last 4 years in gravimetry and, more generally, in geodesy.

Terrestrial gravimeters are generally cumbersome, expensive, and tricky to use, which limits their contribution to Earth study, but the next generation of gravimeters may change that picture (Rymer, 2016). Cold atom (Debs et al., 2013) and MEMS (microelectromechanical system; Middlemiss et al., 2016) gravimeters are under development; they would be more transportable, would be absolute in the case of atom instruments, and may become less expensive if more instruments are produced.

2. Measuring Gravity

There are two families of gravimeters: the absolute and relative ones. Absolute gravimeters give direct access to the gravity value, whereas relative instruments provide gravity variations only. A comprehensive review of these instruments is beyond the scope of our paper; details on spring gravimeters, pendulum gravimeters, and classical ballistic gravimeters can be found in the comprehensive paper of Niebauer (2015) and in

Crossley et al. (2013), Hinderer et al. (2015), and Torge (1989), while superconducting gravimeters, as well as data processing, are described in detail by Hinderer et al. (2015). A short description of atom gravimeters is given by Debs et al. (2013).

In principle, measuring absolute gravity is quite straightforward: time and distance of a free-falling object are measured, as conceptualized by Galileo Galilei, and gravity is inferred from the simple equation of motion: $x = gt^2/2$. In practice, if high precision is requested, difficulties arise, among other reasons, because the mass travels a distance of 1 m within half a second, which would require the measurement to be accurate at the 10^{-10} level for the time and 10^{-9} for the distance for a measure of gravity at the 10 nm/s^2 level. Until the 1960s, those precision levels were out of reach, and the most precise, easiest way to determine gravity was to determine the period of a pendulum and its length (Faller, 1967; Niebauer, 2015). Pendulums then acted as absolute gravimeters and achieved an accuracy of a few parts in 10^{-7} (Cook, 1965b; Torge, 1989). This level could be obtained because of the relatively slow and repeated motion but remained mostly limited by friction at the suspension point (Faller, 1967). It was easier to use pendulums as relative meters, given that systematic errors caused by the determination of the length or the friction forces are much reduced. Bouguer (1749) used this instrument as early as the eighteenth century to reveal the latitude dependence of gravity, as well as altitude, at the 10^{-3} g or 10 mm/s^2 level.

Concurrently to the pendulum, another way to stabilize a test mass is to suspend it with a spring and measure its deformation caused by gravity changes. The stretch of the spring is proportional to the gravity, the mass, and the spring constant k, which represents the stiffness of the spring. The test mass, its displacement, and the spring constant are not known with enough precision to provide the gravity value directly. But, by calibrating the deformation at reference stations, the spring gravimeters provide an indirect measure of gravity. Although springs provide relative instruments only, they have dominated field gravity measurements since the 1930s, when one became able to produce sufficiently stable springs.

2.1. Absolute Gravimeters

2.1.1. Classical Free-Fall Gravimeter

The ballistic absolute gravimeters (AGs) could only be achieved with sufficient accuracy in the 1950s, when electronics, quartz clocks, and vacuum technology made it possible to reach the then required accuracy level of 10^{-5} (Cook, 1965b; Torge, 1989). The test mass travels in a vacuumed dropping chamber, but this was not the most challenging issue. As stated above, the most difficult task consists in measuring time and distances with the required precision. In the 1950s, distance/time measurements were performed through photography of the falling object (Preston-Thomas et al., 1960; Thulin, 1958; Volet, 1946, 1952). Later on, interferometric measurements were performed at three positions using white light source during the falling, as pioneered by Faller in 1962, who used the Sun as a bright light source (Faller, 1965). Photographic and interferometric methods allowed a precision of a few 10^{-6} g (Cook, 1965b). Eventually, the advent of coherent laser sources made it possible to increase to a much larger extent the number of positions, allowing to reach the 10^{-7} g or 1 μm/s^2 level.

Another challenge was to develop a stable reference frame to measure the distance. In an absolute gravimeter, a test laser beam bounces off the free-falling body before being reflected back to the interferometer, where the test beam interferes with a reference one. While the dropped mass is completely isolated from the Earth's vibrations during its fall, anthropogenic and natural microseismic noises continuously modify the position of the reference mirror of the interferometer. Even in the absence of an earthquake, the displacements of the Earth's surface are persistent and location and season dependent, reaching up to a few micrometers close to the coast (Kedar et al., 2008), while one should measure the free-fall distance at the 1 nm precision level in order to achieve a precision on gravity of 10 nm/s^2. In the first white-light gravimeter, the measurements of gravity were corrected by using the records from a 1 s period seismometer. Early in the 1980s, Rinker (1983) developed the so-called Super Spring, that is, a modified seismometer providing an inertial reference system at periods shorter than about 1 min—the suspended mass of a seismometer provides an inertial reference frame, independent from the motions of the Earth, at periods shorter than the resonance frequency (Aki & Richards, 2002). The challenge consisted in producing a suspension device of which the free period is about 1 min, that is, longer than the periods ranging 5–20 s, where microseism is the strongest. Introducing this long-period seismometer increased the precision of the absolute gravimeter by 2 orders of magnitude (Figure 1). This allowed achieving the few 10^{-9} g level. Nowadays, apart from

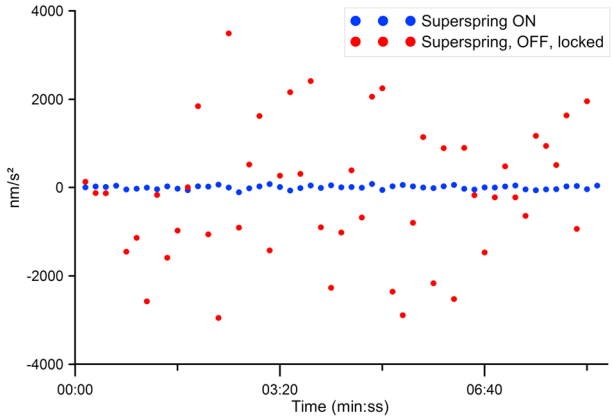

Figure 1. FG5 gravity measurements with operational and locked superspring. Standard deviations are 41 and 1,957 nm/s^2, respectively. The data were taken at the Rochefort station (50.1552°N, 5.2256°E), 28 March 2017, 07:15 (superspring locked) and 07:43 UTC (superspring operational). The average gravity value 9.81011440 m/s^2 has been removed.

the Super Spring device, other absolute instruments use passive and active insulating methods (Hensley et al., 1999). In passive systems, the interferometer signal is corrected by using the acceleration measured by a seismometer (Le Gouët et al., 2008); in active devices the signal of the seismometer stabilizes the position of the reference mirror (Hauth et al., 2013; Hensley et al., 1999; Wu et al., 2017). Due to the stabilizing mechanical device, the active method is more complex to implement and would make field instruments heavier and more difficult to set up.

Absolute instruments are also sensitive to tilts, which introduces an optical length perturbation. An appropriate design of the interferometer can ensure that the gravimeter is only second-order sensitive to tilts of the ground. This was realized by keeping the test and reference interferometer arms in a vertical line (Niebauer et al., 1995). During the setup of an FG5 instrument (Figure 2), a pool of alcohol serves as a horizontal mirror, which is used to level the gravimeter with a precision within 44 μrad to ensure a measurement of gravity at the level of 10 nm/s^2.

Concurrently with the free-fall instruments, rise and fall instruments have been developed since the 1960s (Amalvict, 2010; Cook, 1965a; Sakuma, 1963). While free-fall instruments require at least three time-position pairs, rise and fall need only two: the separation between two positions and the transition time differences between rise and fall (Faller & Marson, 1988; Torge, 1989). This was considered as advantageous in the 1960s but not nowadays, as both types record more than 1,000 time-position pairs. An advantage of the rise and fall method is that being symmetric, it is less sensitive to the effects of the residual air and some timing errors (D'Agostino et al., 2008; Faller & Marson, 1988). However, throwing a mass vertically is challenging, because of the important release velocity (Marson, 2012). The main advantage of the free-fall method is its mechanical simplicity, making it easier to attain a high sampling rate, that is, a drop every few seconds in classical instruments or a few tenths of a second in atom gravimeters.

Figure 2. (left) The FG5#202 absolute gravimeter at the Membach station, Belgium and (right) an FG5X at the Walferdange station, Luxemburg. The box with the red connector is the ion pump, maintaining a vacuum in the dropping chamber (upper cylinder) at the 10^{-9} atmosphere level. Credit: K. Vanneste, Royal Observatory of Belgium (Figure 2, left), O. Francis, U. Luxemburg (Figure 2, right).

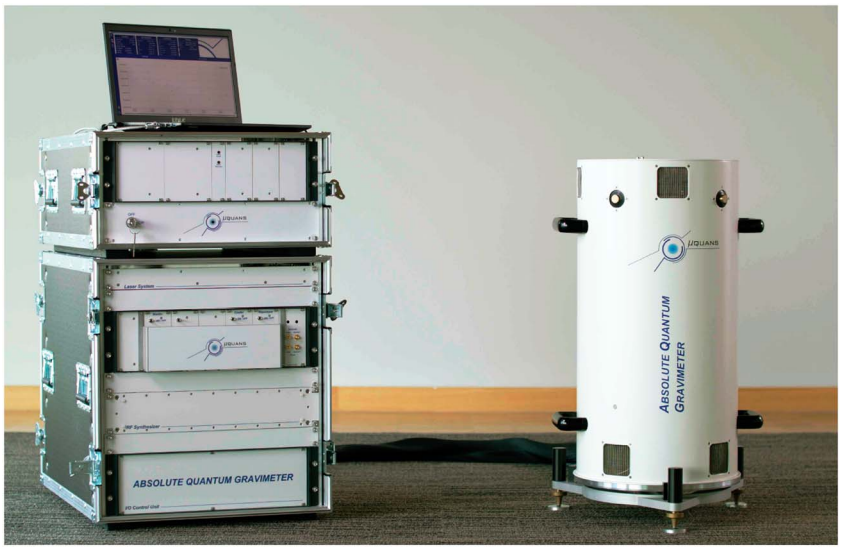

Figure 3. The Muquans absolute quantum gravimeter, based on laser-cooled atoms. Credit: Muquans.

For completeness, let us mention the A10 portable absolute gravimeter from Micro-g LaCoste, which is easier to use outdoors, in harsh field conditions (Ferguson et al., 2008). The A10 instrument is smaller than an FG5 one, it has automated leveling, both the vacuum and interferometer base are temperature regulated, and it has a dropping rate of 1 Hz, allowing acquiring a large quantity of data in a very short time. However, it is about 10 times less precise and accurate than an FG5 gravimeter.

In summary, modern rise and fall and free-fall instruments use an interferometer, a highly stabilized laser, a vacuum chamber in which the test mass travels vertically, a long-period seismometer providing a reference frame, a fringe detector, a counter, and a computing unit for data acquisition and the calculation of *g*. An atom clock and the wavelength of a laser act as time and length standards. Given that the meter definition is reduced to a time measurement (Giacomo, 1984), absolute gravity measurements are directly connected to the International System base unit of time.

2.1.2. Quantum Free-Fall Gravimeter

In the 1990s it became possible to produce atoms cooled down to microkelvin. Cold atoms have opened new paths in physics (Phillips & Metcalf, 1987). Among others, it allowed using cold atoms as test masses to measure gravity (Peters et al., 1999, 2001; Zhou et al., 2015). Hence, one benefits from the wave-matter duality of atoms, which are used as both test mass and wave to measure the traveled path. A great advantage of atom instruments consists in the absence of moving parts, avoiding mechanical wear. Results from laboratory tests show that the atom gravimeters provide an accuracy and precision similar to classical ballistic gravimeters (Freier et al., 2016; Gillot et al., 2014). Atom gravimeters also measure at a higher sampling rate, in principle up to a few hertz, which makes the mitigation of microseismic noise easier. As these instruments (Figure 3) are still being developed, new achievements may make them even more competitive in the near future. Note that by comparing atom and classical FG5 gravimeters, Peters et al. (1999) provided the best test of the equivalence principle, showing that cesium atoms and macroscopic objects fall with the same acceleration, to within 7 parts in 10^9.

2.2. Relative Gravimeters

In relative gravimeters, a proof mass is suspended by using a mechanical spring in classical gravimeters or through magnetic levitation in superconducting instruments.

2.2.1. Spring Gravimeters

The spring instruments are mostly used for regional mapping of gravity. The gravimeter reading is taken at a reference station where gravity is known. This could be achieved with spring gravimeters in the 1930s when Lucien LaCoste invented the zero-length spring, which made it possible to produce spring-based suspensions stable and sensitive enough to measure gravity changes in space with a fair precision.

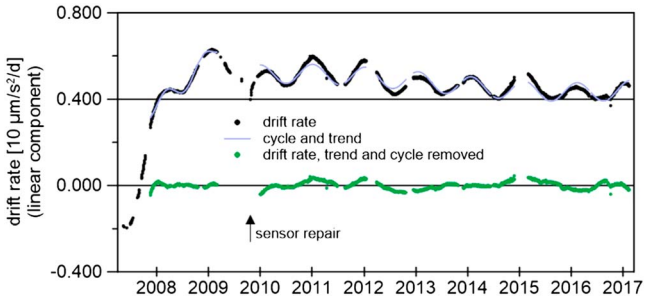

Figure 4. Drift rate (linear component) of the instrumental drift of CG-5 Scintrex Autograv SN-070340236 (black dots), adjusted 332 day cycle and trend (blue solid line), and drift rate after removing the adjusted cycle and trend (green dots). As for Gettings et al. (2008), we do not have any explanation for this oscillation.

Before the advent of electronics in the 1960s, the displacement of the suspended beam was measured optically, and, as a modern electronic instrument, the meter was returned to a reference null position. This was achieved by adjusting a screw system (Hinze et al., 2013; Niebauer, 2015; Torge, 1989). The number of revolutions of the screw system was calibrated to convert a change in displacement of the beam into actual gravity changes.

Time-varying gravity monitoring is not straightforward, as relative gravimeters are not stable enough at long or very long term—a few days for poor spring instruments to a few months for superconducting and outstanding spring gravimeters—and most of the present absolute gravimeters cannot be operated continuously, as they rely on mechanical devices that are subject to wear. Continuous measurements are thus achieved using relative spring or superconducting gravimeters, which allow long-term monitoring but with a quasi-linear instrumental drift. The drift affecting relative instruments may be linear or exponential (Bonvalot et al., 1998; Okiwelu et al., 2011; Parseliunas et al., 2011; Schilling & Gitlein, 2015; Van Camp & Francis, 2007). It reaches up to thousands of nm/s^2/d for spring gravimeters (Figure 4) and a few tens of nm/s^2/yr for superconducting gravimeters (Fores et al., 2017; Hinderer et al., 2015; Van Camp & Francis, 2007). The drift is estimated by comparing the relative meters with absolute measurements or by repeating relative surveys at a reference station where gravity is measured or supposedly stable (Debeglia & Dupont, 2002; Hinderer et al., 2016).

In the future, continuous measurements could also be performed by absolute atom gravimeters, which are not subject to wear. However, they are constrained by the lifetime of the laser.

Among the spring instruments, metal springs, as in Micro-g LaCoste gPhone and Burris gravimeters (Jentzsch, 2008; Niebauer, 2015; Schilling & Gitlein, 2015), or quartz spring gravimeters, as in Scintrex CG-3, CG-5, and CG-6 instruments (Niebauer, 2015; Seigel et al., 1993), were the most common in the 2010s (Figure 5). A change in gravity induces incremental vertical force acting on the test mass, counteracted by a feedback voltage acting on capacitor plates in order to maintain the test mass in position, which ensures linearity (Levine et al., 1986; Wielandt, 2002). The measurement of the spring gravimeter is the feedback voltage, as it is proportional to the gravity change.

Quartz spring gravimeters appeared in the early 1990s. Advantages of a quartz device are as follows: quartz is easy to work, allowing fusing the frame, the spring, and suspension points, hence providing a monolithic construction, which reduces the possibility of slippage or deformation; quartz is not influenced by external magnetic fields; and quartz gravimeters are more resistant to tares than metal spring meters, and they do not need a clamping system. However, the temperature dependence of quartz is larger than most metal springs by 3 orders of magnitude ($5.3 \cdot 10^{-4}$ K^{-1} versus $5.5 \cdot 10^{-7}$ K^{-1} for low-temperature coefficient metal), and these instruments also suffer from a strong, changing drift (Figure 4). They can nevertheless be used for tidal

Figure 5. Three relative gravimeters: (left) Micro-g LaCoste gPhone (metal spring); (middle) Scintrex CG-6 Autograv (quartz spring); (right) Burris gravimeter (metal spring). Credit: Micro-g LaCoste, Scintrex Ltd, and ZLS Corporation.

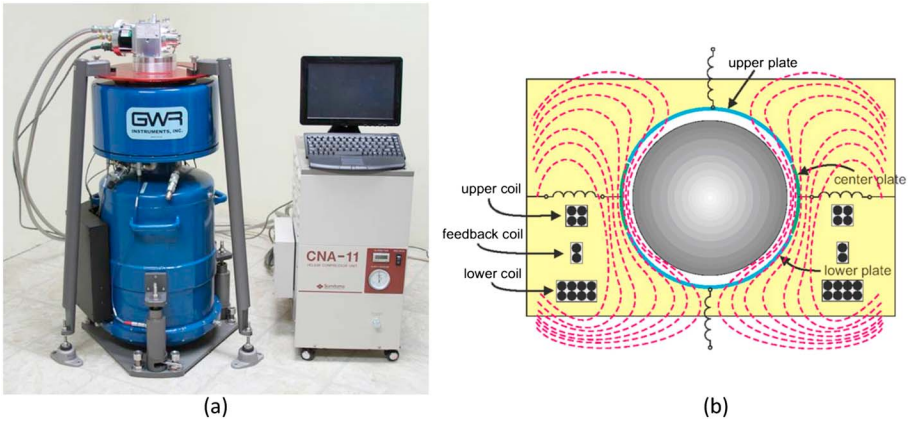

Figure 6. (a) GWR iGrav superconducting gravimeter, with the cryocooler on the right; (b) diagram of the gravity sensing unit: Sphere and upper, center, and lower plates of displacement transducer; with magnetic flux (red dotted lines) from upper and lower coils expelled from sphere interior. Credit: GWR Instruments, Inc.

analyses (Bonvalot et al., 1998; Ducarme & Somerhausen, 1997; Meurers, 2012) but are useless for phenomena with a period longer than a few days. Metal spring gravimeters are more stable and have been used for continuous monitoring in a broad range of applications such as studies of active volcanoes (Branca et al., 2003; Carbone et al., 2006, 2007; Gottsmann et al., 2011; Hautmann et al., 2014; Jousset et al., 2000). However, the long-term stability of spring gravimeters is usually not sufficient to resolve weak gravity signals, as those (typically smaller or equal to 100 nm/s^2) caused by hydrological systems. In the 2010s, the new Micro-g LaCoste gPhone and gPhoneX gravimeters reached a precision sufficient to detect hydrological effects (Sugihara & Nawa, 2012; Tanaka et al., 2013; Van Camp, Francis, et al., 2016). The gPhone instrument obeys the same operating principle as the classical LaCoste gravimeters, with an improved thermal system and vacuum seal. The gPhoneX benefits from an improved electronics, which lowers its noise level between 1 and 20 mHz (Figure A11). This makes the instrument insensitive to temperature changes and buoyancy effects due to atmospheric pressure variations.

The gPhone gravimeters are very sensitive to power outages, as the thermostatization is lost and the instruments need several weeks before they stabilize again. Hence, it is recommended to provide an efficient uninterruptible power system.

2.2.2. Superconducting Gravimeters

The most precise relative instrument is the superconducting gravimeter (SG) (Figure 6), as introduced by Prothero and Goodkind (1968). The first two commercially available instruments were installed in 1981 in Brussels, Belgium, and Bad Homburg, Germany (Hinderer et al., 2015). The fundamental component of the superconducting gravimeter, also called cryogenic gravimeter, consists in a hollow superconducting sphere, used as a proof mass, that levitates in a persistent magnetic field generated by currents in a pair of superconducting coils (Goodkind, 1999; Hinderer et al., 2015). The superconducting property of zero resistance allows the currents that produce the magnetic field to flow forever without any resistive loss. This could be achieved, for example, for more than 22 years in Metsähovi (Finland), a record that was broken in Membach (Belgium) on 18 September 2017 (van Camp, 2017). Superconductivity is obtained by immersing the sensing unit in a liquid helium bath at 4 K (−269°C). Early instruments required 200 L of liquid helium every month; nowadays, a cryocooler allows liquefying gaseous helium and operating the instrument without almost any helium loss. In the case of power outage, the Dewar contains enough liquid helium (16 L) to ensure about 10 days of cryogenic conditions.

A change in gravity induces a vertical force on the sphere. As in modern spring gravimeters, the mass is kept at a constant position, by injecting a current in an auxiliary feedback coil. Current SGs have a power spectral density noise level ranging typically 1–10 (nm/s^2)^2/Hz (Figure A11), which means that they are able to detect temporal gravity change ranging 0.1–0.3 nm/s^2 (or 10–30 nGal) within 1 min (Fores et al., 2017; Rosat & Hinderer, 2011; Van Camp et al., 2005). Superconducting gravimeters are provided with tiltmeters and thermal levelers, which compensates for tilts larger than 3 μrad, corresponding to 0.05 nm/s^2 (Hinderer et al., 2015).

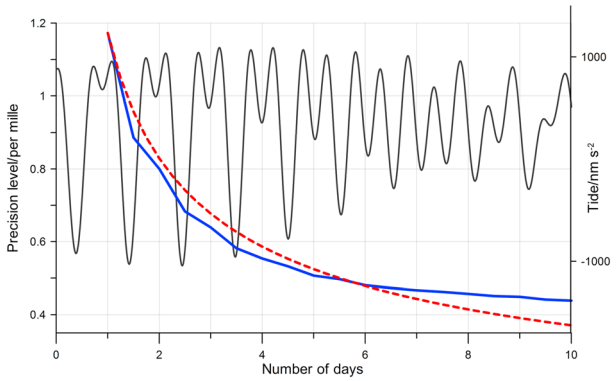

Figure 7. In dark gray, the tidal signal simulated at the Membach station (Belgium, 50.61°N, 6.01°E, days since 8 July 2014, 00:00). In blue, evolution of the error on the calibration (per mille) as a function of the number of days. In red, the $1/\sqrt{N}$ law normalized on the first value of the standard deviation. Due the decreasing amplitude in the tidal signal, the precision does not decrease as $1/\sqrt{N}$. The absolute gravimeter time series are synthesized by adding a Gaussian white noise of amplitude 70 nm/s^2 to the tidal signal (10 s sampling interval, continuously). Modified from Figure 1b of Van Camp, Meurers, et al. (2016).

2.2.3. Microelectromechanical Systems

In 2016, a microelectromechanical system (MEMS) device was first used as a gravimeter (Middlemiss et al., 2016). MEMS are microscopic mechanical devices made from semiconductor materials. Presently, sensibility to tilts, temperature, and internal friction (Chin et al., 2005) limit the stability in time of the MEMS-based gravimeter. Its noise level is insufficient for geophysical studies: 10^7 versus respectively 10^1–10^4 $(\text{nm/s}^2)^2/\text{Hz}$ for superconducting and spring gravimeters at the frequency of 0.1 mHz. Moreover, the ability to measure location-dependent gravity variations has not been demonstrated yet. However, those light instruments could revolutionize expensive air- and sea-borne gravimetry, for example, if such a device could be installed on a drone and be able to monitor gravity changes with a precision better than 1,000 nm/s^2. Because of their low consumption and potential low cost, they could also be deployed as a dense array around specific structures such as volcano, hydrothermal, or karst systems.

2.2.4. Calibration and Tilts

Relative instruments must be calibrated. Usually, spring gravimeters are calibrated by measuring gravity differences along a calibration line, that is, between different stations where gravity is determined by absolute gravity measurements. The superconducting gravimeters measure continuously at a station; they are usually calibrated at the per mille—that is, one thousandth—level by measuring side by side with an absolute gravimeter (Francis et al., 1998). It is possible to reach the per mille level by measuring for 48 h at spring tide (Figure 7) and increasing the sampling rate to one drop per 5 s. Then, the experiment must be repeated at least seven times to achieve the per mille level with a 99% confidence interval (Van Camp, Meurers, et al., 2016). Given that the peak-to-peak amplitude of the tidal signal amounts about 2,500 nm/s^2, calibrating a gravimeter at the 1‰ level means that the peak-to-peak amplitude of the tides is measured with an uncertainty of 2.5 nm/s^2.

Other methods, as moving a known mass round the instrument (Achilli et al., 1995), installing the gravimeter on a calibration platform (Richter et al., 1995), or comparing with spring gravimeters (Meurers, 2012), also provide an estimation of the calibration factor at the per mille level. When comparing gravimeters, one assumes that the superconducting instrument is error free. In practice, this is not the case and may induce a systematic negative bias in the estimation of the calibration factor. This is known as attenuation or regressions dilution bias (Hutcheon et al., 2010). If the standard deviation of the noise affecting the superconducting gravimeter is at least 100 times lower than the RMS amplitude of the tidal signal used to compute the calibration factor, then the attenuation bias remains lower than the 1‰ level (Van Camp, Meurers, et al., 2016). This can be achieved by measuring when the microseismic noise is low or by applying a least squares filter with cutoff frequency of 0.05 Hz and length of 60 s. This is an appropriate choice as the microseismic noise is strong above 0.05 Hz and because this frequency remains high enough not to remove a common signal to the two gravimeters.

Gravimeters are sensitive to tilts θ with respect to a vertical orientation, which causes, at the first order, gravity to diminish by

$$-\frac{1}{2}g\theta^2 = -4.9\ 10^9\theta^2\ \text{nm/s}^2 \tag{1}$$

where θ is in radians. One microradian subtends an arc length of 1 mm at a distance of 1 km. The long-term observations of the gPhones can be further improved by providing them with an active tilt control system, such as the one built at the University of Luxemburg (Francis et al., 2014). It allows stabilizing the instrument at periods longer than a few days. Meanwhile, Micro-g LaCoste introduced the commercial Odin leveling platform, which uses the temperature controlled hydraulic legs to correct for tilts with a subarcsecond resolution (Scintrex Ltd, 2017). It is also possible to compensate tilts affecting LaCoste and Romberg instruments by applying a posteriori a correction computed from electronic levels data (Carbone & Greco, 2007).

Scintrex CG-5 and CG-6 gravimeters allow for numerical correction of plumb line misalignments by using the signals of tilt sensors. As those show time-variable offsets and sensitivity, they need to be regularly calibrated. Levelers were also used on a Scintrex CG-3M spring gravimeter to monitor gravity changes on the seafloor. Hence, using a 446 day record made in the North Sea by ROVDOG (Remotely Operated Vehicle-deployed Deep-Ocean Gravimeter), Sasagawa et al. (2008) could obtain a standard deviation on 100 s averages, tide-corrected time series of 44 nm/s^2 and even 13 nm/s^2 when selecting 11 quiet days when the microseismic noise was low. The North Sea experiences also showed that it is possible to perform seafloor gravity surveys with an uncertainty smaller than 50 nm/s^2 (Nooner et al., 2007; Sasagawa et al., 2003).

2.3. General Issues

In principle, the best way to measure time-varying gravity consists in measuring continuously using a relative instrument at given stations. However, instruments are expensive, typically US$100,000–300,000 for relative instruments and US$500,000 for absolute ones, and operating a station implies maintenance tasks. Moreover, a relative gravimeter requires calibration and correction of its instrumental drift, which is done using absolute measurements that must be performed once a year at least. Hence, to reduce costs, it is more common to repeat gravity measurements using spring or absolute gravimeters at different points. More details on field techniques, data processing, and noise sources of terrestrial measurements are beyond the scope of this paper but of sufficient relevance to be given in Appendix A.

The Gravity Recovery And Climate Experiment (GRACE) mission has demonstrated the feasibility of measuring from space the gravity signature of a broad spectrum of phenomena that also affect terrestrial gravimeters: groundwater and ice mass balance, coseismic and postseismic effects, or glacial isostatic adjustment (Tapley, 2004; Wouters et al., 2014). GRACE consists of two identical satellites in near-circular orbits at 500 km altitude; separated from each other by 220 km. Space variable gravity potential of the Earth generates perturbations of the satellite orbits, which alter the distance between the satellites. By measuring this distance as a function of time through a microwave ranging system, one can infer information on the mass distribution and its movements within the Earth system.

GRACE provides relative measurements, such as spring and superconducting gravimeters. But the spatial resolution is very different from what can be achieved with ground instruments. Groundwater storage is heterogeneous in space and variable in time at scales below the spatial and temporal resolutions of GRACE, preventing one from retrieving local hydrological effects (Van Camp et al., 2014a, 2014b, 2010). Terrestrial measurements provide high-precision information about the time evolution of mass distribution in the few kilometers square around the instrument (Creutzfeldt et al., 2008; Güntner et al., 2017), whereas GRACE, with a 400 × 400 km^2 resolution, provides high-quality information about the mass distribution at the regional and global scales. Van Camp et al. (2014a, 2014b) showed that it is meaningless to compare the hydrological signal as seen by terrestrial gravimeters to GRACE, as it is not possible either to assess the mass distribution in the close vicinity of the instrument or to average out the local contribution by using a coarse network, considering the sparse distribution of terrestrial instruments.

For completeness let us mention other satellites such as the Laser Geodynamic Satellite (LAGEOS) (Seeber, 2003), the Challenging Minisatellite Payload (CHAMP) (Reigber et al., 2002), and the Gravity field and steady-state Ocean Circulation Explorer (GOCE) (Pail et al., 2011). These missions were appropriate to the measurements of the mean, static gravity field. By combining the data of GRACE, GOCE, and LAGEOS with surface data, one could provide a high-resolution model of the global, static gravity field with a spatial resolution of about 100 km (Förste et al., 2014).

2.4. Main Components in Time-Varying Gravity Signals

When initiating measurements with a gravimeter at the surface of the Earth, the strongest signal that appears is due to Earth tides, of which the peak-to-peak amplitude reaches about 3,300 nm/s^2. As already explained, this periodical phenomenon is relatively easy to correct at a few nm/s^2 level. However, it remains difficult to reach the nm/s^2 level (Ducarme, 2009; Kroner et al., 2005; Van Camp, de Viron, Pajot-Métivier, et al., 2016). When this is done, natural and anthropogenic microseismic signals are clearly visible at periods shorter than 50 s. When this high-frequency signal is removed using a low-pass filter, a strong correlation between the gravity time series and the atmospheric pressure appears. This can be corrected as described in

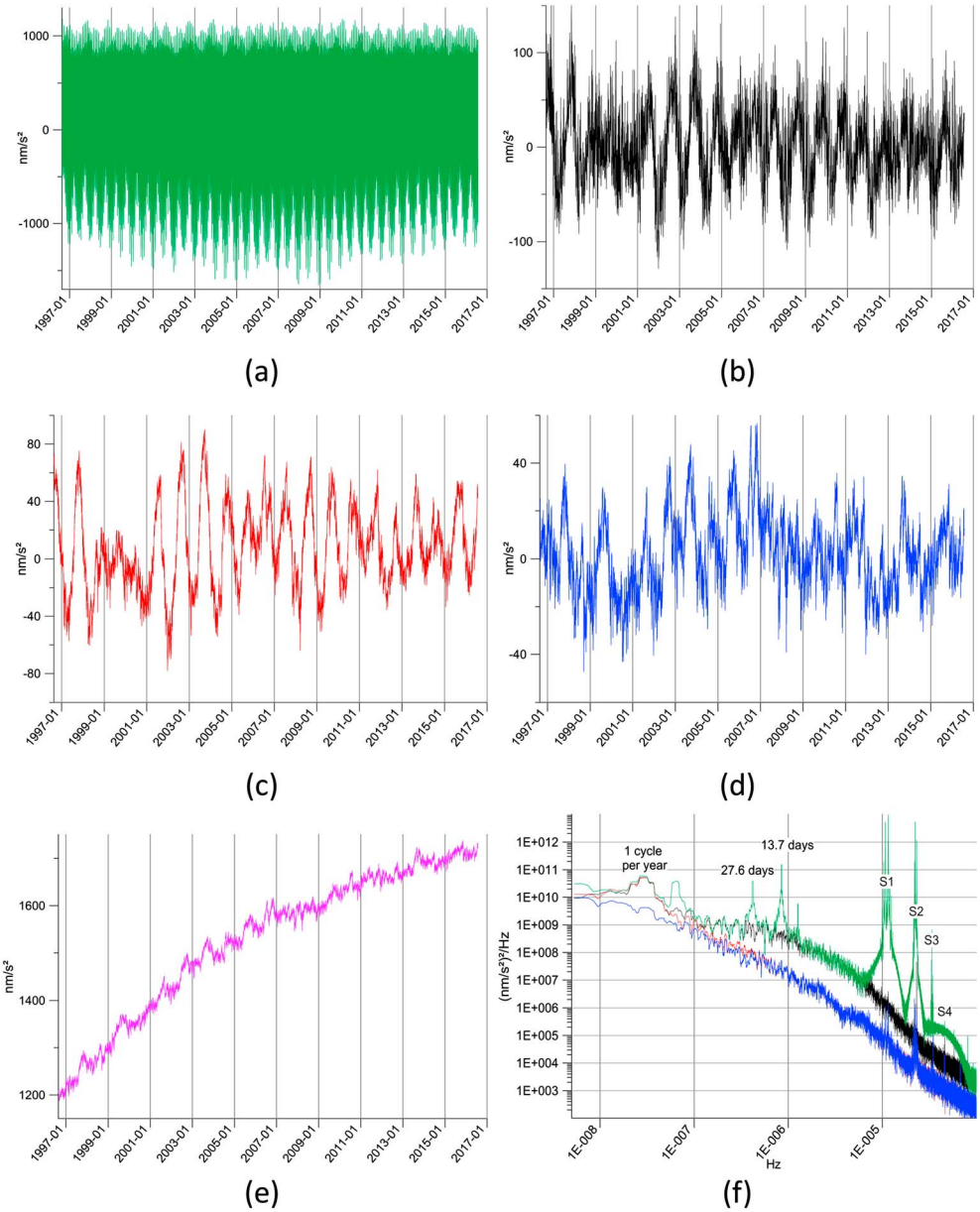

Figure 8. Hourly time series from the superconducting gravimeter GWR#C021 installed at the Membach station, Belgium. Data were taken from August 1996 until July 2016. (a) Time series after correcting for the instrumental drift; (b) same as Figure 8a after correcting for tidal effects; (c) same as Figure 8b after correcting for atmospheric pressure effect using an admittance of -3.3 nm/s^2/hPa; (d) same as Figure 8c after correcting for the polar motion effects; (e) same as Figure 8d but without removing the exponential instrumental drift which amounts $-667\times \exp(-0.108t)$nm/s^2/yr, equivalent to about +10 nm/s^2/yr in 2016; (f) power spectrum densities of the series shown in Figures 8a–8d. The quartdiurnal, terdiurnal, semidiurnal, and diurnal bands S4–S1 are shown, as well as the fortnightly and annual periods.

Appendix A; then, with lower amplitude, centrifugal effect change due to polar motion is easy to observe and correct (Figure 8). What subsequently remains are hydrological effects, residual tidal and atmospheric signals, and background free oscillations ("hum"). There are also earthquakes that can have a very large but still transient signature.

A specific signal coming from one of these phenomena can be properly investigated only if processes with similar signatures are not recorded in the signal. For example, a phenomenon having a semidiurnal S_2 or diurnal S_1 component will be lost in the tidal analysis process. Conversely, the tidal parameters will be

influenced by this signal, and separating them will be very difficult unless independent information is available. In practice, this is what is achieved with the atmospheric signal: a barometric time series is used as an additional input in tidal analyses in order to separate the atmospheric pressure effects from the tidal ones. This is also done with the polar motion, which can be modeled using astronomical observations. Concerning evapotranspiration of ground water by a forest during sunny summer days, this signal is diurnal, such as the S_1 component of the tidal and atmospheric effects; nevertheless, it was possible to extract it because the temporal signature of evapotranspiration is completely different: it looks like a stair-like effect rather than a sine wave, because evapotranspiration nearly stops during the night (Van Camp, de Viron, Pajot-Métivier, et al., 2016).

Other instrument-dependent noise sources are described in Appendix A.

3. Monitoring Geophysical Phenomena

The position of ground gravity in the global Earth observation system is defined by the properties of the observable, which has to pass a Socrates Test of Three:

1. Is it large enough? Ground gravity integrates the effects of mass around the instrument, weighted by the inverse of the square of their distance to the instrument. In addition, any vertical ground displacement results in a displacement of the instrument with respect to the Earth, which changes gravity by nearly 20 nm/s^2/cm (De Linage et al., 2007; Van Camp et al., 2011). Hence, ground gravity can be successfully used for studying two types of phenomena: mass distribution change down to 10 kg at a distance of 1 m (Figure A7) and vertical ground motion down to 1 mm.
2. Is it unique and separable? A pervasive problem in gravimetry is that surface gravity measurements do not provide a unique measure of the mass distribution within the subsurface. Is there a way to separate the signature of the phenomenon from the other contributions to gravity, with the required precision? Gravity is integrated, which means that a unique value includes the action of all the existing masses around the instrument, close or very far away. Separation is possible if the phenomenon is so strong that the other signatures can be considered as noise. This is also the case when even a very small phenomenon exhibits a distinct time/frequency signature, such as (pseudo)periodic phenomena, of which the return period is short enough to provide a good signal-to-noise ratio after stacking, or long-term processes so that the signatures from other sources average out. In addition, phenomena that can be observed by both gravity and some other techniques can also be separated in the gravity time series. Separating the signals does not only help to better observe a geophysical phenomenon but also to subtract its effect from the gravity, allowing to reveal further other phenomena.
3. Is it useful? Considering the very local focus of ground gravity, will that measure bring usable information about the phenomenon of interest? Do we benefit from a model good enough to interpret the measurements? The precisions of the relative and absolute measurements are at the level of one for 10^{-11} and 10^{-9}, respectively, making them very sensitive to small or remote phenomena. The response to Newtonian effects of the terrestrial gravity measurements has a transfer function that amplifies strongly the local scale and is much less sensitive to everything farther away than 100 m.

Measuring gravity changes at the nm/s^2 level makes it a very appropriate tool to estimate the groundwater mass balance: if the process responsible for the gravity variation is homogeneously distributed in the space close to the gravimeter (e.g., water table or hydrothermal systems changes), the problem can be simplified as a Bouguer Plate Effect (BPE).

To quantify our purpose, let us consider an infinite, 1 cm thick flat plate of water. Following the Bouguer approximation, the corresponding BPE corresponds to

$$\Delta g = 2\,\pi\,\rho G h = 4.2\ \mathrm{nm/s^2} \tag{2}$$

with ρ the density of water, G the gravitational constant, and h the thickness of the slab. Considering that the precision of measurements performed using a superconducting gravimeter can reach a level of 0.1 nm/s^2 (Van Camp, de Viron, Pajot-Métivier, et al., 2016, p. 2016), the groundwater signal can be detected with a layer as thin as 0.02 mm. Additionally, one can demonstrate, as it is done in Deville (2013), that 90% of the BPE comes from a volume represented by a cone of which the base radius equals about 10 times its height. Indeed, relating 90% of the BPE to the vertical component of the gravitational attraction of a horizontal

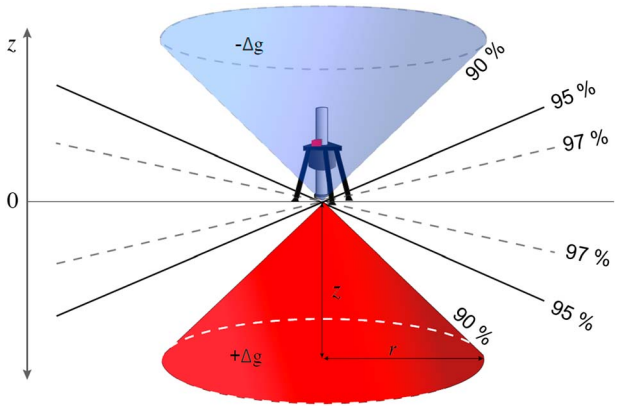

Figure 9. Cone of sensitivity for masses above and underneath a gravimeter. The mass in each colored zone contributes 90% of the gravity signal as monitored by the gravimeter; the ratio between vertical distance and the radius of the cone is $z = 9.95r$ (90%), $z = 19.97r$ (95%), and $z = 33.32r$ (97%). For legibility, the actual aperture angles of 169°, 174°, and 177° could not be drawn. Another representation of the sensitivity distribution can be found in Kennedy et al. (2014).

thin disc of which the center is placed vertical to the gravimeter, based on a formulation similar to that of Singh (1977), leads to

$$\Delta g = 0.90 \times 2\ \pi\ \rho G h = \left(1 - \frac{z}{\sqrt{z^2 + r^2}}\right) \times 2\ \pi\ \rho G h \qquad (3)$$

where z is the distance between the gravimeter and the disc center, and r is the radius of the disc, as described in Figure 9. Developing this relationship ends up with $d = 9.95\ r$. This is valid both if the disc is placed below or above the gravimeter. Thus, 90% of the gravity signal originating from hydrological processes takes place in a volume represented by an "hourglass" of which the center is the gravimeter, defining the gravimetric sampling volume (Figure 9). However, for investigating shallow processes in the presence of strong topography at the measurement site, it is recommended to compute specific gravity site effect based on 3-D models made of, for example, rectangular prisms or spherical bodies. Such an alternative approach is required when dealing with spatially limited hydrological targets such as confined reservoirs and saturated karstic features. This is also an approach that should be preferred for imaging gravity variations related to volcanic activity.

Figure 10 shows the expected gravity signal for two volcanic sources: magma transport in brittle rock, that is, a dike intrusion and a Mogi model (Mogi, 1958), that is, a spherical cavity. Two typical dike intrusions (Rivalta et al., 2015) in an existing fissure are modeled: 3 km high and 2 and 5 m wide dikes. The 2 m thick shallow dike induces a gravity change of about 10 nm/s^2 at 11 km, this increases to 17 km for the 5 m thick one. For deeper dikes, extending from −5,000 to −7,000 m as observed around the Bárdarbunga volcano (Gudmundsson et al., 2016; Sigmundsson et al., 2014), the distances become 7 and 14 km for density contrasts of 300 and 1,000 kg/m^3, respectively. For the Mogi source, changes of 10^{10} kg at a depth between 2 and 6 km induce gravity variations larger than 10 nm/s^2, which can be measured at a horizontal distance of up to 4 km. For a mass change of 10^{12} kg, at depths ranging 2 to 6 km, a 10 nm/s^2 gravitational effect can be measured at distances up to 24 km (Figure 10).

If the response to any of those three questions is no, then ground gravity is useless, and other measurements should be planned. Otherwise, the signals worth being studied can be local or very large scale:

1. *Local*. The sensitivity of the ground gravimeter is essentially limited to 1 km^2 around the instrument. Phenomena of interest saturate the signal at the kilometer length scale and are small scale enough to be largely sampled by one or a few instruments. In such contexts, monitoring gravity changes delivers gravity time series that provide an integrated vision of the evolution of the targeted process, which could be too deep for surface techniques. Such information is often not reachable by other means, being too local for space-based sensors. Often, the local phenomena are strong, reaching at least a few thousands of nm/s^2. When they are weak, a careful measurement procedure and identifying the potential temporal signature improves the chances to detect them. Local phenomena concern, for instance, volcanic and hydrothermal systems, water or CO_2 injection sites, karst systems, subsidence processes, landslides, ice melting areas, erosional processes, or Newtonian noise on gravitational wave detectors (section 3.1).
2. *Very large scale*. If the length scale of the phenomenon is very large or if its geographical pattern is known, measuring local gravity magnitude in a few isolated locations is sufficient to fully sample the phenomenon. This is the case of the periodic Earth tides, free oscillations after major earthquakes, the episodic seismic slips at plate boundaries, and of long-term gravity changes related to glacial isostatic adjustment and the seismic cycle (section 3.2).

Independently from geophysics, it is also relevant to monitor gravity for questions related to metrology and fundamental physics, as described in section 3.3. All the phenomena described in this section are summarized in Table 1.

3.1. Local Phenomena

When using gravimeters to investigate local phenomena, of which the typical length scale is a few hundred meters, one deals with Newtonian effects or local displacements. The possible related vertical displacements

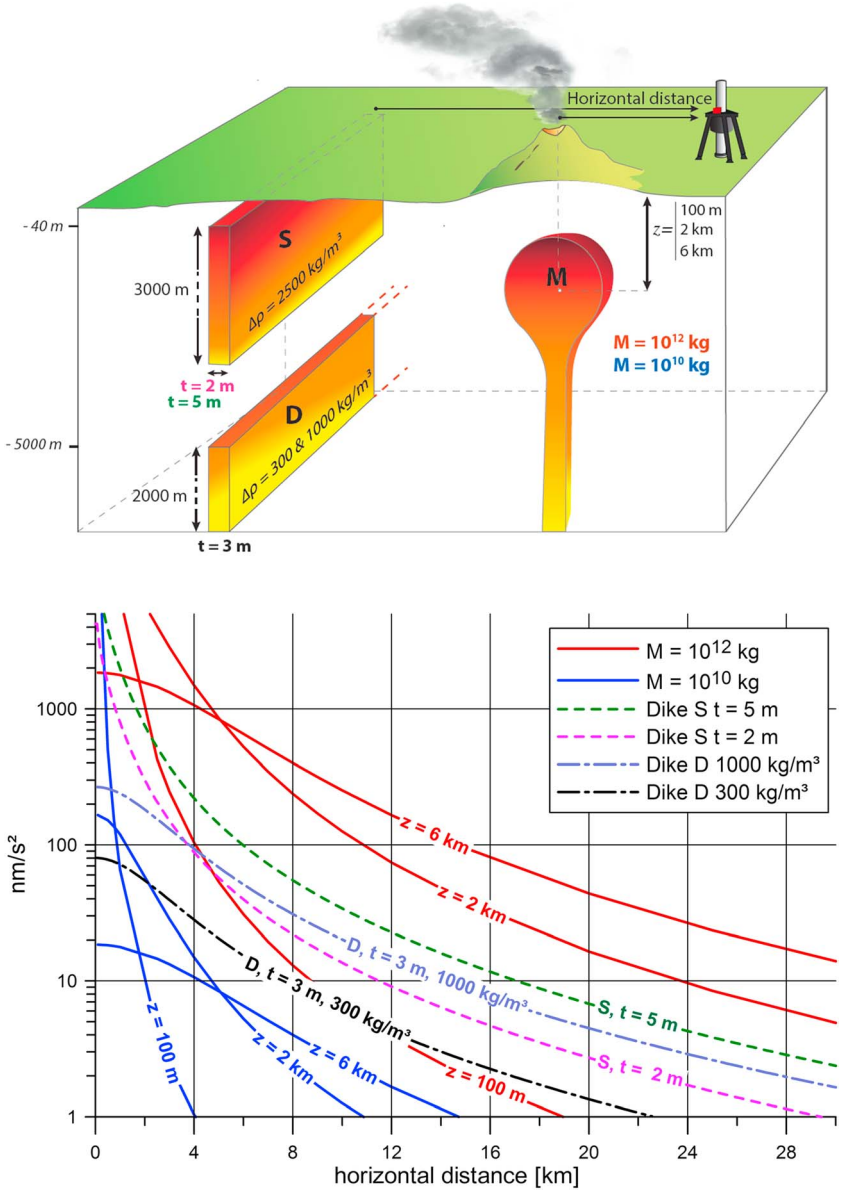

Figure 10. Effects of a Mogi point and dike sources as a function of the horizontal distance, for three depths and two masses for a Mogi source (Williams-Jones & Rymer, 2002) and two thicknesses for a shallow dike (Dike S similar to Mount Etna (Branca et al., 2003), or two density contrasts (300 and 1,000 kg/m^3) for the deeper case Dike D, extending from −5,000 to −7,000 m, with a thickness of 3 m; D is similar to the Bárdarbunga intrusion (island) (Gudmundsson et al., 2016; Sigmundsson et al., 2014). All the dikes are 48 km long and modeled according to Nagy (1966).

are supposed to be corrected for by using Global Navigation Satellite Systems (GNSS), satellite radar interferometry, or repeated leveling methods.

3.1.1. Hydrogeology

Gravity measurements inform on local groundwater mass balance, infiltration rates, effective porosity, or hydraulic conductivity of aquifers and contribute to model calibrations (Kennedy et al., 2016). In a changing world, accurately assessing the terrestrial hydrological cycle remains a key challenge of the geosciences, as sustainability requires knowing the availability of freshwater, mitigating the flood hazard, or identifying actual evapotranspiration.

The first application of gravimetry in hydrogeology, often called hydrogeodesy or hydrogravimetry (Christiansen et al., 2011; Ferré et al., 2009), was published by Montgomery (1971), who investigated

Table 1
Summary of the Geophysical Phenomena Described in Section 3

Phenomenon and Scientific Challenge	Period	Expected Signature Level (nm/s^2)	Required Precision (nm/s^2)	Difficulties and Required Improvements	Added Value of Gravity
Hydrogeology: Ground water mass balance	1 min to decades	0.1 to a few hundred	<0.1	Building a comprehensive model and correcting atmospheric effects	Mass integrated at local scale
Volcanology: Determining the functioning of the volcanic plumbing system	1 min to decades	0.1 to 10^6	1–10	Separating hydrological effects and harsh field conditions	Density changes and mass transport
Reservoir monitoring: Monitoring water storage and migration, oil, natural gas, or CO_2 storage	1 min to decades	0.1 to a few thousands	<0.1	Complete model and modeling atmospheric effects	Mass integrated at local scale and transfer of masses
Subsidence: Determining compaction processes, cause of the subsidence	Months to decades	10–500	1	Separating hydrological effects	Density change
Tides: Identifying the best solid Earth tidal model	6 h to decades	Up to 3,000	<0.1	Instrumental hazard, minimizing tares, precise instrumental transfer function: stable calibration factor, determined at better than the 0.1% level; instrumental time lag with a precision of 0.01 s Improving ocean loading models, better separating atmospheric and hydrological effects	Amplitude and phase of the gravity tidal waves
Earth free oscillations: Improving Earth's model, 3-D tomography of the mantle and inner and outer cores	100 s to 3,240 s	Up to 10	<0.01	Modeling atmospheric effects Determining precise instrumental transfer function	Accurate eigenfrequencies, quality factor of each mode (i.e., its attenuation), and calibrated amplitudes
Slow slip events: Physics of the phenomenon, for example, role of water	Minutes to years	Up to a dozen	<1	Separating hydrological effects	Mass changes, migration of fluids, and measuring low-frequency oscillations
Glacial isostatic adjustment: Ice load history, viscoelastic models of the mantle, separating present, elastic adjustment from the past, viscoelastic one	Years	Up to 50/yr	<1	Accuracy of the AG Separating hydrological effects, long-term climate changes	Providing the gravity rate of change to estimate the $\frac{\dot{g}}{\dot{z}}$ ratio
Preseismic and coseismic cycle: Role of water in triggering earthquakes, anelastic effects, source process, and early warning	Seconds to decades	0.1 to a few thousands	<1	Accuracy of the AG Separating hydrological effects	Slow and fast mass displacements
Postseismic relaxation: Viscoelastic models of the mantle and poroelasticity	Seconds to decades	1 to a few hundreds/yr	<1	Accuracy of the AG Separating hydrological effects	Providing the gravity rate of change to estimate the $\frac{\dot{g}}{\dot{z}}$ ratio, ground water transport
Metrology: Determining the Planck constant, redefinition of the S.I. base unit; traceability of geodetic and seismic measurements	When required	-	<10	Accuracy of the AG	Gravity value
Gravitational waves: Reducing the Newtonian noise in gravitational waves detectors	30 Hz to a few seconds	?	?	Separating the atmospheric and hydrogeological effects	Monitoring mass movements

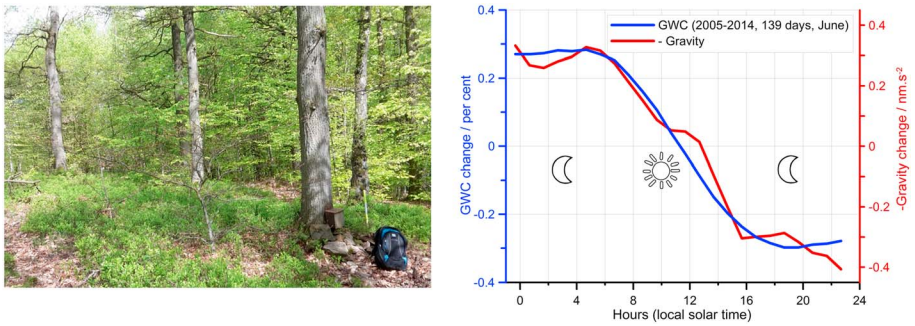

Figure 11. (left) Deciduous forest; the back is 48 m above the gravimeter; (right) gravity water content (GWC, blue, in percent) and inverted gravity signal (red, in nm/s^2; the actual gravity signal increases because the gravimeter is underground, below the surface soil moisture). Time is in hours (local solar time). Stacked values for 139 dry days. The stacking is performed in the months of June from 2005 to 2014. Between 4:40 and 17:40 the gravity water content diminishes by 0.57 ± 0.02 percentage point and gravity increases by 0.66 ± 0.14 nm/s^2, which is equivalent to 1.7 ± 0.3 mm of water. The subsurface lateral flow was separated from the diurnal evapotranspiration signal by removing a linear trend fitted over the nighttime pattern. From Van Camp, de Viron, Pajot-Métivier et al. (2016).

ground water specific yield by performing time lapse microgravity measurements. The high uncertainties on measuring techniques at that time limited the use of time lapse microgravimetry in hydrology.

Nowadays, gravimetric techniques allow us to monitor hydrogeological effects at a scale of up to 1 km^2, for signal ranging a few thousands of nm/s^2 to less than 1 nm/s^2. Several studies have demonstrated the strength of gravity observations for monitoring quantities related to the water cycle, such as soil moisture, rainfall, groundwater storage, hydrothermalism, or snow covering (Creutzfeldt et al., 2014; Hector et al., 2015; Hemmings et al., 2016; Imanishi et al., 2006; Jacob et al., 2008; Pool & Eychaner, 1995; Van Camp et al., 2006; Wilson et al., 2012).

Gravity measurements have also been used to support the monitoring of evapotranspiration, the process whereby liquid water is converted into water vapor by the vegetation. Its assessment is critical to estimate ground water recharge and strongly controls energy transfer between the Earth and the atmosphere. Using a superconducting gravimeter, Van Camp, de Viron, Pajot-Métivier, et al. (2016) observed the diurnal evapotranspiration from a deciduous forest. They identified average daily changes in gravity at the level, or smaller than 1 nm/s^2, which corresponds to 1.7 mm of water per sunny summer day. This is at the limit of the terrestrial measurements (Van Camp et al., 2005) and could be effectively enhanced through a stacking process. As with tides, it is the repeated nature of the phenomenon that allows its precise identification (Figure 11). As measuring evapotranspiration by other methods is challenging, its direct measurement at the 50 ha scale using a gravimeter appears as a promising method. Because evapotranspiration returns more than 50% of the precipitation back to the atmosphere, it plays a major role in terrestrial ecosystem functioning and the recharge of aquifers. Gravity measurements provide an independent way to validate new methods developed to estimate evapotranspiration (Figure 12).

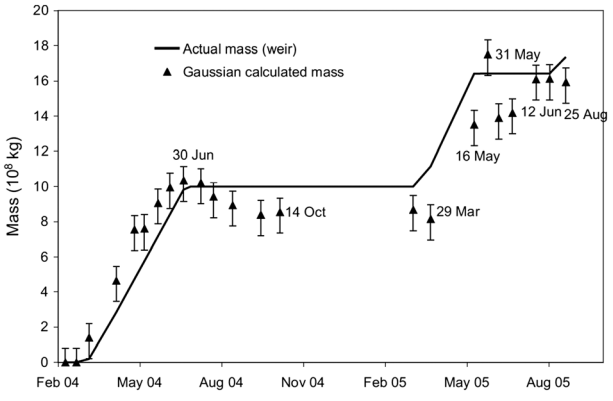

Figure 12. Mass of weir-measured infiltrated water (solid line) compared with the mass estimated from the integration of gravity measurements performed at the infiltration pond at the mouth of Weber Canyon, northern Utah. Measurements performed using a CG-3M Scintrex quartz spring gravimeter. The maximum gravity changes were 1,110 nm/s^2 in 2004 and 1,300 nm/s^2 in 2005. From Chapman et al. (2008).

Aquifers are underground zones where water saturates the pores and fractures of the material; they are of vital importance in many regions. The amount of water available in the saturated zone is usually determined using a piezometer, which measures the water pressure, which can be converted to an equivalent height of a column of water. When the upper surface, known as the water table, is open to the atmosphere through the permeable material, the aquifer is said to be unconfined. The pressure of water is in equilibrium with the atmosphere, and the water level in the borehole corresponds directly to the water level in the aquifer. When the aquifer is surrounded by impermeable layers, it is said to be confined, and the water is stored in the expansion of the

aquifer matrix, that is, its solid structure, and the compressibility of water. Pressure is higher than what would be associated with the water weight only and may reflect the effects from recharge at a higher elevation or from the weight of the overlying rock and soil, and the well level balances this total pressure. As the compressibility of both the aquifer matrix and the water is weak, large piezometric variations are only accompanied by small gravity changes in confined aquifers. The piezometers, often installed in boreholes, do not establish whether an aquifer is confined, or not. Hence, piezometric head and gravity measurements can be used to identify unconfined aquifers, as head changes correlate with gravity changes only in unconfined aquifers (Pool, 2008). In unconfined aquifers, combining gravity and piezometer levels, or known volumes of injected water, provides direct information on the porosity of the aquifer (Chapman et al., 2008; Davis et al., 2008; Pool & Eychaner, 1995).

In the unsaturated or vadose zone, it is usually not possible to efficiently pump groundwater. In the soil, capillary forces hold the moisture too tightly. To estimate the soil moisture, gravimeters can act as a weighing lysimeter, a device that estimates the amount of water percolating through the soil. The advantage of a gravimeter is that it can noninvasively sample 10^6 m^3 of undisturbed ground volume, versus typically 1 m^3 of soil volume for a lysimeter, which is an invasive technique, not applicable to water percolating through porous hard rocks (Wang & Dickinson, 2012). Comparing soil moisture measurements using gravimeters and lysimeters was performed by Creutzfeldt et al. (2010).

Continuous terrestrial gravity measurements provide valuable information for assessing the water mass balance in the saturated and unsaturated zone at the mesoscale, which cannot be observed by satellite techniques due to their coarse resolution (Peng et al., 2017; Van Camp et al., 2014a, 2014b).

It remains challenging to discriminate between the gravitational effect of water storage change in the unsaturated zone and the aquifer. In a karst area, where the vadose zone is usually thicker than in other contexts, combining gravity measurements at the surface and inside accessible caves is a way to separate the contribution from the unsaturated zone lying between the two instruments, from the saturated zone underneath the cave, and the common mode effects from the atmosphere or other regional processes. Continuous measurements provide information on the ground water mass changes as a function of the degree of saturation at different timescales, from flash floods events to seasonal and interannual scales. The functioning law of the aquifer can then be inferred by combining continuous gravity and geophysical and hydrological measurements. A karst system is a complicated, nonlinear system, but an extraordinary characteristic in some cases is the ability to observe the saturated zone directly ("underground streams"). The advantage of gravity measurements is that they provide information on the masses of water, integrating vertically and horizontally the karst subsystems several hundreds of meters around the instrument. This is not the case with classical hydrological monitoring systems, which are soundings affected by their own near environment and the karst heterogeneity.

3.1.2. Separating Hydrogeological Effects From Other Geophysical Processes

Even if there is no interest in performing hydrogeological investigations using a gravimeter, the gravity signal is such that separating the contribution of surface hydrology from other geophysical processes in gravity measurements is a major challenge. This is especially true for volcanoes, most of which are located along or surrounded by oceans, hence experiencing strong rainfalls, where water, either meteoric or marine, mixes with hot magmatic fluids and convects within porous rock and sediments.The separation can be done by three methods, as discussed hereafter: (1) the hydrological signal is known with a precision sufficient to allow subtraction of the hydrology signature from the gravity data, (2) one disposes of sensors with a response to hydrological load and tectonic effect different from that of the gravimeter, or (3) the space-time behavior of the two signals differs to such an extent that it is possible to use data processing technique to separate them. The third method is not practical because of the sparsity in time and space of microgravimetric surveys (Van Camp, de Viron, & Avouac, 2016).

Method 1 requires precise independent information about hydrology. Estimating subsurface water storage changes is notoriously complex, and it is even more at the very local scale, where the gravity transfer function is the most sensitive (Creutzfeldt, Güntner, Thoss, et al., 2010; Creutzfeldt, Güntner, Wziontek, et al., 2010; Meurers et al., 2007; Mikolaj et al., 2015; Van Camp et al., 2006). This is difficult because very local parameters such as soil characteristics, lithology, bulk rock porosity, or hydraulic conductivity influence water storage and, consequently, local gravity variations. Thus, knowledge of such parameters is crucial for extracting the

local hydrological signal from other sources of gravity perturbations. Geological investigations are useful and, often, even necessary to identify possible reservoirs or structures that may facilitate water transfers throughout the ground. Additional measurements from other types of sensors such as soil moisture sensors, piezometers, time lapse electrical resistivity surveys, dye tracing, and seismic ambient noise monitoring may strongly help in validating geological assumptions (Singhal, 2010) and monitoring local hydrogeological processes. However, this cannot be performed at each gravity station. In addition, correction of the hydrological signature by applying global hydrological models such as the Global Land Data Assimilation System (GLDAS) (Rodell et al., 2004), or European Re-Analysis (ERA) (Uppala et al., 2005), or space-based observations from GRACE (Wouters et al., 2014) is questionable, given their limited time and space resolution.

Method 2 requires additional data of a different kind. For example, combining repeated leveling, GNSS or InSAR (Interferometric Synthetic Aperture Radar) and gravity measurements, one can separate the gravity signal caused by the vertical land movement from other effects. Simultaneous gravity measurements at depth and the surface (Jacob et al., 2009), or at different locations on the surface (Kennedy et al., 2014), have also been proved useful to separate the signal of interest.

Method 3 is powerful when measuring long-term gravity changes. Based on the spectral content of modeled hydrogeological effects and of superconducting gravimeter time series, (Van Camp et al., 2010) investigated the hydrological effects on gravity measurements extending several years. They showed that the time required to measure a gravity rate of change of 1 nm/s^2/yr at the 1σ level was of the order of 10 years but highly dependent on the location, assuming continuous, hourly sampled gravity time series at the existing SG stations. In the case of repeated absolute gravity measurements, the continuity of measurements is broken, and the setup noise must be taken into account. Presently, the easiest and practical way to mitigate hydrological effects in long-term gravity measurements is to perform measurements for years, at the same epoch of the year—the impact of seasonal variations is then minimized, and for a sufficiently long time period, interannual variations average out. This procedure is only approximate due to long-term variability of the hydrological signal and to the possible long-term drift of groundwater storage. Van Camp, de Viron, & Avouac (2016) showed that for 10 yearly campaigns, performed with an absolute gravimeter at the same epoch of the year, an average uncertainty ranging 3–4 nm/s^2/yr can be achieved in most of the places of the Earth (this study did not include Antarctica nor Greenland). But, for shorter periods, it remains challenging to correct for them and, when a correcting model is available, it may not only be insufficient, it can also add artifacts. The addition of continuous measurements from a relative gravimeter mitigates the error in the estimation of gravity rates of change caused by the presence of long-period, interannual, and annual signals in the AG data (Van Camp et al., 2013), but this remains unpractical. Mitigation could be powerful by repeating measurements around a site (Naujoks et al., 2008) or installing a regional network of continuously measuring instruments, as it would allow separating common mode signals from very local ones; however, this is presently not logistically or financially sustainable.

3.1.3. Volcanoes and Hydrothermal Systems

Magmatic systems are complex structures, where many physical and chemical phenomena occur, and eruptions result from both slow and fast processes occurring at depths ranging from the Moho to the surface. Most magmas stall and cool, de-gas, crystallize, and evolve to lower density and chemically evolved melts within the crust (Sparks & Cashman, 2017; Wright et al., 2012).

Geophysical phenomena associated with and prior to volcanic eruptions include magma generation by partial melting of the upper mantle and crust, vertical and horizontal motion, melting, crystallization, and magma fluid exsolution, but the relative importance of the various phenomena vary to a large extent. Part of the eruptions is triggered by melt replenishment in a shallow reservoir, while for others, primitive lavas show no evidence of storage. Eruptions are fed by either a single or multiple magma bodies tapping the plumbing system (Dzurisin, 2003). Understanding how magma and associated fluids decouple to each other, move through the crust, and accumulate in shallow chambers before erupting remains challenging (Cashman et al., 2017; Christopher et al., 2015; Sparks & Cashman, 2017). The variety of possible eruption types is just huge, and the same is true for their possible geophysical signatures.

Precursor events, such as ground deformation, changes in seismic velocities, seismic activity, magnetic field, electrical resistivity, ground water levels, heat flow, and change in gas composition and gravity, are associated with the magma approaching the surface. By monitoring gravity changes, it is possible to detect

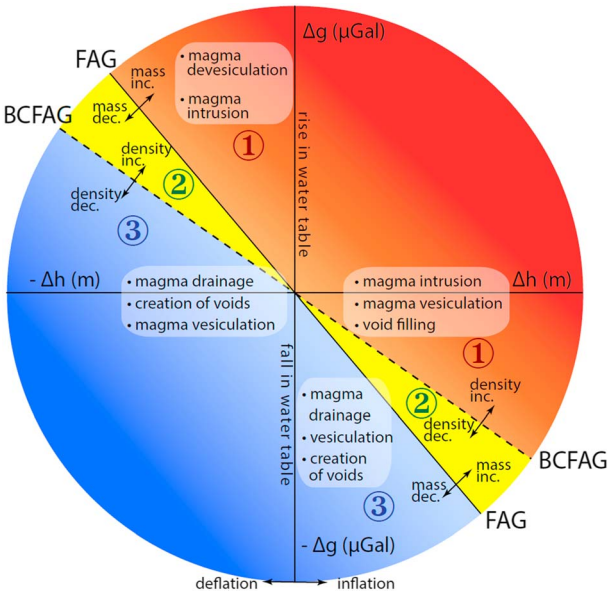

Figure 13. During periods of inflation, increasing elevation (Δh) is accompanied by decreasing gravity (negative Δg), and conversely. Region 1 represents gravity increases larger than the FAG during subsidence or decreases smaller than the BCFAG during uplift, caused by mass or density increases. Conversely, region 3 represents gravity decreases larger than the FAG during uplift or increases smaller than the BCFAG during subsidence, caused by mass or density decreases. Modified from Figure 2 of Williams-Jones and Rymer (2002).

shallow and deep processes before eruption precursors such as gas fluxes, earthquakes, surface deformation, or the creation of voids leading to caldera collapse (Battaglia, 1999; Battaglia et al., 2003; Branca et al., 2003; Carbone, 2003; Carbone et al., 2017; Rymer, 1994; Rymer & Brown, 1989).

Combining gravity and deformation measurements permits discrimination between gas, water, and magma intrusion (Bagnardi et al., 2014; Bonvalot et al., 1998; Carbone & Greco, 2007; Hautmann et al., 2014), assessing voids opening (Carbone, 2003; Furuya et al., 2003), magma density changes associated with degassing (Bagnardi et al., 2014; Poland & Carbone, 2016) or overturn of resident magma in a reservoir (Rymer et al., 1998). Terrestrial gravity measurements can also support the investigation of dike growth and migration, which can be induced by vertical intrusion (Gudmundsson, 1995, 1998; Wright et al., 2012) or lateral outflow of magma (Einarsson & Brandsdottir, 1978; Gudmundsson et al., 2016; Sigmundsson et al., 2014) (Figure 10).

Hence, gravity measurements can contribute to building the new conceptual models that are currently addressing questions related to magma evolution and the behavior of volcanic systems.

When a volcanic phenomenon occurs, it is associated with a change in the mass distribution, which affects the vertical gravity gradient. Investigating change in that gradient allows a better physical understanding and discrimination between the types of events (Rymer, 1994; Rymer & Williams-Jones, 2000; Williams-Jones & Rymer, 2002): Figure 13 represents the gravity variation as a function of deformation, assuming coincident mass and pressure changes. A separation of the phenomena between three distinct classes can be observed in the figure, separated by the linear relation between gravity change and deformation associated with the free air gradient (FAG) and the Bouguer-corrected free air gradient (BCFAG). The FAG represents the gravity changes that would be observed when moving a gravimeter up and down, without mass displacements. On a flat surface, the theoretical FAG value is $-3{,}086$ nm/s^2/m but can vary by about 10% depending on the local terrain and Bouguer anomaly (Rymer, 1994). The BCFAG represents the amount by which gravity varies with elevation, taking into account the mass accompanying the deformation. For a spherical point source (Figure 14), the BCFAG ranges from $-2{,}530$ to $-2{,}330$ nm/s^2/m for magma densities of 2,000 to 2,700 kg/m^3, respectively. Gravity change following the BCFAG means that ground deformation is not accompanied by subsurface density change.

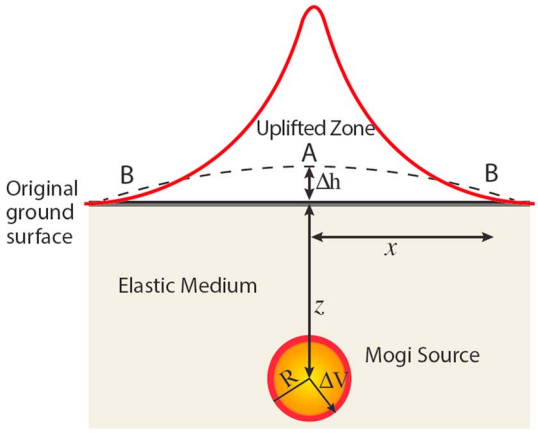

Figure 14. Magma reservoir modeled as a spherical body (Mogi source) in an elastic half-space, associated deformation (gray shaded line) and gravity effect (red line). The inflation or deflation source is due to injection or withdrawal of new magma in the spherical chamber. Modified from Figure 1 of Rymer and Williams-Jones (2000).

In region 1, at the right of the figure, for gradient and deformation included between the horizontal zero gradient and the BCFAG, an anomalous small gravity decrease (smaller than expected from the BCFAG) is accompanied by inflation as one would expect from magma intrusion, which increases the density of the magma chamber, hence reducing the decrease in gravity, which would be expected from the uplift. Conversely, for region 3, at the left of the figure, experiencing subsidence, the weak gravity increase, or even the decrease in gravity, can be caused by magma drainage, the creation of voids (Furuya et al., 2003), or magma vesiculation, which refers to the formation of bubbles.

During inflation, the lower part of region 2 indicates mass and volume increase, resulting in a density decrease. This can be interpreted as the buildup of gas or water within the magma chamber. This buildup of gas pressure within magma is a precursor to eruptive activity and is important to detect for hazard mitigation (Vigouroux et al., 2008). Conversely, during deflation, in the higher part of region 2, mass decreases while

density increases. Such an observation is reported by Battaglia et al. (2006), who assumed that the subsidence was caused by migration of water out of aquifers in a caldera.

Considering gradient and uplift in the area delimited by the FAG line and the vertical axis, region 3 at the bottom right of the figure corresponds to shallow processes such as groundwater changes or fluctuation of magma and gas in the feeder conduit. The anomalously large gravity decrease (larger than expected from the BCFAG) has different possible causes, such as magma drainage, the creation of voids, vesiculation, or fall in the water table. In region 1 at the top left of the figure, subsidence is accompanied by an anomalously large increase in gravity, induced by devesiculation associated with gas losses, magma intrusion, or rise of the water table.

By combining gravity and deformation measurements, several studies deciphered the nature of volcano processes acting below the surface. For example, Furuya et al. (2003) could identify the formation of an empty space underneath the Miyakejima volcano (Japan). Although the ground was subsiding, the void induced a decrease in the gravity of 1,450 nm/s^2, reflecting the formation of a large void beneath the volcano 2 days prior to a caldera collapse in July 2000. It is hypothesized that a voluminous lateral flow of magma broke the lithostatic balance between the magma chamber and surface crust, thereby forming a void. Another strong gravity decrease was observed on the Sierra Negra volcano, Galapagos, Ecuador: Vigouroux et al. (2008) reported on a gravity drop by 9,500 nm/s^2 associated with a diminution of the density in the magmatic system. Combining the gravity data with geochemical measurements, the authors interpreted the density decrease as a magma vesiculation, providing a driving force for explosive eruptions. They could infer the sill thickness and bubble content (10–50 volume percentage). The Sierra Negra gravity change is the largest ever monitored gravity variation on an active volcano.

A 4,000 nm/s^2 decrease was also reported at Mount Etna (Italy) in October 2002, which lasted for less than 6 h and was supposed to be caused by the opening of a dry fracture 1 km away from the gravity station (Branca et al., 2003; Carbone et al., 2007) (Figure 15). Using gravity measurements, the authors could demonstrate that magma from the central conduit entered the fracture system passively, that is, using this existing structure as a path for the eruptive vents. The filling of the newly formed voids roughly compensated the decrease observed in Figure 15a. The gravity decrease allowed the authors to deduce that the magma overpressure did not cause the fracture opening, possibly caused by external forces. Still at Mount Etna, during the 2002–2003 eruption, Carbone et al. (2006) interpreted joint tremor/gravity anomalies as caused by the accumulation of a foam layer in the conduit.

On the Campi Flegrei caldera, west of Naples, Italy, inverting gravity, leveling, and trilateration, Battaglia et al. (2006) could show that a fluid, of which the density is close to water, was the main source of the 1980–1984 inflation. At Nisyros Caldera, Greece, 350 nm/s^2 peak-to-peak gravity variations were observed over periods of 40 to 50 min (Gottsmann et al., 2005). By cross-coupling gravity measurements with ground deformation and seismic and electromagnetic data, it was assumed that the gravity changes were caused by the degassing of the magmatic source, inducing thermohydromechanical disturbances within the hydrothermal system. Gottsmann et al. (2011) applied a similar multiparameter experience at the Soufrière Hills Volcano, Montserrat (Lesser Antilles, UK). Different fingerprints could be revealed a few minutes before two different vulcanian explosions in July and December 2008. The authors inferred important constraints for investigations of the effusive to explosive transition; gravity measurements were valuable to investigate the response of a shallow aquifer and fluid-saturated fault damage zones to stress changes during pressurization and depressurization of the plumbing system (Hautmann et al., 2014).

Table 2 summarizes the different applications of the monitoring of time-varying gravity on volcanoes.

On volcanoes, discrete, time lapse gravity measurements are performed at most once a day or a week, often once a year or lesser, due to logistical problems such as costs, snow, staff and instrument availability, and the necessity to reduce staff exposure in a hazardous area (Carbone & Greco, 2007). Continuous measurements reduce these logistical issues, allow investigating high-frequency or transient phenomena, improve dramatically the signal-to-noise ratio, and avoid aliasing (Van Camp et al., 2013). Continuous monitoring is important to monitor magma accumulation and withdrawal, revealing new physical properties of magmatic plumbing systems as the dynamics of intrusive sources (Battaglia et al., 2008; Poland & Carbone, 2016). This is especially true on persistently active volcanoes where significant variations on the daily and hour scales have been reported and are important for eruption forecasting (Branca et al., 2003; Gottsmann et al., 2007).

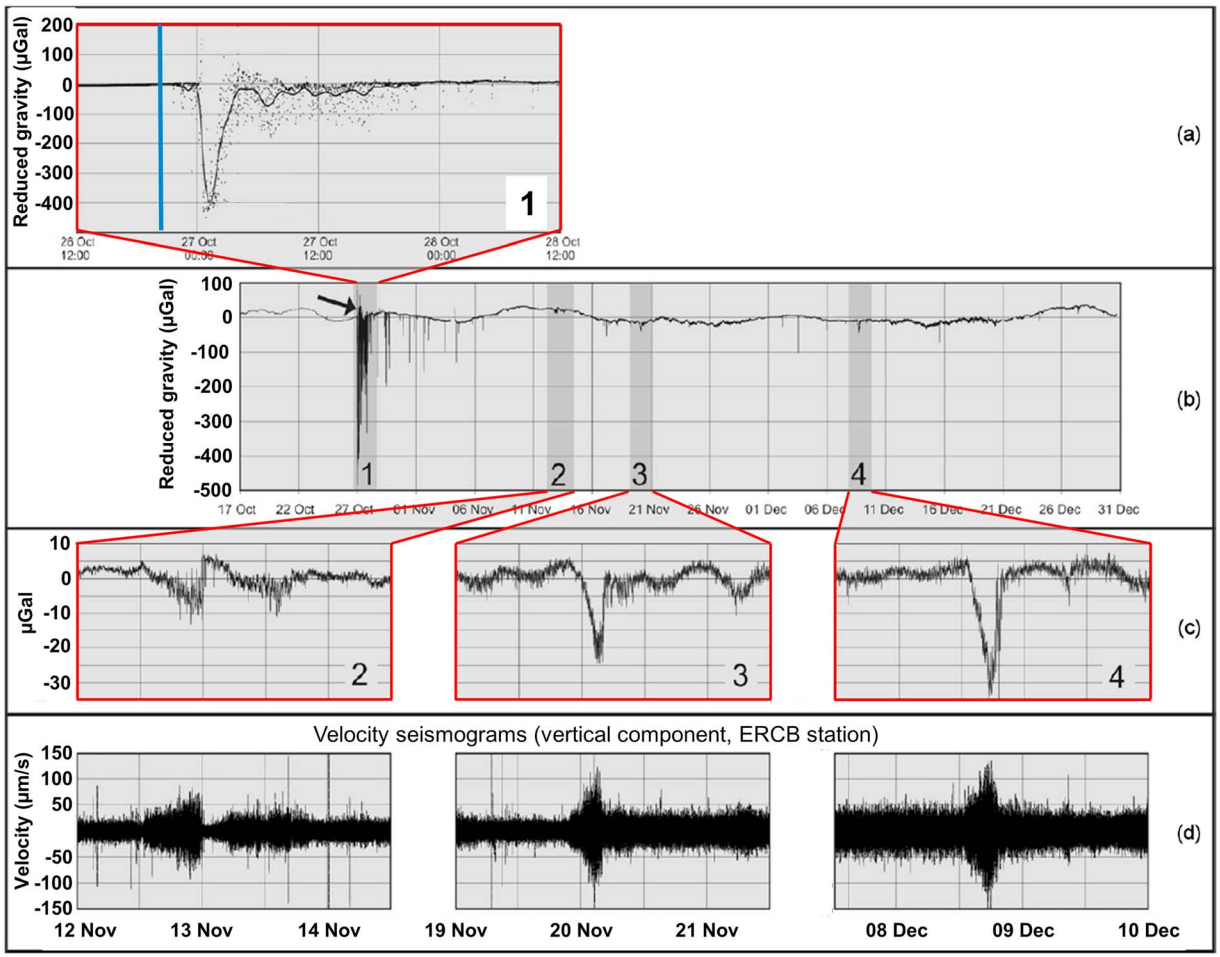

Figure 15. (b) Gravity sequence acquired at the summit northern slope of Mount Etna volcano, at an elevation of 2,820 m above sea level, during the 17 October to 31 December 2002 period and zooms over (a) the 48 h signal encompassing the start of the 2002–2003 eruption (black arrow in Figure 15b), and (c) the three 60 h signals encompassing the gravity decreases contemporaneous to volcanic tremor increases; (d) the signal from ERCB seismic station is shown. A low-pass filter (cut-off frequency of 24 cycles per day) is applied to the signal in Figure 15a (continuous black line) to better evidence the main change of the gravity field relative to the strong background noise (unfiltered series appears as dots). The vertical blue line in Figure 15a marks the start of the seismic swarm before the eruption. The time series are corrected for tides and instrumental drift. Modified from Figure 2 of Carbone et al. (2007).

Moreover, volcanoes store a large amount of water in their porous layers, cracks, lakes, and cavities. Changes in groundwater masses not only mask other mass transfers that can be monitored by gravimeters but also pose hazards: "wet" volcanoes can induce magmatic and steam-driven (hydrothermal or phreatic) eruptions. Steam-driven eruptions are particularly hard to predict and may expel steam, water, and fragments of preexisting rocks. Continuous or repeated gravity measurements are appropriate to monitor groundwater changes and to build and assess hydrogeological models (Kazama & Okubo, 2009; Kazama et al., 2012; Mouyen et al., 2016). Ideally, and realistically, combining time lapse spatial surveys and continuous measurements at reference stations is probably an optimal option (Carbone & Greco, 2007; Williams-Jones et al., 2008). Given their great sensitivity, superconducting gravimeters can provide useful information on volcanic phenomena sufficiently early, even several kilometers away from the magmatic source, which is a logistical asset (Figure 10). The sensitivity of high-precision gravimeters to mass changes may, therefore, shed light on the causes of volcanic unrest and can become critical for assessing volcano hazard and issuing a warning.

A network of continuously measuring gravimeters may nicely complement other geophysical and geochemical methods for a better understanding of the rifting cycle, the crust and mantle properties, and the dynamic transport of magma, gas, and water. In particular, long-term gravity monitoring, for decades as done in Membach (Figure 20) and other reference stations (Crossley & Hinderer, 2009; Van Camp et al., 2011), could provide valuable insights on the slow volcanic phenomena. Note that gravity measurements

Table 2
Application of Measurement of Time-Varying Gravity in Volcanology

Context	Phenomena
Magma movements on different timescales (not necessarily accompanied by observable deformation)	Intrusion of magma leading to eruption Rising of a gas slug Fracture opening, intrusion of dike Magma overturn or convection Magma drainage out of a reservoir, magma migration from central conduit to fractures Magma storage Accumulation of magma at depth, increasing pressurization in the volcanic conduit and potential for explosive eruption Gas exsolution Vesiculation (density decrease) and crystallization (density increase)
Volcano-groundwater interactions	Discriminating between the intrusion of magma and water/gas Groundwater dynamics within a volcanic edifice (potential for slope failure, lahar generation, and steam-driven eruptions) Monitoring mass changes without significant vertical deformation
No magma nor hydrothermal fluid movements	Gravitational attraction due to an extruding lava dome (Jousset et al., 2000) Microfracturing rate (Carbone, 2003; Carbone et al., 2009; Greco et al., 2010)
Continuous gravity monitoring enables	Avoiding aliasing from intermittent 4-D gravity campaigns Recovering functioning laws and, therefore, discriminating clearly between models for sources of volcano unrest Investigating short period (minutes to hours) gravity changes (e.g., bubble formation and collapse in Strombolian activity) Development of an accurate surface hydrological model to achieve 1 nm/s^2 (or 0.1 microGal) precision Precise modeling of Earth and ocean tides and atmospheric signals Changes in the mechanical response of the edifice to the tidal forces Providing a precise reference point to anchor microgravity surveys
Integration and correlation with other techniques	Combining with GNSS or InSAR—most powerful combination to separate and interpret change in gravity with expansion, deflation, or stability of volcanoes' surface Correlation with seismic activity and very long and ultralong period seismic signals

should systematically be accompanied by measurements of ground deformation, to correct for free-air gravity effects.

3.1.4. Geothermal and Other Reservoirs

As in hydrogeological systems, gravity offers a method for mapping the redistribution of subsurface masses and assessing geothermal, CO_2, oil, and magma reservoir driving mechanisms (Sugihara & Ishido, 2008).

Time lapse microgravimetry has been successfully applied to monitor natural variations of geothermal fluids in Japan (Nishijima et al., 2016), Yellowstone (Arnet et al., 1997), and Taïwan (Mouyen et al., 2016). Monitoring geothermal reservoirs is important for improving industrial processes, as it allows monitoring the quantity of net mass withdrawal but also, as for volcanoes, to map the redistribution of the subsurface mass (Nordquist et al., 2004). Measuring gravity variations is important to constrain the mass balance within reservoirs and its lifetime, which is difficult to estimate (Ishido et al., 1995; Sugihara & Ishido, 2008). This is also required to mitigate the associated earthquake hazard, which depends on the amount and location of displaced fluid (Deichmann & Giardini, 2009; Holland, 2013; McClure, 2015; Mukuhira et al., 2016).

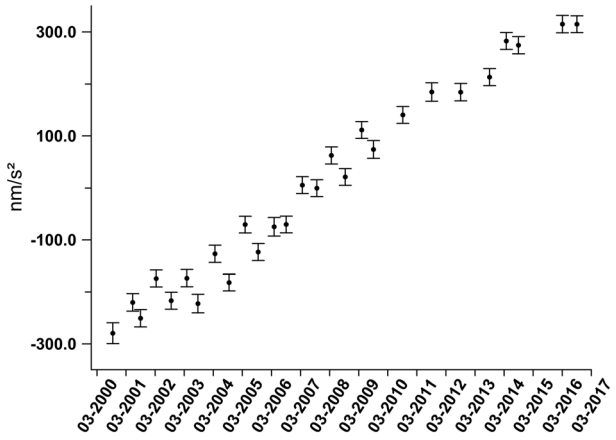

Figure 16. Absolute gravity measurements at the Jülich station, Germany (50.91°N, 6.91°E) (Van Camp et al., 2011). A gravity rate of change of 39 ± 2.5 nm/s^2/yr and a seasonal effect of 30 nm/s^2 are observed.

Gravity was shown to be useful to monitor fluids in oil fields: Brady et al. (2010) performed repeated absolute gravity measurements to monitor the gas-cap water injection under harsh arctic conditions in the Prudhoe Bay oil field. Repeated microgravity surveys are operationally used in the industry; their first use in the context of the geothermal industry was undertaken in New Zealand in 1961. Since then, this has proved to be a powerful tool for monitoring extraction (Hunt, 1995) and reinjection (Hunt & Bowyer, 2007) in a reservoir during exploitation.

Injecting CO_2 into a reservoir decreases the density; hence, gravity may be used to monitor CO_2 storage (Gasperikova & Hoversten, 2008). Monitoring CO_2 sequestration relies on the density contrast between CO_2 and the aquifer fluids. This excludes the applicability of gravity surveys from reservoirs where no significant mass change occurs as CO_2 is absorbed, such as depleted coal beds, displacing the naturally present methane gas (Harpalani & Mitra, 2010; Nooner et al., 2007).

3.1.5. Subsidence

Subsidence is a downward vertical movement of the Earth's surface, which theoretically causes an increase in the gravity of −2 nm/s^2/mm (Bouguer-corrected free-air gradient BCFAG). It can be caused by tectonic activity, sedimentary, water or ice loading, sediment compaction or consolidation, and from places where the fluid is expelled from sediments. Anthropogenic subsidence results in downward motion that can amount several tens of cm/yr, for example, caused by the collapse of underground mine or water, oil and natural gas extraction (Doornhof et al., 2006), or drainage projects, which can induce organic sediment decomposition and compaction. Pressurized fluid induces pore fluid pressure; when fluid is extracted, the pore pressure diminishes, increasing the vertical effective stress acting on the solid matrix. This causes matrix compaction and hence, subsidence, which depends on the compressibility of the rock, faults, local lithology, and the boundary conditions. Subsidence is a complicated, partly irreversible process and is characterized by a great space and temporal variation. Discriminating shallow subsidence from deeper processes is challenging and requires learning about the sources of the subsidence (Jones et al., 2016). For example, it is important to know if subsidence is caused by recent sediment compaction or by lithospheric loading from sea level change, a deposit of sediments, and glacial isostatic adjustment. In addition to its scientific interest, the question is important as it determines the way buildings must be footed. Subsidence may damage roads, bridges, and wells; cause cracking or tilting of buildings or cause serious concerns in low-lying zones such as Shanghai (Dong et al., 2014), Hanoi (Dang et al., 2014), New Orleans (Dixon et al., 2006; Jones et al., 2016), or Venice (Teatini et al., 2011, 2012); and disturbs oil and natural gas extraction fields. Overall damage from subsidence is estimated at the level of several billions of dollars per year (Gambolati & Teatini, 2015).

Better understanding of subsidence processes and geomechanics (elastoplasticity, viscoelastoplasticity, pore volume change, pore pressure change, closing fractures, cavity collapse, and volume units that compact, stretch, and change shape) is paramount for mitigation procedures (Gambolati & Teatini, 2015; Showstack, 2014). Since 2000, we have monitored gravity in Jülich, a zone experiencing man-induced subsidence caused by brown coal mining activity in the Lower Rhine Embayment, Germany (Van Camp et al., 2011). A gravity rate of change of 39 ± 2.5 nm/s^2/yr is observed (Figure 16); using the Bouguer ratio − 2 nm/s^2/mm implies a gravity rate of change of 27.2 nm/s^2/yr, which differs by 12 nm/s^2/yr from the observed trend. The difference could be caused by the compaction causing the subsidence (Bear & Corapcioglu, 1981). By combining gravity and deformation measurements, one could infer valuable information on the compaction processes and fluid migration associated with subsidence. As far as we know, this has never been done.

3.2. Periodic, Pseudoperiodic, and Long-Term Phenomena

3.2.1. Tides

As understood by Newton in 1687, tides result from the action of the Moon, the Sun, and, to a much lesser extent, Venus and Jupiter on the Earth (Hartmann & Wenzel, 1995; Roosbeek, 1996; Wenzel, 1997b). The celestial body gravitational attraction generates global scale vertical ground displacement at semidiurnal and

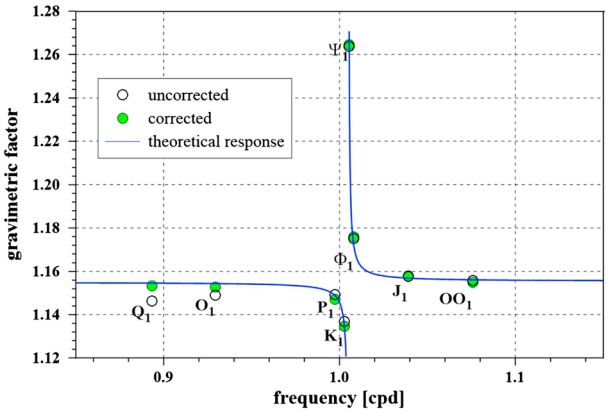

Figure 17. Observed gravimetric factor in the diurnal frequency band at the Membach station, using a time series from June 1998 to July 2016. The smooth curve represents the theoretical response of the nearly diurnal free wobble resonance based on the nonhydrostatic body tide model of (Dehant et al., 1999. White dots represent the gravimetric factor without correcting for ocean loading effect, the green dots after applying the Hamtide model (Taguchi et al., 2014). For details on the data processing see Meurers et al. (2016).

diurnal timescales that can reach 50 cm and gravity signal, 3,300 nm/s^2. Apart from strong transients from magmatic or hydrothermal systems, this is the largest time-variable contribution to gravity. Their magnitude and phase are also affected, to a small extent, by the local and global rheological properties of the Earth. As Earth tide phenomenon can be described with only a few parameters, their knowledge does not provide much information on the rheology of the Earth (Agnew, 2015). Differences in the symmetric structure of the Earth's mantle, as expected from seismology, cause changes in the response of the Earth to tidal forcing, known as the tidal parameters (Métivier & Conrad, 2008; Zürn, 1997), but discriminating between solid Earth models or determining regional effects remains beyond observation possibilities. A resonance in the nearly diurnal frequency band, linked to the free core nutation of the Earth, amplifies the ψ_1 solar tidal wave, which increases the gravimetric factor by 10% at a period of 23.87 h (Figure 17). The net effect is small, given that the amplitude of the wave is only 4 nm/s^2 at midlatitude, 2 orders of magnitude smaller than the largest, lunar diurnal O_1 and semidiurnal M_2 waves that amount about 400 nm/s^2. Retrieving the resonance frequency based on tidal parameters, therefore, remains challenging (Rosat et al., 2017).

Note that 200 to 300 Myr ago, when the Earth was rotating faster by a few hours per day, the resonance was excited by another, stronger tidal wave. This may have led to strong geological effects as a change in geomagnetic field and destabilization of the *D″* region at the core mantle boundary, causing widespread volcanism as Siberian traps and mass extinction (Greff-Lefftz & Legros, 1999).

Historically, tides were measured using tiltmeters (Agnew, 1986). In the 1930s, the achievement of fairly stable spring relative gravimeters made it possible to continuously monitor gravity. Hence, tidal effects were the first time-variable gravity changes to be investigated. Terrestrial measurements of tides with state-of-the-art technology such as superconducting gravimeters allow a precision of 0.1 nm/s^2, outperforming by far space techniques (Zürn, 1997).

The gravimetric factor and phase lag tidal parameters derived from superconducting gravimeter data could be useful to validate or discriminate between different body tide models (Baker & Bos, 2003; Bos & Baker, 2005; Ducarme et al., 2014). However, the quality of ocean models required for correcting the ocean load effects still limits the validation process. It also requires knowing the transfer function of the gravimeter with sufficient accuracy to separate instrumental artifacts (per mille level in amplitude and 0.01 s in phase) from the actual geophysical signal (Baker & Bos, 2003).

Another field of research studies the time variation of the tidal parameters. The superconducting gravimeters allow investigating the variations of the tidal gravimetric factors at the 0.2‰ level corresponding to an amplitude change smaller than 0.1 nm/s^2 in the case of M_2. The causes of these amplitude changes are mainly a modulation due to the insufficient frequency resolution of the limited time series, making it impossible to separate all constituents of the discrete tidal spectrum. A tidal potential is expanded into scalar spherical harmonics of different orders and degrees. As the response of the Earth to ocean loading is degree-dependent, this leads to a modulation effect when common tidal parameters are adjusted for all constituents within a tidal wave group. Other causes of the modulation are possible temporal variation in the ocean loading caused by meteorological forcing or changes in the calibration of the gravimeters (Meurers et al., 2016). For Earth body tide model validation, time series covering a multiple of 1 year periods are required to mitigate the M_2 modulation problem. Intervals equal to or longer than 8 years reduce the modulation effect to 0.1‰. The M_2 gravimetric factor modulation can also be used for detecting and quantifying tiny calibration factor changes below the 1‰ level (Meurers, 2017).

Pole tides are due to the pole motion that is the displacements of the Earth's rotation axis relative to a frame fixed to the Earth. As the centrifugal acceleration depends on the angular distance of a location from the instantaneous rotation axis, the centrifugal acceleration and, hence, gravity will change (Agnew, 2015). The pole motion is dominated by an annual wobble and the Chandler wobble at roughly a 433 day

period (Gross, 2007). As their periods are close together, their addition generates a 6–7 year beat period. The annual wobble is a forced motion only, mainly by the atmosphere, while the Chandler wobble is a resonant oscillation forced by the atmosphere and the oceans (Bizouard et al., 2011; Plag, 1997). The Chandler wobble can be considered as a continuously or, at least, frequently excited, damped harmonic oscillation.

The theoretical pole tide amplitude maximally reaches up to ±50 nm/s^2 at midlatitudes and can be predicted by using the International Earth Rotation Service (IERS) daily pole coordinates. As for the tides, the Earth reacts to the force field by deformation (Wahr, 1985), which can be described by a gravimetric factor applied to the theoretical effect of a rigid Earth. The observed gravimetric factor is influenced by the gravity effect of the ocean pole tide, which is the response of the ocean to the time-variable centrifugal effect (Plag, 1997), taking loading and self-gravitation into account (Chen et al., 2009). Determination of this factor is challenging, as other loading processes, for example, by the atmosphere or hydrology, contribute as well in this period range. SGs provide sufficiently long and appropriate gravity time series due to their temporal stability and low instrumental drift allowing for a retrieval of the gravimetric factor (Loyer et al., 1999). Stacking methods making use of a set of SG time series (Xu et al., 2004; Ziegler et al., 2016) and wavelet filtering (Hu et al., 2007) have been used for that purpose. The gravimetric factor needs to be known at the 2% level for making gravity observations at different epochs comparable at an accuracy level of 1 nm/s^2.

Nowadays, Earth tides are not a hot research topic anymore. This might change if further progress is made in improving the accuracy of ocean load models and instrumentation. Nevertheless, correcting for tidal effects is paramount to investigate elusive gravity changes and can only be done thanks to the great theoretical and instrumental developments achieved during the second part of the twentieth century (see the monograph *Tidal Phenomena* of Wilhelm et al., 1997, which provides a comprehensive overview of the subject).

3.2.2. Earth Free Oscillations

The Earth, as a massive body, is characterized by vibration eigenfrequencies that are excited by earthquakes. The frequencies of the Earth's modes depend on its shape and its profiles of density, shear, and compressibility. The associated standing waves, known as seismic free oscillations or seismic normal modes, induce repeated variations of gravity and were for the first time clearly identified after the great 1960 Chilean earthquake (M_w 9.5). They can be observed after major earthquakes ($M \geq 7.5$); the gravest, spheroidal ${}_0S_2$ mode has a period of 53.9 min. Their study is fundamental to seismology as, from their spectra in the frequency band from 0.3 to 20 mHz, information on the structure of the Earth can be retrieved (Laske & Widmer-Schnidrig, 2015; Park et al., 2005; Woodhouse & Deuss, 2015). The study of free oscillations, or terrestrial spectroscopy, is not much limited by the uneven distribution of seismometers and earthquakes. Modes are largely unaffected by local structure, so that they sample long-wavelength phenomena, not accessible to body waves, hence allowing retrieving the mean rheological parameters. For example, the modes indicate a weak stratification of the outer core (Masters, 1979) and provide the best evidence that the inner core is solid (Dziewonski, 1971), and of its—still discussed—anisotropy (Makinen & Deuss, 2013; Romanowicz & Bréger, 2000; Romanowicz et al., 2016; Souriau & Calvet, 2015). Modes are one of the bases of the spherically symmetric nonrotating Preliminary Reference Earth Model (PREM) model (Dziewonski & Anderson, 1981), are used to retrieve focal mechanism and to compute magnitude of large earthquakes (Okal, 1996; Stein & Okal, 2005), and provide a method to compute seismograms by summing them (Aki & Richards, 2002; Woodhouse & Deuss, 2015).

In the 1960s, there was no instrument sensitive and stable enough to allow a comprehensive investigation of the free oscillation's spectrum. In the late 1970s, it was proposed to use gravimeters through the International Deployment of Accelerometers (IDA, after Cecil and Ida Green, benefactors of the Earth sciences) network, based on about 20 LaCoste spring gravimeters (Agnew et al., 1976, 1986). The gravimeters, relatively small and low noise, were a way to provide well-calibrated, low-drift (compared to seismometers) measurements at a reasonable cost. Note that in the free oscillation frequency band, gravimeters mainly monitor inertial acceleration associated with the ground movement; this differs from the usual application of gravimeters at longer periods, where the Newtonian effects dominate. IDA provided precise frequency and attenuation measurements and valuable information on seismic source studies. However, gravimeters are not appropriate to monitor toroidal oscillations, associated with rotational horizontal displacement; those are measured using long-period seismometers, as the STS-1 deployed in the Global Seismic Network (GSN)(Bent, 2013), STS-2, or strainmeters and tiltmeters (Zürn et al., 2000).

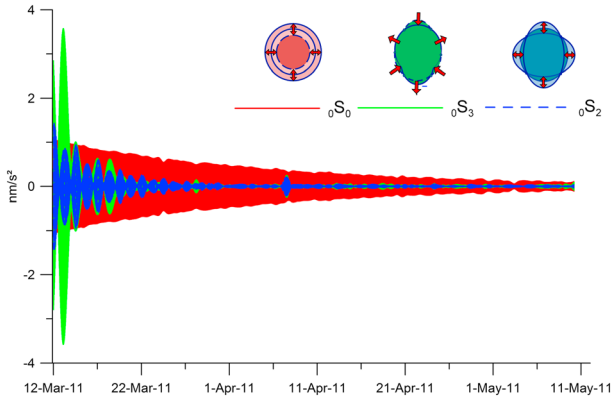

Figure 18. Filtered time series from the SG C021 at the Membach station, Belgium (50.61°N, 6.01°E), after the March 2011, M = 9.1 Tohoku megathrust earthquake. The data are corrected for tidal and atmospheric pressure effects. Band-pass filtered time series to isolate the $_0S_0$ (red, period ~54 min), $_0S_2$ (blue, period ~20 min), and $_0S_3$ (green, period ~35 min) normal modes. The modulation of $_0S_2$ and $_0S_3$ is due to the beating between the five and seven different multiplets of $_0S_2$ and $_0S_3$, respectively. This "Zeeman" splitting is due to the Earth's small departure from spherical symmetry, that is, the Earth's diurnal rotation, ellipticity, and 3-D structure. The attenuation quality factor of the long-period fundamental modes is high, such that the oscillations of, for example, $_0S_0$, $_0S_2$, or $_0S_3$ can still be observed in the time series 2 weeks after the event. After 2 weeks, $_0S_0$ dominates the series for more than 2 months.

Early in the 2000s, the new generation of superconducting gravimeters achieved lower noise levels than the other sensors for frequencies lower than 0.8 mHz (Rosat, 2005; Rosat & Hinderer, 2011; Van Camp, 1999; Widmer-Schnidrig, 2003; Zürn et al., 2000). Hence, using superconducting gravimeters, Rosat (2003) reported on the first observation of the overtone $_2S_1$, a translation of the core in the mantle that, as the other modes at frequencies lower than 0.8 mHz, provides valuable information on the 3-D density structure in the Earth's mantle and core. The stability of SGs makes them also valuable to investigate the lateral density structure and the attenuation factor of the modes (Figure 18).

Some free oscillations, termed as Earth's hum, have frequencies such that they are excited permanently; they were first discovered by Nawa et al. (1998) using a superconducting gravimeter in Antarctica. The excitation of the hum is still a hot topic of study, but the probable mechanisms are pressure on the Earth's surface by the atmosphere and infragravity waves in the shallow and deep ocean (Laske & Widmer-Schnidrig, 2015; Nishida, 2013; Webb, 2007). Even if the excitation mechanism remains uncertain, the hum can be used to infer 3-D upper mantle structure and can be considered as a part of the new field of ambient noise tomography (Laske & Widmer-Schnidrig, 2015; Nishida, 2013; Shapiro, 2005).

In the subseismic frequency band, that is, periods longer than 53.9 min, other elusive modes have been investigated using superconducting gravimeters: the Slichter mode $_1S_1$ and inertial gravity oscillations in the Earth's core. Unlike the classical seismic modes, of which the restoring force is elastic and described by the shear and compressibility moduli, the main restoring force of the core undertones is the much weaker Archimedean force, which results in lower periods. The Slichter mode $_1S_1$ would be a translational oscillation of the inner core about its equilibrium position; its period is expected between 4 and 6 h. This mode is controlled by the density jump between the solid inner and fluid outer cores, and the buoyancy force produced by the outer core. Several authors claimed the detection of this mode, but no detection using state-of-the-art instruments has been reported so far. Known attempts remained unsuccessful (Rosat et al., 2003, 2006), even after the great 2004 Sumatra-Andaman earthquake (Ding & Shen, 2013). Note that Rosat (2007) showed that a vertical deep-slip M_w 9.7 event should be required to excite the Slichter mode up to a detectable level. However, studies are still ongoing to analyze the possibility of searching for the Slichter modes in superconducting gravimeter records (Shen & Luan, 2015).

Melchior and Ducarme (1986) reported on the detection of gravity oscillations in the Earth's core in the times series of the superconducting gravimeter at Brussels. The reported period was 13.9 h. The restoring forces of this oscillation are Coriolis (inertial), Archimedes (buoyancy), and Lorentz (Alvén), hence the name MAC (Magnetic, Archimedes, Coriolis) waves (Gubbins & Herrero-Bervera, 2007). Observations of the MAC oscillations would provide valuable information on the stratification of the outer core (Vidal & Schaeffer, 2015). This mode could never be confirmed ever since (Zürn et al., 1987). The spectral peaks reported by Melchior and Ducarme (1986) were probably caused by instrumental artifacts. Let us just recall that, at that time, recordings of this prototype instrument, installed in an urban area on sediments, were still performed through chart recorders.

In the subseismic frequency band, there are also modes related to the geometry of the Earth: the aforementioned nearly diurnal free wobble and also the Chandler wobble (Wahr, 1985). As described in the last section, research is ongoing to determine the gravimetric factor of the pole tide; meanwhile, one uses the precise astronomical observations to correct the gravity time series from the polar motion effect.

Superconducting gravimeters are appropriate instruments to monitor the seismic free oscillations, and, in our opinion, their use is one of the best successes of the Global Geodynamics Project GGP, the network of superconducting gravimeters established in 1997 (Crossley & Hinderer, 2009), which became in 2015 the International Geodynamics and Earth Tide Service (IGETS) and collects the data from two dozen stations.

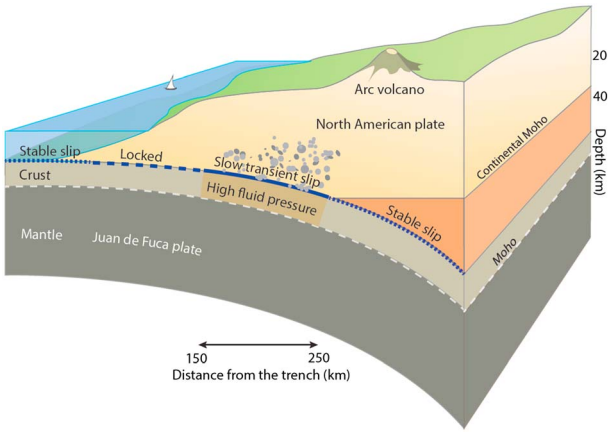

Figure 19. Schematic cross section of the Cascadia subduction zone as reported by Audet et al. (2009, 2010). The various slip modes believed to occur along the plate interface are given by the dashed, dotted, and continuous blue lines, and the corresponding observed phenomena indicative of each are listed above. The zone of high fluid pressure is inferred from seismic images and corresponds to the E zone, the top of which has been inferred recently to be the plate interface where aseismic slow slip occurs. Tremor source location estimates concentrate at and above the interface (gray dots), albeit with large uncertainties.

3.2.3. Episodic Aseismic Slip at Plate Boundaries

For the last 15 years, long-term GNSS positioning surveys have revealed the existence of slow slip events (SSE), corresponding to a fast trenchward relaxation motion. The SSE, also known as silent earthquakes, are associated with tremors and observed at many subduction zones, for example, Japan (Obara, 2002), Cascadia (Rogers, 2003), Central America (Jiang et al., 2012; Radiguet et al., 2016), South America (Vallée et al., 2013), or New Zealand (Beavan et al., 2007; Wallace et al., 2016) (Figure 19). The SSEs are somewhat similar to earthquakes, but their slow motions result in a different and not fully understood physics, with different scaling laws (Ide et al., 2007). The SSEs take place at about 30–40 km depths and can release a seismic moment equivalent to a magnitude 6–7 earthquake. In different regions, a striking characteristic is that SSE and tremors appear regularly, with periods from several months to a couple of years, with a characteristic duration of weeks. The episodic tremors and slips (ETS) are widely assumed to dissipate strain energy accumulating from ongoing convergence along the deeper region of the plate interface (Schwartz, 2015). It remains difficult to locate with precision the mass changes associated with the SSE events, as well as to investigate the possible release and migration of fluids suggested by Boyarko and Brudzinski (2010) and Dragert et al. (2004). Progress is ongoing in developing and applying geodetic techniques to detect the aseismic slip events.

Gravity observations could provide a better picture of the ETS zone, which remains fuzzy, because of difficulties in tremor detection and location (Ghosh et al., 2009). Monitoring the flow of water toward the surface would provide information on the permeability of the subduction interface as well as the overlying hanging wall. Being able to monitor dehydration processes of the ocean crust plunging into the mantle is paramount for the understanding of arc volcanism and the seismic cycle in the subduction zones experiencing megathrust earthquakes.

The slow events have anomalously large characteristic durations. Hence, they are enriched in low frequency relative to other classical events of comparable magnitude and may be prone at exciting Earth's free oscillations (Beroza & Jordan, 1990). The stability and sensitivity of superconducting gravimeters could contribute to the study of the slow and silent earthquakes, but no result has ever been published.

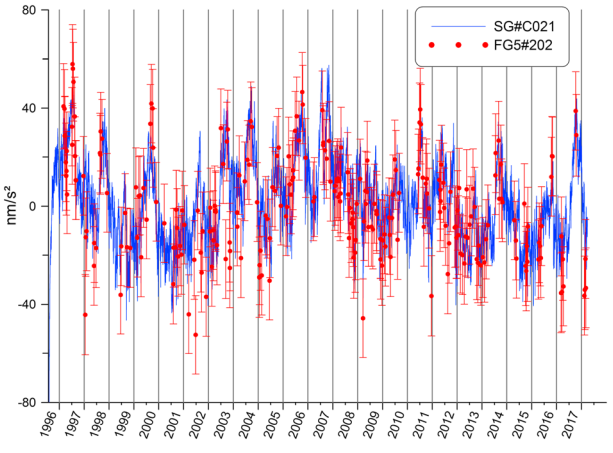

Figure 20. Gravity residuals from the superconducting GWR#C021 and absolute FG5#202 gravimeters at the Membach station, Belgium. Usually, gravity is lower during the winter because water accumulates in the unsaturated zone above the underground gravity station (Van Camp et al., 2006). The origin of the multiannual variation, about 70 nm/s^2 peak to peak, remains unknown. The instrumental drift of the SG was corrected by using the AG measurements.

3.2.4. Long-Term Gravity Changes

The viscoelastic glacial isostatic adjustment, present elastic loading changes as caused by ice melt, water withdrawal, climate change, and tectonic deformations all can induce long-term variations in gravity that may consist in a trend or in oscillating phenomena of which the periods range from a few weeks to years (Figure 20). Relative and absolute terrestrial gravity measurements are appropriate to measure those long-term gravity changes, which might reflect either vertical ground motion or mass redistribution.

Gravimeters have been used to monitor glacial isostatic adjustment (Lambert et al., 2006; Mäkinen et al., 2005; Mazzotti et al., 2011; Sato et al., 2012; Steffen et al., 2009), slow vertical ground displacements (Djamour et al., 2010; Mazzotti et al., 2007; Van Camp et al., 2011; Zerbini et al., 2007), crustal tectonics (Mouyen et al., 2014), or mass redistribution by erosion (Mouyen et al., 2013). Terrestrial measurements have also been used to study slow, climate-driven oscillations in gravity (Jiang et al., 2011; Lambert, Henton, et al., 2013; Lambert, Huang, et al., 2013; Van Camp et al., 2010, 2011).

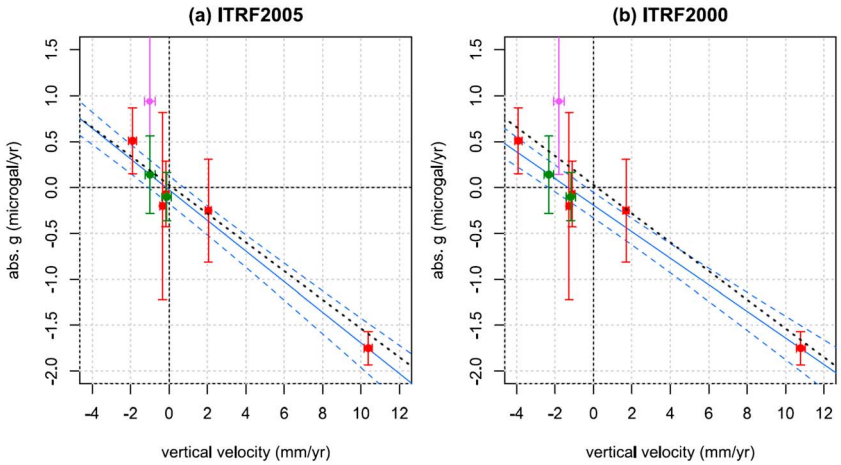

Figure 21. Absolute gravity (1 μGal = 10 nm/s^2) versus GPS uplift rates in Canada and the northern U.S. GPS vertical velocities aligned to (a) International Terrestrial Reference Frame ITRF2005 and (b) ITRF2000. Red and green symbols show absolute gravity and GPS uplift rates with 95% confidence intervals at collocated and interpolated sites, respectively. From left to right, gravity stations are Iowa City, Wausau, Priddis, Pinawa, Int. Falls, Flin Flon, and Churchill. The Saskatoon station is shown by the purple symbol and is not used in the fit, given the shortness of the time series (8 years instead of 13–15 years elsewhere and the strong hydrogeological effects). Blue solid and dashed lines show best fit linear regression and its 95% confidence interval, respectively. Black dashed line shows model-predicted, center-of-mass-aligned, linear relation based on rates predicted by the Multi-Dome-1/VM2 glacial isostatic adjustment model. From Mazzotti et al. (2011).

The GNSS technique is quite appropriate for measuring relative deformations, but estimating absolute deformation (i.e., not with respect to another station allegedly fixed but with respect to a stable reference) requires a much better mastery of the vertical reference frame than is presently achieved. It remains challenging, using relative measurements, to determine if northern Europe is moving vertically as a whole or not, at least at the millimeter precision level; such a precision is required when dealing with sea level changes (Wöppelmann & Marcos, 2016). In addition, from the metrological point of view, it would be dangerous to rely on measurement from only one technique to determine the vertical motion, even more so if the vertical component is the well-known weakness point of the technique. Indeed, repeated absolute gravity measurements allowed the determination of a bias in the GNSS velocities at the mm/yr level when expressed in the ITRF2000 reference frame (Mazzotti et al., 2007, 2011; Teferle et al., 2006) (Figure 21).

Though the gravity has the capacity to detect and separate a trend from other techniques, separating the different geophysical contributions from a trend is challenging and can only be achieved by either subtracting known contribution or by modeling of better known contributions.

3.2.4.1. Glacial Isostatic Adjustment

Glacial isostatic adjustment (GIA) refers to the crustal deformation induced by the present and past change in the ice load at the Earth surface (Steffen & Wu, 2011; Wake et al., 2016). For example, Fennoscandia rebounded by up to 300 m after the end of the last glaciation (Steffen & Wu, 2011). Because the crust is partly elastic, it reacts instantaneously to changes in the ice masses, but as the underlying mantle is viscoelastic, part of the adjustment takes time so that Fennoscandia and northeastern Canada are still uplifting at rates up to about 1 cm/yr. Assessing ice mass balance using altimeters is biased because they cannot discriminate between ice and snow, and because they cannot distinguish between the signal from present-day deformation of the Earth and the delayed viscoelastic effects from past glaciation. Hence, investigating the GIA is necessary for studies of past and present ice mass balance (Ivins et al., 2013; Mémin et al., 2011; Omang & Kierulf, 2011). It also provides insights on the rheology of the Earth (Mazzotti et al., 2011; Nielsen et al., 2014; Sato et al., 2012; Wahr et al., 2001).

Wahr et al. (1995) demonstrated that by measuring gravity and vertical deformation, one can discriminate between the past, viscoelastic, and present elastic effects of ice loading by computing the ratio $\dot{g}/\dot{z}$, which is expected to range -1.0 to -2.6 nm/s^2/mm (De Linage et al., 2007; Teferle et al., 2009; Wahr et al., 1995). This ratio depends on the position of the load, the wavelength, the rheology, and the history of the deformed layers.

It also depends on whether there is elastic response due to past and contemporary ice changes, earthquakes or other tectonic processes (Mazzotti et al., 2007), and nontidal sea level variations, such as the Baltic sea level decrease due to the Fennoscandian postglacial uplift (Olsson et al., 2009). Unfortunately, the precision of the measured ratios $\dot{g}/\dot{z}$ (e.g., as reported by van Dam et al., 2017; Mazzotti et al., 2007; Ophaug et al., 2016; and Sato et al., 2012) yet does not allow discrimination between different models. Extending the times series and better modeling the hydrogeological effects on gravity measurements are key to achieve this goal. This would improve our knowledge on the viscosity in the mantle and on the thickness and extension of the past ice cap.

3.2.4.2. Preseismic, Coseismic, and Early Postseismic Effects

During an earthquake, abrupt frictional sliding along a part of the fault zone causes coseismic deformations and mass displacements. After the main shock, postseismic deformations occur, resulting from different phenomena (Marone et al., 1991; Smith & Wyss, 1968). First, an immediate after-slip can be observed, due to aseismic slip or coseismic slip associated with the aftershocks. It decreases quickly, within weeks or months after the earthquake. Second, deformation is dominated by poroelasticity effects such as dilatation and compression associated with faulting disturbance of pore fluid pressure, causing the fluid to diffuse from compressed regions to dilated ones (Jónsson et al., 2003; Nur & Booker, 1972) and possibly triggering earthquakes (Masterlark & Wang, 2000). Third, as the mantle is viscoelastic, it cannot accommodate the stress induced by the coseismic deformation and must relax. This viscoelastic motion flows for decades, in response to major earthquakes, until a new state of equilibrium is reached and the fault relocks (Bedford et al., 2016; Remy et al., 2016). The associated deformation is called postseismic relaxation (Azúa et al., 2002; Barbot & Fialko, 2010; Perfettini & Avouac, 2004; Pollitz, 1997, 2001).

A gravimeter placed on the Earth surface records variations in the gravity associated with the postseismic relaxation. These variations are due to the vertical deformation of the Earth surface and of the internal boundaries separating layers at depth with different densities. Once the deformation part is determined from GNSS measurements of the surface deformation, gravity data provide direct information on mass redistributions at depth and place new constraints on the viscosity structure. For example, if only small gravity changes are observed, a suite of low-viscosity models would be ruled out, because the predicted variation of the Newtonian term decreases with increasing viscosity of the mantle. In addition, these direct gravity measurements are also particularly sensitive to the effects of lateral variations in the rheological parameters of the mantle, of which the wavelengths are smaller than the present resolution of satellites. Ergintav et al. (2007) used repeated GNSS and gravity measurements to investigate 3-D postseismic deformation for the 1999, $M = 7.4$ Izmit earthquake in Turkey, but the interpretation of the gravity campaigns is limited by the precision (about 50 nm/s^2) of the measurements and the hydrogeological effects.

Using three superconducting gravimeters located at epicentral distances of 3.4°, 6.9°, and 9.4° from the 2003 $M_w = 8.0$ Tokachi-Oki earthquake, Imanishi (2004) observed gravity changes at the few nm/s^2 level and demonstrated the ability of gravity measurements to infer information on the nature of dislocations in the earthquake source region. Transient gravity changes have also been observed at the onset of a major earthquake, as reported by Montagner et al. (2016) who investigated time series after the 2011 Tohoku-Oki $M_w = 9.0$ earthquake, using a superconducting gravimeter located 510 km away from the epicenter. The authors observed a transient signal of a few nm/s^2, before the arrival of seismic waves. It is suggested that a network of sensitive gravimeters could reduce the time required to release a warning and enable faster earthquake magnitude estimation.

Preseismic gravity changes have been reported in Tibet by Chen et al. (2016), which they interpret as related to interseismic mass change around the locked plate interface under the Himalayan-Tibetan Plateau, but Van Camp, de Viron, and Avouac (2016) demonstrated that the reported effects can be explained by instrumental artifacts and hydrogeological effects. Hui et al. (2011), Shen et al. (2011), and Zhan et al. (2011) also reported on gravity precursors in China. However, these studies are essentially based on repeated relative surveys, of which the results must be analyzed in light of hydrological effects and mainly instrumental artifacts, especially as the measurements were performed on long profiles in strong topography. Hence, given the correlation with the topography of Tibet, Xinjiang, and eastern plains observed in Hui et al. (2011) and Zhan et al. (2011), this supports the hypothesis that calibration errors and/or malfunctioning seals play a significant role. Another puzzling point is that for the same campaigns, Hui et al. (2011) and Zhan et al. (2011) report significantly different gravity changes.

On the other hand, repeated gravity measurements provide upper limits on the elusive vertical land motion in slowly deforming, intraplate areas (Camelbeeck et al., 2007; Van Camp et al., 2011) or at plate boundary zones (Mazzotti et al., 2007; Mouyen et al., 2014).

3.2.4.3. Postseismic Relaxation in Subduction Zones

Megathrust earthquakes generate huge coseismic stress changes affecting a volume, with dimensions of ~1,000 km both laterally and vertically and, thus, trigger the largest postseismic deformations. Little is known about the viscosity of the shallowest upper mantle layers: models predict viscosity ranging between 10^{19} and 10^{22} Pa s. These values are known through the investigations of the postglacial isostatic adjustment, laboratory experiments, and a few postseismic relaxation observations. In subduction zones, the problem is even more complicated than at other plate boundaries because the viscoelastic processes are controlled by the 3-D geometry of the subduction (Hu et al., 2016; Pollitz et al., 2008; Suito & Freymueller, 2009; Thatcher & Pollitz, 2008). For example, near Sumatra, the subducting Indo-Australian slab can act as a strong boundary to the viscous mantle flow (Pollitz et al., 2008). In South America, the viscosity is supposed to increase by over 2 orders of magnitude from the arc toward the hinterland, which influences the postseismic responses over a distance of a few hundreds of kilometers from the trench (Li et al., 2017). A deeper understanding of the viscoelastic processes through new measurements is essential to obtain information on the rheology of the Earth's mantle and the stress evolution in the crust and to learn about subduction processes.

Assessing the viscosity of the most shallow upper mantle layers in subduction zones and investigating if postseismic viscoelastic processes are able to cause failures of neighboring megathrust faults or not has been addressed by measuring the surface displacements caused by the postseismic relaxation, using GNSS, and gravity change, using GRACE (Broerse et al., 2015; Han, 2006; Panet et al., 2010). GRACE has provided information on coseismic and postseismic effects but at a resolution which remains poor compared to the expected spatial variations of viscoelastic effects (Hu et al., 2014). Moreover, GRACE could not monitor the effect of earthquakes of magnitude lower than 8 (Han et al., 2016; de Viron et al., 2008). The last point worth investigating is the study of Mantle's water mass poroelastic diffusion, which is discussed by Ogawa and Heki (2007) but has never been confirmed since. However, subduction models still lack direct information on 3-D mass movements at depth, at scales ranging tens to thousands of kilometers. Repeated or continuous gravity measurements can contribute to gaining insights on the 3-D viscosity structure after large earthquakes and the related seismic cycle. Repeating well-positioned absolute gravity measurements can further probe the physical parameters of the mantle surrounding a subduction megathrust fault (Mazzotti et al., 2007). Measuring the ratio between deformations and gravity rates of change could also provide information on inelastic deformation and fluid transfers during the seismic cycle (Fulton & Brodsky, 2016).

The Sunda megathrust zone in Sumatra would be a very interesting case study as, unlike most seismically active subduction zones, the presence of islands close to the trench and above the seismogenic portions of the Sunda megathrust makes it possible to use geodetic monitoring and paleogeodetic (e.g., corals; Meltzner et al., 2006) studies to constrain seismic, postseismic, and interseismic deformations. In particular, coral data provide reliable information on vertical land movements and the unique possibility to constrain viscoelastic mass movements precisely. Another advantage is the absence of glacial isostatic adjustment, which complicates the study of the still ongoing postseismic response to the great 1964 Alaska earthquake.

To mitigate the disastrous effects of megathrust earthquakes, it is important to understand the preseismic, coseismic, and postseismic processes. Numerical inversion methods are promising to model the megathrust cycle, but they lack high-quality physical parameters. Gravity measurements would sharpen estimates of the viscosity in the upper mantle in the region surrounding the rupture zone. Depending on the chosen viscosity, models predict postseismic gravity rates of change ranging between 5 and 100 nm/s^2/yr. Such rates of change can be perfectly monitored by repeated AG measurements.

Together with free oscillations, tides, and glacial isostatic adjustment, measuring viscoelastic processes in subduction zones provides the transfer function of the Earth at various timescales related to the elastic and viscoelastic properties of our planet.

3.3. Metrology and Fundamental Physics

A last but not least important point is the contribution of gravimetry in metrology and physics. On the one hand, well-calibrated gravimeters provide traceable seismic and geodetic measurements. On the other

hand, moving away from geosciences, absolute gravity measurements are to play a key role in the new definition of the kilogram and research in fundamental physics.

3.3.1. Metrology

Gravimetry forms a relationship between metrology and geodesy because gravity is one of the techniques necessary to determine the geoid, which is the standard reference surface for altitude in the World Geodetic System (WGS). Major earthquakes modify the geoid height by moving layers of different densities and by changing the density of rocks. For example, the great 2004 Sumatra-Andaman earthquake modified the geoid height by about 1 cm in the vicinity of the rupture zone (Broerse et al., 2011; Fuchs et al., 2013; Ogawa & Heki, 2007). The glacial isostatic adjustment also modifies geoid at rates up to 1 mm/yr in Greenland, Antarctica, and Fennoscandia (Fleming et al., 2004; Vermeersen & Schotman, 2008; Wu et al., 2010). This can be monitored locally by terrestrial gravity measurements and globally using satellite observations.

In metrology, gravity is also a key to the new realization of the kilogram with the Kibble balance experiment, weighing electrical and mechanical powers (Stock, 2013) (formerly known as the Watt balance, the Kibble balance was conceived by Bryan Kibble in 1975 (Kibble, 1976) and was renamed after his death in 2016). Hence, gravity is expected to play a key role in the redefinition of the SI base unit (Fischer & Ullrich, 2016; Van Camp & de Viron, 2016). For that purpose, gravity must be known, hence measured, at the 10^{-8} level in laboratories housing a Kibble balance (Merlet et al., 2008). Used as standards, absolute gravimeters must participate regularly in intercomparison campaigns to look for possible biases (Francis et al., 2015; Jiang et al., 2011; Pálinkáš et al., 2017; Vitushkin et al., 2002).

The last point, rarely discussed in seismology, is the traceability and calibration of the measurements. After the 2004 Sumatra-Andaman earthquake, it was found that the Global Seismic Network and the Federation of Digital Seismographic Networks (FDSN) exhibited a scatter of 5–10% in the calibration factors (Park et al., 2005). Davis and Berger (2007) proposed to use predicted tidal signals to calibrate the GSN at the 1% level, but, in our opinion, this method does not meet the metrological standards nor the traceability that one expects from measuring instruments. The superconducting gravimeters, being calibrated at the 0.1% level in order to assess tidal models (see section 3.2.1), could be used to verify the magnitude of large earthquakes.

3.3.2. Gravitational Wave Detectors

The recent detection of gravitational waves produced by a binary black hole system (Abbott et al., 2016) opens the field of gravitational wave astronomy. This was achieved in the 35–250 Hz frequency band and required insulation of gravitational wave detectors by using active seismic isolations devices. However, down to 30 Hz, another challenging task consists in eliminating the Newtonian noise that is predicted to influence the second-generation gravitational waves detectors (Coughlin et al., 2016). This noise refers to the gravitational effects of terrestrial density variations in the vicinity of the detectors. These fluctuations are caused by the ground displacement associated with seismic surface waves and also by moving air and water masses (Harms & Venkateswara, 2016). Investigating gravitational waves at frequencies lower than 30 Hz will open new paths in astrophysics, related to merging galaxies, neutron stars coalescence, the speculative mass of gravitons, supernovae, or cosmic expansion (Blair et al., 2015; Castelvecchi, 2016). We believe that the research performed by geodesists to understand the influence of the atmosphere and hydrosphere on gravity measurements will benefit from the developments of new gravitational wave detectors, and conversely.

3.3.3. Fundamental Physics

Gravimeters provide a tool to measure the Newtonian constant of gravity *G*. This could be achieved by measuring the perturbation due to a well-known mass to the acceleration of the free-falling object of an absolute gravimeter (Schwarz et al., 1998). Free-fall experiments using two different materials were also performed to look for a violation of the equivalence principle and, consequently, attempt to reveal a fifth force (Niebauer et al., 1987); this speculative fundamental force may be as weak as the gravitational one.

For completeness, let us mention that tides influence the alignment and, hence, the measurements of particle accelerators (Boerez et al., 2012; Xu et al., 2013), but this must be additionally monitored using strainmeters and tiltmeters, as deformations and tilts are of concern rather than gravity changes.

4. Meeting the Next Challenges of Terrestrial Gravimetry

Among the challenges of present and future geophysics, improving our integrated understanding of the processes active in the Earth interior and of the water cycle is required to enhance our ability to answer important societal issues, such as risk mitigation and water availability. The precision of present terrestrial gravity measurements makes it a key technique to gather information on mass transport within the Earth system. Considering the technique accuracy, abilities, and limitations, investigation through terrestrial gravimetry of hydrogeological, volcanic, and hydrothermal systems can bring new pieces of information, which are required to develop a comprehensive understanding of those structures and the associated physical and chemical phenomena. A better knowledge of the ratio between gravity changes and vertical displacement is also expected, as it provides a key value to understand viscoelastic and elastic processes related to glacial isostatic adjustment and postseismic relaxation, especially in subduction zones.

We live on a dynamic planet, which requires long-term continuous quantification of its changes. Enhancing our understanding of the dynamic Earth system by quantifying our planet's changes in space and time allows for better decision making at all levels. This is the raison d'être of the Global Geodetic Observing System (GGOS) (Plag & Pearlman, 2009).

Most of the geophysical phenomena are associated with mass transport and affect to some extent the ground gravity measurements. Nevertheless, a phenomenon is worth to be studied by gravimetry only under these three conditions:

1. The gravimetric signature is above the instrumental noise level.
2. The signature can be separated from the ones of other phenomena.
3. The local information obtained through gravimetry is useful for the understanding of the phenomena.

In the future, those conditions will still hold. Nevertheless, evolutions of the instruments can broaden the range of phenomena that can be studied and the relevance of the information brought by gravimetry.

The precision and accuracy of the state-of-the-art instruments are not a limitation anymore. On the other hand, those instruments are heavy, expensive, and operator demanding. They also depend on main power supply. Those characteristics make it difficult to densify the observation network with more instruments and/or more measurements. They also limit the usability of the best instrument in harsh conditions, such as volcanoes, or remote areas, such as Antarctica. Lighter, more precise and less power-demanding future instruments will open new horizons for developing new observational systems, such as drone-borne gravimeters, that could fill the gap between terrestrial and satellite-based gravity. Cheaper gravimeters could be deployed in dense arrays at selected sites, to address well-posed phenomena, improving the source separability and diminishing the local impedimenta. Deploying a network of instruments can be achieved to some extent by pooling the resources, as presently achieved in the U.S. by the University NAVSTAR Consortium that facilitates geoscience research and education using geodetic tools as GNSS, borehole strainmeters and seismometers, airborne mapping, InSAR, and terrestrial laser scanning (Herring et al., 2016).

Ground gravity has to be considered as a part of a multi-instrument observation network, where the combination of information with different transfer functions improve the separability of the signals and to which gravity can bring, even with a local information, the missing piece of the puzzle. For example, Steffen et al. (2012) provided detailed sensitivity maps and highlighted areas that need more absolute gravity measurements to further improve the modeling of different ice processes, lithospheric thickness, background viscosity, and lateral mantle viscosity variations. Similarly, making sensitivity maps should be done in rifting and subduction zones where, for example, the presence of volcanoes and postseismic motion must be taken into account. In hydrogeology, it must be supported by geological and pedological investigations. Depending on local environmental conditions, external data from piezometers, soil moisture measurements, dye tracing, electrical resistivity or self-potential surveys, meteorological data, or remote-sensing techniques are also strongly recommended. In volcanology, ground deformation and seismic and geochemical studies complete this list. The combination of different instruments also requires developing statistical and processing techniques, to elucidate cause-effect relationships between the multiple time series, taking into account that correlation does not imply causation (Sugihara et al., 2012).

The best days of geophysics and, in particular, time-varying gravimetry are still ahead! New, less expensive, and easier to implement techniques will make it possible to deploy arrays of gravimeters to monitor systems that need comprehensive investigations to understand their functioning, such as volcanoes, specific hydrogeological and hydrothermal systems, or postseismic and postglacial relaxation.

Glossary

Absolute gravimeter (AG): instrument measuring the value of the gravity, ranging 9.78 m/s^2 at the equator to 9.83 m/s^2 at the poles. Absolute gravimeters—as opposed to relative gravimeters, which only measure the difference in the gravity value—can be ballistic or based on a pendulum.

Accuracy: absolute difference between the measured value and the true value.

Aliasing: distortion of the signal due to undersampling, resulting in a change of frequency, where periods shorter than two sampling periods appear as being longer. When a signal is decimated, low-pass filtering prior to decimation limits aliasing.

Atom absolute gravimeter: ballistic gravimeter using laser-cooled rubidium atoms used as test mass (Debs et al., 2013).

Ballistic absolute gravimeter: instrument measuring the gravity through the monitoring of the free fall of a test mass.

Bouguer-corrected free air gradient: see free air gradient.

Capacitive sensor: a device used as a precise and linear displacement transducer, as the capacitance is inversely proportional to the distance between two conducting plates.

Cold atom gravimeter: see atom gravimeter.

Cryogenic gravimeter: see superconducting gravimeter.

Drift (instrumental): apparent continuous time gravity change due to instrumental artifacts affecting spring or superconducting relative gravimeters.

Exsolution (or vesiculation): the process of bubble formation in magma.

Free-air gradient: correction to observed gravity values to account for variation of gravity with altitude, typically −3,086 nm/s^2/m. If the movement of the gravimeter is due to ground deformation, one must account for displaced masses; the correction is known, in this case, as the Bouguer-free air corrected gradient and amounts −2,000 nm/s^2/m.

Free-fall absolute gravimeter: ballistic absolute gravimeter.

Gas slug: a conglomerate of high-pressure gas bubbles.

Generalized Gauss-Markov (GGM) noise: similar to the first-order Gauss Markov process, but the power law can take any spectral index.

GNSS: Global Navigation Satellite System (such as the Global Positioning System GPS, Glonass, or Galileo).

Gravimetric factor: see tidal parameters.

Interferometer: an optical device used to precisely measure distances based on the interference between two light waves.

Karst: landscape formed from the dissolution of soluble rocks such as limestone, dolomite, and gypsum; it is characterized by caves, sinkholes, and efficient underground drainage.

Gal: the Gal (symbol Gal) is a centimeter-gram-second (CGS) unit of acceleration; 1 Gal = 1 cm/s^2.

Microseism: background noise during periods of earthquake quiescence. It consists in persistent vibrations of the ground, with the dominant period between 2 s and 40 s. They are mainly caused by oceanic waves, anthropogenic activity, atmosphere, and hydrothermal and volcanic systems.

Mush: slushy material that is part magma and part solid crystal.

Pendulum absolute gravimeter:gravimeter where the observable is the period of a pendulum.

Piezometer: device measuring the hydraulic head within an aquifer, usually measured as a liquid surface elevation.

Power spectral density (PSD): distribution of power of a signal into frequency components composing that signal.

Precision: stability of the measurements, that is, deviation of the individual measurements with respect to the average value.

Relative gravimeter: instrument that measures the changes in the gravity in space and time.

Sill: horizontal sheet intrusion between older layers of sedimentary

Spring gravimeter: relative gravimeter, where a proof mass is suspended by a spring.

Superconducting gravimeters (SG): relative gravimeter, where the proof mass is a superconducting sphere levitating in a magnetic field, and the measurement is the current required to keep it levitating at a constant position.

Tare: undesirable element in gravity time series; it consists of a gap, a step, or a spike.

Tidal parameters: gravimetric (or amplitude) factor δ and phase κ of the response of the Earth to the tidal forces.

Trend: (here) actual geophysical rate of change.

Trilateration: the process of determining a position by measuring distances.

Uncertainty: this parameter characterizes the dispersion of the value that could reasonably be attributed to the quantity subject to measurement. Uncertainty comprises, in general, many components, as an experimental standard deviation and systematic effects. The other components are evaluated from assumed probability distributions based on experience or other information (Joint Committee for Guides in Metrology, 2012). See also Accuracy and Precision.

Vertical gravity gradient: variation of gravity along the vertical line (dg/dz).

Yield (specific): volume of water per unit volume of an aquifer that can be extracted by gravity drainage.

Appendix A: Data Processing, Field Techniques, and Sources of Noise

A.1. Processing the Gravity Time Series

Time-varying gravity data supplied by an instrument at a given location consist of one variable time series, most of the time at a fixed sample rate. Except for absolute gravimeters acting as standards, the first step in processing data from relative gravimeters is the calibration. Then, the microseism, tidal effects, atmospheric pressure variations, and polar motion effects are routinely corrected in the time series prior to physical interpretation, except of course when those are the studied phenomena.

A.1.1. Microseismic Noise

Gravimetry time series from everywhere in the world are affected by microseismic perturbation, coming from the interaction of the waves with the coastal areas. This noise reaches a maximum at a period of about 6 s and ranges $8\ 10^3$–$8\ 10^7$ $(nm/s^2)^2/Hz$ (Peterson, 1993). This corresponds to displacements ranging 0.02–2.5 μm. In the vicinity of urban and industrial areas, the microseismic perturbation is larger, especially above 1 Hz. Microseism causes an increase of the power spectral density (PSD) only at periods shorter than 50 s; hence, applying a low-pass filter to recording systems of relative instruments allows removing easily this effect; a drawback of this method is that any other short-period signal is also removed.

A.1.2. Tidal Effects

The Scintrex CG3 and CG5 instruments are provided with an algorithm based on Longman (1959), which corrects tidal effects directly (Bonvalot et al., 1998); the new CG6 instrument is provided with a state-of-the-art software, the same as in the FG5 absolute gravimeters, allowing to apply more accurate corrections (Van Camp, 2003). Before the 2000s, early absolute gravimeters also used an old-fashioned tidal model (Munk & Cartwright, 1966; Van Camp, 2003). However, this model considers a frequency-independent tidal parameter for an oceanless Earth. Imprecisions in the model contaminate the gravity time series at the 10 nm/s^2 level for an oceanless Earth and, for the real Earth, can amount 100 nm/s^2 along coastlines (Figure A1). Another drawback is due to round-off errors, as CG3 or CG5 acquisition softwares store the results with a resolution of 10 nm/s^2. If one wants to restore the tidal signal computed by the gravimeter, round-off errors will affect the measurements (Meurers, 2012). Hence, for high-precision gravity investigation, at or below the 10 nm/s^2 level, a more accurate tidal model should be applied after switching off the correction available in the instrument.

The tidal signature corresponds to the sum of the direct gravitational attraction on the test mass, of the change of distance to the Earth's center due to Earth deformation, and of the Earth's internal mass redistribution (see section 3.2.1). To the first order, the equilibrium tide can be calculated using a radial Earth model for an inelastic nonhydrostatic, oceanless Earth (Dehant et al., 1999). Nevertheless, the actual gravity transfer function differs from that of the model by up to about 2%, due to the loading of ocean tides. The ocean loading effect on gravity is caused by the attraction of the moving water masses and the deformation of the crust due to the water load, with an induced vertical displacement that can reach a dozen centimeters. Numerous

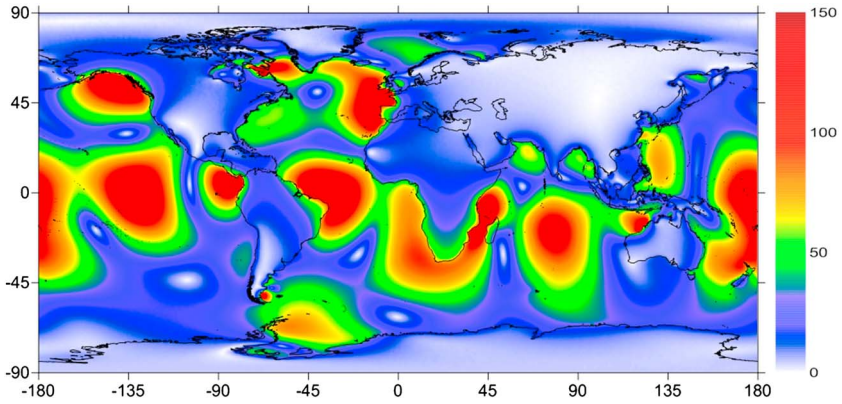

Figure A1. Amplitude (nm/s^2) of the semidiurnal M_2 wave ocean load based on applying the SPOTL package (Agnew, 2013) to the TPXO7.2 model.

models have been developed to correct for the dynamic ocean tide effects, but a correction at the nm/s^2 level is still challenging, due to the rather complicated distribution of the continents and the bathymetry. Presently, the best way to correct for tidal effects is by adjusting tidal parameter sets on the time series, as it allows correcting for both the solid Earth and ocean loading tidal contributions to gravity at the station (Hinderer et al., 2015; Neumeyer, 2010). Tidal analysis software, such as ETERNA (Schüller, 2015), estimate the frequency transfer function of the Earth (solid body plus oceans)-station-sensor system through a least squares adjustment of the Earth tide observations on the well-known astronomic forcing function or tidal potential (Wenzel, 1997a). As already explained, this periodical phenomenon is relatively easy to correct at a few nm/s^2 level. However, reaching the nm/s^2 level or below is not straightforward (Ducarme, 2009; Kroner et al., 2005; Van Camp, de Viron, & Avouac, 2016).

Ocean loading parameters can also be computed from existing ocean tide models, for example, by the free ocean tide loading provider from the Onsala Space Observatory (Bos & Scherneck, 2017). More than two dozen ocean loading models are available. The best choice is station dependent; the load tide amplitude may scatter from one model to the other by about 0.5 nm/s^2 or 5% for midcontinental sites in Europe, for example.

From observed or modeled tidal parameters, packages such as the Tsoft software (Van Camp & Vauterin, 2005) allow predicting Earth tides as well as ocean loading contributions.

A.1.3. Atmospheric Effects

The atmospheric mass also affects the gravity, by both the direct Newtonian attraction of air masses above the instrument (-4 nm/s^2/hPa) and the loading on the crust (+1 nm/s^2/hPa) (Merriam, 1992; Warburton & Goodkind, 1977). The effect is at the level of -3 nm/s^2/hPa and frequency dependent. At midlatitude, this means a standard deviation of gravity of 30 nm/s^2 as the standard deviation of the barometer recording is 10 hPa. The local air pressure recording and a single admittance factor allow correcting for about 90% of the atmospheric effects (Boy, 2005; Boy et al., 2009, 2002; Hinderer et al., 2014; Klügel & Wziontek, 2009; Merriam, 1992).

The quality of the correction using a single admittance approach differs within the frequency range due to the frequency dependence of air pressure admittance. This can certainly be improved by applying a 3-D model of the atmosphere and local barometric measurements (Boy, 2005; Boy et al., 2002, 2009; Hinderer et al., 2014, 2015; Karbon et al., 2014; Klügel & Wziontek, 2009; Merriam, 1992; Neumeyer, 2010) (Figure A2). However, the correction of atmospheric pressure effects remains imperfect, even with the most sophisticated treatments due to the limited spatial and temporal resolution of 3-D atmosphere models.

Even if the atmospheric pressure correction remains imperfect, the PSD of the barometric signal flattens at periods longer than 50–100 days; hence, atmospheric effects are not expected to influence the measurements of long-term gravity changes. At shorter periods, the barometric signal is autocorrelated. After removing tidal and polar motion effects, when correcting the gravity recordings for the pressure signature, the standard deviation decreases easily by 50% (Membach: from 30 to 15 nm/s^2) and the PSD level decreases

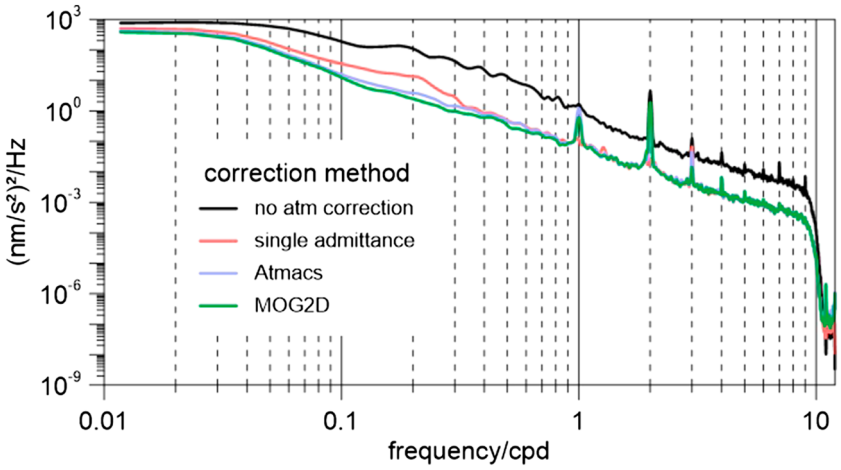

Figure A2. Power spectral densities (PSDs) of superconducting gravimeter time series (Conrad Observatory, Austria): Residuals before (black) and after atmosphere correction using a single admittance (red); atmacs (blue, Klügel & Wziontek, 2009) and MOG2D (green, EOST Loading Service, Boy et al., 2009) models.

by up to 10 dB at periods shorter than 100 days. Despite correction models, atmospheric effects can limit the ability to monitor subtle gravity changes at the nm/s^2 level, especially fast ones. Rapid strong mass exchanges within the atmosphere, at the kilometric or even smaller scale, are very difficult to model.

Another indirect atmospheric effect is the nontidal sea loading, caused by variations in the sea level, primarily driven by wind stress. This effect was observed for the first time along the Baltic Sea in Finland (Virtanen & Mäkinen, 2003) and along the North Sea in Belgium (Fratepietro et al., 2006) using superconducting gravimeters and was later evidenced using GNSS measurements (Geng et al., 2012; Nordman et al., 2015). Other seasonal atmospheric pressure-driven sea level changes also influence gravity measurements, as shown along the Adriatic Italian coast by (Zerbini et al., 2004). These nontidal effects—reaching a few dozen nm/s^2—can be accounted for by applying appropriate models (Boy et al., 2009; Fratepietro et al., 2006; Virtanen & Mäkinen, 2003).

Modern relative gravimeters are sealed in such a way that direct buoyancy effect of atmospheric pressure changes on the suspended mass does not influence gravity measurements. However, damaged seals make the gravimeters sensitive to the Archimedean effects of atmospheric pressure changes (Figure A3). This is even more critical if imperfectly sealed gravimeters are calibrated by measuring at different elevations, as pressure changes would bias the calibration process.

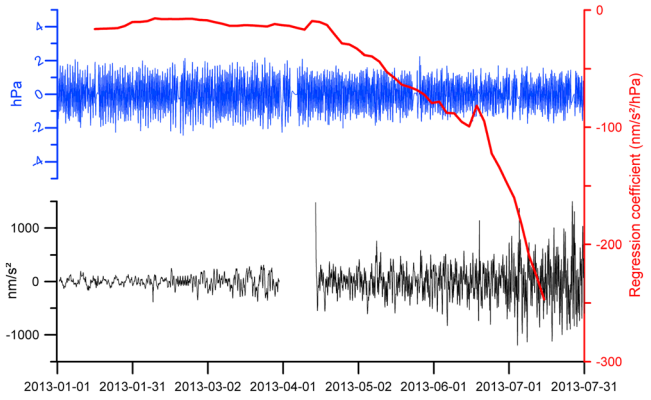

Figure A3. Influence of the atmosphere pressure variation on the B28 Burris gravimeter, of which the seals are leaking, slowly increasing the response of the instrument to barometric changes. Instrument installed at Montserrat, Lesser Antilles, 16.75°N, 62.23°W. Black: gravity after removing a synthetic Wahr-Dehant tidal signal (Dehant et al., 1999); blue: barometer time series; red: regression coefficient between pressure and gravity. Both pressure and gravity signals are high-pass filtered with a cutoff frequency of 0.5 cycle per day.

Changes of solar irradiation cause, among other phenomena, dynamic global air pressure changes known as atmospheric tides (Agnew, 2015). The associated load on the Earth's surface causes deformation and gravity variations. Boy and Hinderer (2006) investigated the gravity effect induced by the diurnal atmospheric tide S_1 at Strasbourg because Earth tides and gravitational ocean loading are small contrary to semidiurnal waves. They achieved some but far from a perfect agreement between observed and modeled tides.

A.1.4. Polar Motion Effects

The polar motion induces a very small variation of the distance to the rotation axis, about a dozen meters, which results in a change in the centrifugal acceleration and in gravity to the level of 130 nm/s^2 peak to peak (Wahr, 1985), which is easily visible with a stable gravimeter. However, other techniques such as radio-astronomy (very long baseline interferometry) allow better measurements of the pole motion so that its effect on gravity can be removed independently.

In practice, software such as the Tsoft package can do this, using the time series of pole coordinates, as provided by the International Earth Rotation Service.

A.2. Types of Monitoring and Experimental Designs

Measuring gravity changes at the 10^{-9} level or better requires a rigorous measurement protocol. Among others, it is very important to benefit from a reference station where gravimeters can be tested and which acts as a reference point for campaign-based microgravimetric surveys.

A.2.1. Designing a Station

A.2.1.1. Limiting Tilt and Vibration Effects

Stable installation of the gravimeter, on the bedrock or a very stable pier, allow to limit tilt and vibration effects; see recommendations of Uhrhammer et al. (1998) in order to ensure the mechanical stability of the pier. Concerning the vibrations, relative gravimeters, given their feedback systems and filters, are not appropriate to investigate phenomena of periods shorter than a few seconds, as the loop gain of a force-balance accelerometer feedback system becomes unstable at short periods (Wielandt, 2002). Hence, they are rather insensitive to anthropogenic vibrations.

As for absolute gravimeters, their seismometer-based isolating device attenuates the microseismic effects. However, when it is strong enough, microseism can significantly deteriorate the measurements, typically when the drop-to-drop standard deviation becomes higher than 150 nm/s^2 for an FG5 instrument. In that case increasing the sampling rate is an additional and efficient way to mitigate for microseismic noise (Van Camp et al., 2005). Strong microseismic noise can also lower the ability of the operator to check the verticality of the instrument. Hence, it is preferable to measure away from the coast or cities, whenever possible; that is, city or ocean are not the topics of the study (Van Camp et al., 2011; Williams et al., 2001).

Concerning tilts, superconducting gravimeters and gPhones are equipped with thermal levelers, which, in principle, compensate for tilts of the ground and decrease the PSD noise level by 1 order of magnitude. However, classical absolute gravimeters are still not provided by such devices and must be installed on a stable platform; it is worth noting that the suspension devices as the superspring or seismometers do not allow compensating for tilts. On the other hand, the cold atom gravimeter developed by Muquans is provided by tiltmeters, of which the recordings are used to correct the gravity value provided that the tilts remain smaller than 1°.

Clay soils swelling with moisture or air pores within sand which react to atmospheric pressure can cause tilts; whenever possible, bedrock must be preferred. Installing a pillar on pads of elastic material is definitely not appropriate for seismic or gravity measurements, given that the pier has the freedom to move and tilt and that resonance effects may occur. In other words, although pads may attenuate the urban noise, they are likely to introduce low-frequency tilts and displacements.

The pillar, ideally in contact with the bedrock, should be made of a rich mixture of 50% cement and 50% sieved sand (Uhrhammer et al., 1998). It should not contain any reinforcing bars nor wire mesh nor rock aggregates, as all have different coefficients of thermal expansion and iron may induce magnetic effects. This seems contrary to traditional concrete construction practice, but the very hard mixture is strong enough to support a gravimeter and its operator! The mixture must be vibrated to remove air which otherwise may expand and contract with passing pressure cells, resulting in high-frequency noise. To ensure thermal insulation and minimize coupling with the floor and the structure of the building, the pier should be surrounded by foam boards. Figure A4 shows the construction of one of the two pillars at the Rochefort station: the foam boards are visible before pouring the cement-sand mixture. Although Uhrhammer et al. (1998) recommend a 50-50 mixture, we used a 35% cement-65% sand mixture, following the recommendation of the Black Forest Observatory, because the 50-50 rich mixture could be too brittle for 1 m^3 large pillar. In order to avoid possible instabilities of the pillar, we chose to install the superconducting gravimeter on the smoothed bedrock directly (Figure A4d). However, for practical reasons a pillar had to be built to host the absolute instrument (Figure A4e). When selecting a site, one should take into account possible building construction or soil sealing around the gravity station, which may modify gravity significantly.

A.2.1.2. Limiting Thermal Influence

Thermal influences on gravimeters are drastically reduced or even canceled through controlling the temperature in the gravity sensing unit. This contrasts with several other geophysical instruments such as broadband

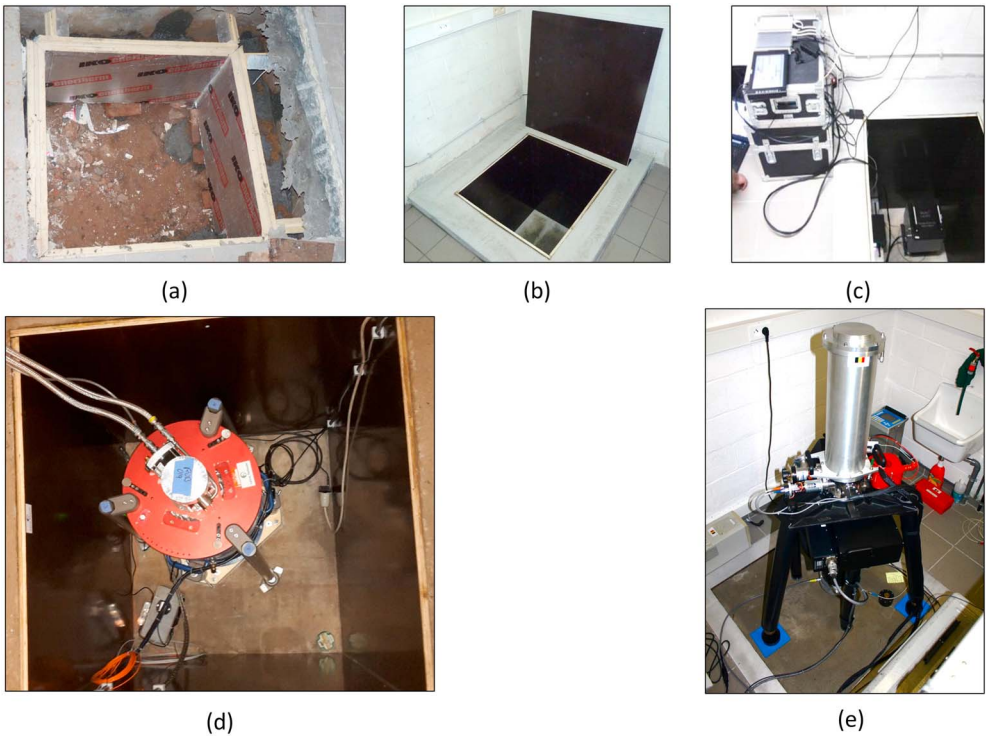

Figure A4. Pillars at the Rochefort station, Belgium (50.16°N, 5.23°E). (a) Digging to reach the bedrock; (b) ready to house the gravimeter; (c) after installation of the gPhone gravimeter; (d) same place, after installation of the GWR iGrav#019 superconducting gravimeter; and (e) same room, the pillar for the absolute gravimeter, made of 35% cement and 65% sand. Credit: Royal Observatory of Belgium.

seismometers that need much more thermally stable conditions (Block & Moore, 1966; Wielandt, 2002): their external insulation must ensure a significant attenuation of the thermal noise in the seismic band (i.e., at periods shorter than 54 min) and preferably also the diurnal signature (Uhrhammer et al., 1998).

State-of-the-art observatory instruments such as superconducting and gPhone gravimeters are thermostated at a level making them insensitive to room temperature changes. For example, let us compare the superconducting gravimeters iGrav#019 and OSG#056. The iGrav#019 is installed in the middle of the Belgian town of Rochefort (50.1552°N, 5.2256°E), in a laboratory where the temperature is only controlled at the 1–2°C level, while the OSG#056 is installed at the extremely stable Black Forest Observatory (Rosat & Hinderer, 2011; Zürn & Widmer, 1995). In particular, the OSG is protected by an airlock that limits temperature fluctuations to less than about 3 mK and acts as a low-pass filter for atmospheric pressure variations shorter than 36 h (Zürn et al., 2007). The OSG#56 is an experimental, dual sphere instrument, provided with a heavier, 17.7 g sphere in the lower sensor and a typical 4.3 g mass in the upper sensor. This was a test to decrease the thermal, Brownian noise of the sensors, which varies as m^{-2}, m being the mass (Hinderer et al., 2015). With a PSD of 2 nm/s^2, the iGrav#019 performs similarly to the upper sensor of the OSG#56 installed at Black Forest Observatory. As for the gPhone instrument, we obtained similar results when measuring at the Rochefort surface laboratory (Figure A4c) and after its installation in the cave, where the temperature is yet much more stable.

Presently, spring gravimeters are shielded from temperature changes by housing the sensor in a single or double oven, at a temperature close to 60°C. However, spring gravimeters can suffer from an improper thermostatization. Recordings from not well temperature stabilized or even not well-sealed spring gravimeters may be improved by compensating for temperature or barometric effects (Andò & Carbone, 2009; Bonvalot et al., 1998; Fores et al., 2016). For example, Fores et al. (2016) showed a linear relation of -5 nm/s^2/°C between two CG5 instruments and ambient temperature. As those effects are instrument and setup specific and may be frequency dependent (Andò & Carbone, 2009), this must in some cases be removed through nonlinear techniques and in a case-by-case fashion.

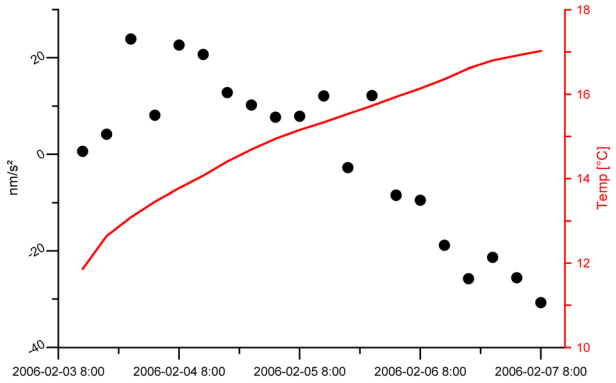

Figure A5. Gravity as measured by the absolute gravimeter FG5#202 (black dots), and room temperature (red line) at the Rochefort station, Belgium. The strong variation in temperature (5°C in 4 days) caused a misalignment of the interferometer, diagnosed by controlling the instrument. This induced an apparent decrease in the gravity of about 30 nm/s^2; such a time series must be rejected. Since 2008, the temperature is regulated at the 2°C level.

To a much lesser extent, classical, mechanical absolute gravimeters are also sensitive to temperature as changes of a few degrees in the operating room can cause a misalignment of the interferometer and consequently modify gravity by a few tens of nm/s^2 (Figure A5). This can be mitigated by stabilizing the room temperature at the 1°C level or by controlling the alignment whenever temperature changes by 2 or 3°. Ancillary temperature recording provides a very useful criterion to reject doubtful measurements.

A.2.1.3. Limiting the Umbrella Effect

When gravimeters are operated to study hydrogeology, it is advisable to limit the impact of the building on the local hydrology, known as the umbrella effect (Creutzfeldt et al., 2010; Deville et al., 2013). This umbrella effect can be drastically reduced by using a small field enclosure (Figure A6).

A.2.1.4. Limiting Nearby Newtonian Effects

Finally, let us mention a special consequence of the outstanding sensitivity of superconducting gravimeters, which detect the presence of operators and nearby vehicles (Van Camp & de Viron, 2016). This induces transients in the time series (Figure A7), which should be minimized and carefully reported in a logbook. Self-attraction of absolute gravimeters must also be considered (Biolcati et al., 2012; Niebauer et al., 2013). Hence, activities that are part of the measuring process do influence the measurand, that is, here, the high-precision gravity measurements. Ironically, this makes us think of similar problem quantum physics faces in many experiments. In our case, however, it is not intrinsic to the physics of the process itself; restricting access is appropriate to mitigate this effect whenever possible.

A.2.2. Microgravimetric Surveys

When the time sampling does not require continuous measurements, it is possible to cover a broader area with the same instrument by revisiting with the right time interval a network of selected sites, using either an absolute gravimeter or a relative gravimeter and a reference station where gravity is known.

Time lapse microgravimetry concerns gravity anomalies down to the 24–50 nm/s^2 level (Alnes et al., 2008; Christiansen, Lund, et al., 2011; Thomas Jacob et al., 2010). Time lapse microgravimetry, also called 4-D, campaign or dynamic gravimetry, allows monitoring temporal variations by repeating the microgravity measurements.

Figure A6. iGrav superconducting gravimeter inside its field enclosure. Credit: GWR Instruments, Inc.

Microgravimetry requires caring about several aspects: as mentioned in section A.1., a precise tidal model must be used and the atmospheric pressure measured. It is advisable to avoid shocks and protect the gravimeter from the wind. The measurements must be performed on small networks (about 100 km^2) such that the drift and calibration of the relative gravimeter can be checked at a reference station within a few hours. This is done by visiting each station at least twice within independent loops (Allis et al., 2000; Debeglia & Dupont, 2002; Gettings et al., 2008). As microgravimetry surveys are performed using a reference station, the best way to monitor the stability of the reference station is by using an absolute gravimeter (Hinderer et al., 2016; Thomas Jacob et al., 2010; Sugihara & Ishido, 2008). In that case, one refers to hybrid gravity measurements (Sugihara & Ishido, 2008). In addition, a superconducting gravimeter may further improve the measurements (Hinderer et al., 2016; Van Camp et al., 2013). Finally, redundancy by using two or three instruments could be a way to better assess the drift and possible calibration changes and to eliminate tares that can appear in recordings (Bonvalot et al., 2008; Sasagawa et al., 2003).

If absolute gravity is known at more than one station, it is not necessary to come back to only one reference point, and one can also control the

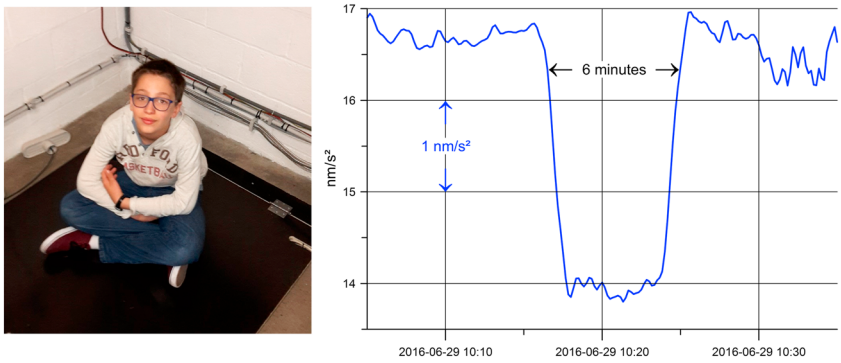

Figure A7. The gravitational effect of a 13 year old, 45 kg boy sitting for 6 min above the superconducting gravimeter iGrav#019 (Figure A4d) at the Rochefort station, Belgium. His navel is about 1 m above the sensor; the mass of the boy induces a decrease in the gravity of 2.8 nm/s^2. Credit: Royal Observatory of Belgium.

calibration of the spring gravimeters. The pyGrav package allows adjusting gravity networks and applying tidal and barometric corrections (Hector & Hinderer, 2016).

A.2.3. Errors Affecting Relative Gravimeter Surveys

In addition to thermal and atmospheric pressure effects, spring gravimeters are subject to precision loss caused by varying calibration factor and the design of the gravity survey.

First of all, remote earthquakes can perturb the measurements. This can be identified by watching the standard deviation of the measurements. To mitigate for these effects, one must wait for from a dozen minutes to a few hours, depending on the magnitude of the event.

The calibration factor of spring gravimeters varies with time (Bonvalot et al., 1998; Deville, 2013; Francis & Hendrickx, 2001) and must be controlled, for example, along calibration lines, which consist of several points experiencing known gravity differences, established using an absolute instrument, sufficiently large to represent the whole range of variations experienced by the gravimeter.

The design of gravity survey influences the results, especially if one runs long distance, in a strong topography. Given the large distances, spring gravimeters undergo shocks, changing magnetic field, pressure, temperature, and strong gravity changes, which influence the drift and the calibration. Even running short distances, the linearity of the drift is not granted (Ergintav et al., 2007; Francis & Hendrickx, 2001) (Figure 4). Typically, a relaxation time, associated with a strong quadratic drift, is observed after moving the gravimeter (Deville, 2013; Flury et al., 2007) (Figure A8). The duration of the relaxation and the intensity of the drift depend on the type of displacement (e.g., gravimeter moved by car or on foot and shocks) and

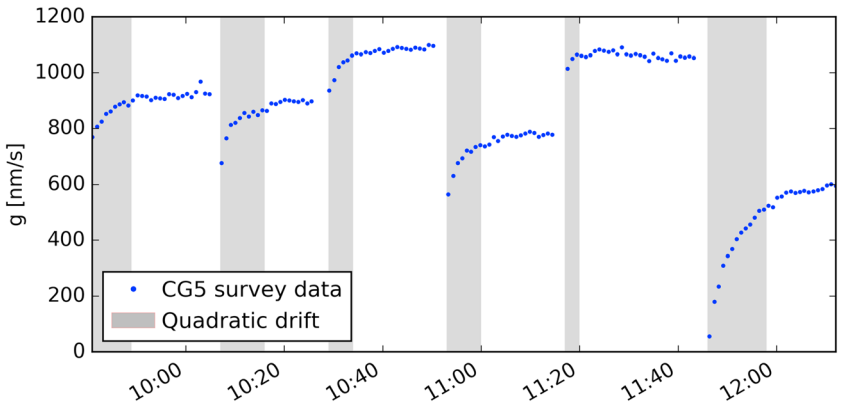

Figure A8. Relaxation of the CG5 spring gravimeter #40542, being displaced at different locations in the park around the Royal Observatory of Belgium. This is similar to the behavior of the results reported by Flury et al. (2007) (CG3 gravimeter) and by Deville (2013, Figure 7.5, CG5 gravimeter).

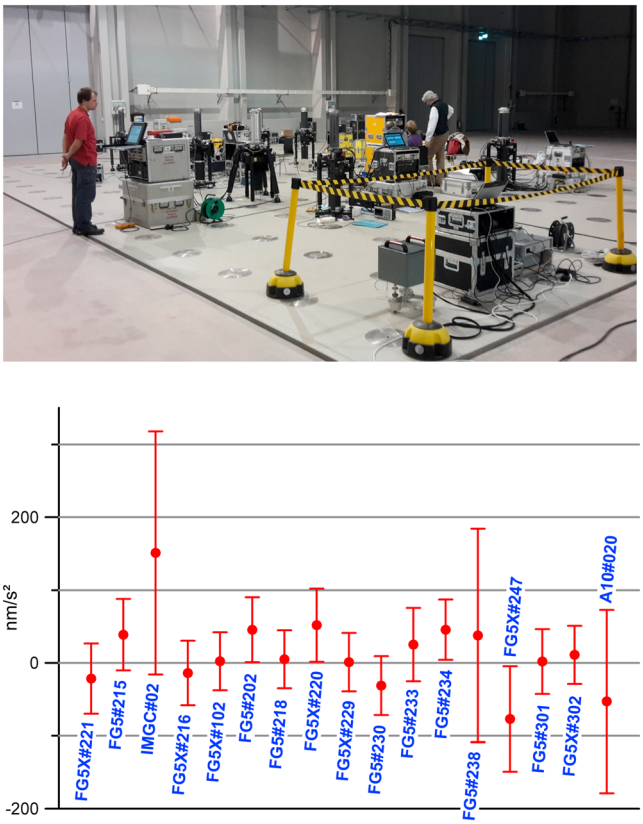

Figure A9. (top) Intercomparison of absolute gravimeters at the University of Luxembourg, November 2015. On the foreground a gPhone relative gravimeter for continuously monitoring gravity changes during the whole intercomparison campaign; (bottom) official results, redrafted from Pálinkáš et al. (2017). The error bars represent the uncertainties at 95% confidence. FG5X is an FG5 gravimeter, both from Micro-g LaCoste, with redesigned dropping chamber (extended free-fall length: 65% longer in distance, redesigned drive system); IMGC: rise and fall gravimeter (D'Agostino et al., 2008); A10 is a portable absolute gravimeter from Micro-g LaCoste (Dykowski et al., 2014). Photo credit: Royal Observatory of Belgium.

are expected to vary from one instrument to another. Measuring for at least 15 min at each station is a way to mitigate the uncertainties due to the relaxation of the spring due to transport (Deville, 2013; Gettings et al., 2008).

In the presence of a strong topography, the gravimeters are operated in quite different pressure and calibration conditions, which induces calibration errors (Atzbacher & Gerstenecker, 1993; Francis & Hendrickx, 2001) and direct atmospheric effects if the seals are damaged. Moreover, if a survey is repeated for several years, a Model G LaCoste Romberg meter will gradually drift to where a different portion of the micrometer adjusting screw is being used. This might introduce errors due to the limited accuracy of the meter's calibration. In particular, the micrometer itself can bias the calibration factor, due to irregularities in manufacturing the gear train and the measuring screw. This causes periodic or circular errors, reaching 400 and 80 nm/s^2 for model G and D LaCoste Romberg gravimeters (Valliant, 1991). Modern spring gravimeters based on LaCoste Romberg sensors are equipped with electronic feedback device, and cyclic errors are no longer a problem provided the feedback range is not exceeded in a survey.

Hence, it is paramount to check any correlation between observed gravity changes and topography, which may support the hypothesis that calibration errors and/or malfunctioning seals play a significant role. Note that part of the reported gravity changes on three epochs (A, B, and C) can be caused by only one poor campaign, as gravity changes are measured by relative surveys, in other words, on gravity differences. This is a problem similar to the ones faced when performing repeated levellings, which can be guessed when trends between epochs A and B and epochs B and C look like reversal images (Camelbeeck et al., 2002).

A.2.4. Errors Due To Offsets Between Absolute Gravimeters

Intercomparison campaigns (Francis et al., 2005, 2010, 2013, 2015; Jiang et al., 2012; Schmerge et al., 2012; Vitushkin et al., 2002) have shown that offsets between absolute gravimeters range commonly 100–220 nm/s^2 (Figure A9). Hence, when absolute gravity measurements are performed, if different AGs are used in the same study, instrument differences should be included in the uncertainty budget (Mémin et al., 2011; Pálinkáš et al., 2013; Sato et al., 2006) or accounted for (Lambert et al., 2006; Lambert, Henton, et al., 2013). Concurrently, the uncertainty due to the setup of the AG instrument should also be taken into account. This noise results from instrumental setup-dependent offsets and can be due to, for example, the middling alignment of the instrument, errors in measuring the installation height between the floor and the interferometer, slight mechanical changes due to transportation, or different instrument floor couplings. For an FG5, the sources of uncertainties can be represented by a normal random distribution, with a standard deviation of 16 nm/s^2 (Van Camp et al., 2005). In some circumstances, larger, isolated systematic errors due to instrumental setup may occur. For example, an error in a hyperfine line of the iodine used to stabilize the laser frequency can induce a shift in gravity of 270 nm/s^2/line; a malfunctioning or not calibrated clock is also possible (2 nm/s^2/mHz for an FG5 instrument), etc. (for a comprehensive review of errors affecting an FG5 gravimeter, see Niebauer et al., 1995). This is difficult to detect but can be mitigated by repeating at least five times the AG measurements (Van Camp, de Viron, & Avouac, 2016) or by side-by-side measurements with a superconducting gravimeter.

Note that offsets between absolute gravimeters do not influence the evaluation of the calibration factor of relative gravimeters (Francis & van Dam, 2002).

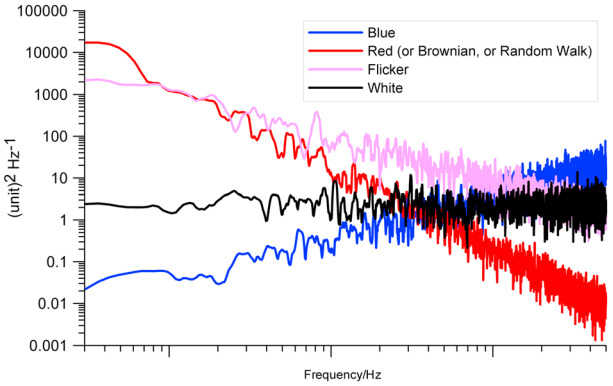

Figure A10. Power spectral densities of blue, red (or Brownian or random walk), flicker (or pink), and white signals (arbitrary units).

A.3. Spectra of the Noise Affecting Terrestrial Gravity Measurements

By analogy with visible light, one refers to colors to classify the noise sources as a function of their power spectral densities (PSDs). The PSDs do not depend on the duration of the analyzed series, making it easy to compare different series or instruments. To compute the equivalent standard deviation σ of the signal at a given period T, one calculates

$$\sigma(T) = \sqrt{\frac{\mathrm{PSD}\,(T)}{2T}}.$$

The noise is said to be white when its PSD is the same in the entire frequency domain; it consists of uncorrelated data with zero mean and finite variance. As the mean does not vary with time, this noise is stationary. When the data distribution follows a Gaussian distribution, the noise is characterized as Gaussian. When more power is concentrated on the lower frequency, the noise is time-correlated: the values of this signal are not, on average, independent from the previous ones. When the power spectrum of a colored noise reads as f^{κ}, with f the frequency and κ the spectral index $-3 < \kappa < -1$, it is said to be a fractional Brownian motion; if $\kappa = -1$, the noise is said to be flicker or pink noise, if $\kappa = -2$, a random walk noise. The random walk, also called red or Brownian signal, can be generated as the integral of a white noise: a value at a given time will be equal to the previous value plus a white noise component. When a spectrum is characteristic of a random walk ($\kappa = -2$) at high frequencies and a flattening at low frequency, it corresponds to a first-order Gauss-Markov process, and a generalized Gauss-Markov model if $\kappa \neq -2$. The noise is said to be blue if the energy is concentrated on the higher frequencies ($\kappa = 1$) (Agnew, 1992; Johnson, 1925; Mandelbrot & Van Ness, 1968) (Figure A10).

When classifying noises, one must keep in mind that this should be done by specifying the frequency band. In gravity time series, after correcting for tidal, atmospheric, polar motion effects and, if needed, instrumental drift, the time series is described by a generalized Gauss-Markov signal at frequencies lower than 1 mHz, with the spectrum flattening at periods longer than a few years, a white noise between 1 and 20 mHz, and a blue or even steeper signal at higher frequencies (Van Camp et al., 2005, 2010; Van Camp, Meurers, et al., 2016) (Figure A11).

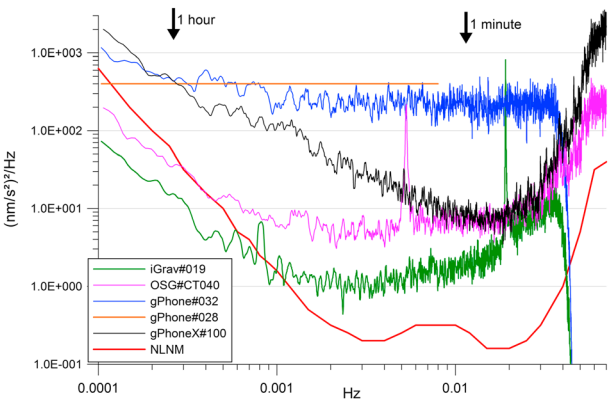

Figure A11. PSDs of the metal spring gPhoneX#100, gPhone#028, and #032 gravimeters, and GWR superconducting gravimeters iGrav#019 and OSG#CT040. Each PSD represents the average of five quiet days. The noise level of the gPhone #028 is inferred from Niebauer (2015). The gPhone#032 is installed in the Rochefort Cave, 40 m underneath the iGrav#019. The OSG#T040 and gPhonesX#100 instruments are at the Walferdange station. Note that the gPhone#032 provided similar results when measuring at the surface laboratory. Hence, the environmental stability in the cave does not play a significant role in this case. At 1 h period, a CG5 gravimeter is at the level of $(10^4\ \mathrm{nm/s^2})^2$/Hz (Riccardi et al., 2011). The peaks at 0.0053 Hz (CT040) and 0.019 Hz (iGrav#019) are caused by an orbital mode of the levitating sphere, typical of the superconducting gravimeters. This mode has a period of 60–200 s, depending on the instrument (Banka & Crossley, 1999; Hinderer et al., 2015).

The instrumental noise, which includes errors from the operational setup (setup noise; Van Camp et al., 2005) and data processing, is often described by a Gaussian white noise model. As the variance of the mean of a Gaussian white noise is inversely proportional to the number of samples, a way to mitigate its effect consists in increasing the number of measurements.

In addition, instrumental artifacts, such as drift, and geophysical signals add a power law signal, of which the spectral signature increases at periods larger than 1,000 s and shorter than 100 s (Agnew, 1992; Agnew & Berger, 1978; Peterson, 1993; Riccardi et al., 2011; Van Camp et al., 2005; Widmer-Schnidrig, 2003).

At periods longer than 2 months, Van Camp et al. (2010) showed that the hydrological signature dominates the gravity signal after correcting for tidal and atmospheric effects. The PSD obeys a Gauss-Markov structure, where the high-frequency, location-dependent power law takes spectral indexes ranging in the interval $[-4.7, -1.4]$. It is physically reasonable that the hydrological effects obey a Gauss-Markov model. Indeed, at a short period, the signal must be nonstationary and correlated, since an amount of ground water at a given time depends on the water stored previously. However, a pure random

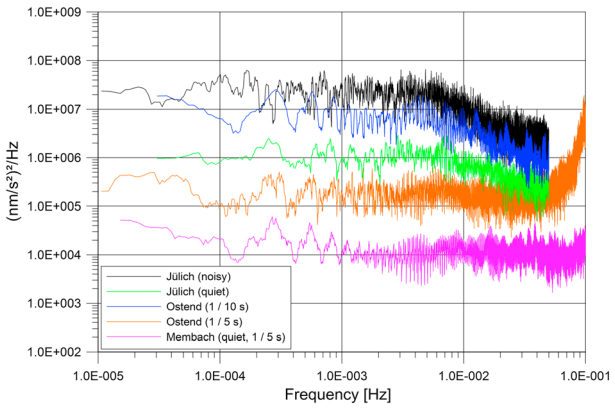

Figure A12. PSD of AG time series at Jülich (Germany), Ostend (Belgian coastline), and Membach (Belgium) stations. In Jülich the PSDs are shown when the industrial noise is low (green, drop-to-drop standard deviation (dtd) = 211 nm/s^2) and very high (black, dtd = 932 nm/s^2). Orange indicates PSD at Ostend (1 drop/5 s, 200 drops per set, one set per hour, dtd = 609 nm/s^2), and blue indicates the same by taking one piece of data out of two (dtd = 609 nm/s^2). This shows the aliasing of the microseismic noise. For comparison the PSD at Membach using the 1/5 s data recorded during quiet days (dtd = 62 nm/s^2). Modified and redrafted from Figure 4 of Van Camp et al. (2005).

walk behavior is impossible as it would theoretically allow the possibility that unlimited quantities of water could be stored or that water may disappear globally over long periods. The spectrum flattens at about 1 year.

To classify instruments and geophysical stations, Peterson (1993) investigated the seismic background noise from a worldwide network of stations. He could establish a new low-noise model (NLNM) and a new high-noise model (NHNM), which are spectra of the lowest and highest observed envelopes of the noise obtained from a set of seismic recordings from 75 stations distributed in the world. By intercomparing long-period STS-1 seismometers, Peterson (1993) showed that the lowest envelope represents the actual geophysical noise level in the periods ranging 1–6,000 s. Hence, the NLNM and NHNM provide an excellent base to discuss the noise level of gravimeters. In the band 50–500 s, the NLNM level can only be reached by outstanding long-period seismometers, superconducting gravimeters, or exceptionally stable and sensitive spring gravimeters (Laske & Widmer-Schnidrig, 2015; Zürn et al., 2000). Spring gravimeters experience an instrumental white noise of which the PSD is about 15 dB higher than superconducting gravimeters, which is equivalent to 400 $(\mathrm{nm/s^2})^2$/Hz from our experience and in the study of Niebauer (2015)(the gPhone is referred to as Portable Earth Tide in his publication). This level is 35 dB higher than the NLNM level (Figure A11). The gPhoneX model performs much better at frequencies higher than 1 mHz, and this results from an improvement within the electronics.

As for the noise level of absolute gravity measurements performed by an FG5 gravimeter, it is 40 to 80 dB higher than the NLNM, ranging 10^4–10^8 $(\mathrm{nm/s^2})^2$/Hz (Van Camp et al., 2005) (Figure A12). This noise is white, but in the case of strong microseismic noise, aliasing induces a negative slope at frequencies lower than 2 mHz, which cannot be directly inferred from the drop-to-drop standard deviation. The level of 10^4 $(\mathrm{nm/s^2})^2$/Hz seems presently the lowest achievable by ballistic instruments. This was demonstrated using an FG5 absolute instrument by the experiment performed in Membach by Van Camp et al. (2005) or an atom gravimeter in Onsala, Sweden (Freier et al., 2016). In the band ranging 50–500 s, the PSD is fairly flat and the cause for the generally low noise is supposed to be the background free oscillations or "hum," as discussed in section 3.2.2.

At periods longer than about 1 day, the performances of absolute gravimeters become similar to the best relative gravimeters and better at periods longer than a few months given that absolute instruments do not experience any drift (Van Camp et al., 2005).

The noise level of Peterson (1993) was obtained using seismic recordings not corrected for tidal and atmospheric effects. At periods larger than 500 s, the Newtonian attraction of moving air masses in the local atmosphere above the sensor is the principal source of the colored signal (Warburton & Goodkind, 1977; Zürn & Widmer, 1995). It is possible to reduce the variance of the signal up to frequencies of about 1–2 mHz (600–900 s periods), by applying a correction based on the atmospheric pressure record performed at the seismic or gravity station (Beauduin et al., 1996; Van Camp, 1999; Zürn & Meurers, 2009; Zürn & Widmer, 1995). This correction is adjusted at each station and is often close to ~ −3.0 nm/s^2/hPa (Merriam, 1992) for longer periods but drops down to 0 at 1–2 mHz. After correcting for tidal and atmospheric pressure effects, the noise level of gravimeters and long-period seismometer becomes smaller than the Peterson's New Low Noise Model at periods longer than 500 s (Rosat & Hinderer, 2011; Zürn & Widmer, 1995).

In conclusion, the quality of a seismic or gravity station must be assessed in given frequency bands, as a function of the scientific objectives. For example, installing a gravimeter in a strong hydrogeological signal context lowers the quality of the station to study tides or slow tectonic deformations. In the opposite, installing a superconducting gravimeter in an arid zone as the Tamanraset GEOSCOPE station, Algeria (Stutzmann, 2000), may provide outstanding data to investigate the tidal spectrum and Earth's free oscillations, while being of lesser relevance for hydrogeology.

Acknowledgments

We thank Christophe Collette, Damien Delforge, Bruno Desruelle, Michel Diament, Marc Hendrickx, Kevin Jourde, Thomas Lecocq, Stéphane Mazzotti, Gwendoline Pajot-Métivier, Isabelle Panet, Frank Pereira dos Santos, Barbara Romanowicz, Annie Souriau, Holger Steffen, Bert Vermeersen, Glynn Williams-Jones, and Walter Zürn for their comments, suggestions, and valuable advice. Stefanie Hautmann and Jo Gottsmann provided the data from Montserrat, for which Eric Tomme provided space for installation, took care of the setup, and downloaded the data from the Burris instrument, of which the installation was part of the National Geographic grant GEFNE34-12. The nice original illustrations of this paper were drawn by Thierry Guyot. Clément Van Camp performed the gravitational experience on Figure A7. The participation of O. d. V. is financially supported by CNES, as an application of GRACE space gravity mission. The work of A. W. is part of the Karst Aquifer Research by Geophysics (KARAG) project (http://www.karag.be) funded by the Fonds de la Recherche Scientifique (FNRS-FRS) and is also supported by the Ernest du Bois Fund, managed by the King Baudouin Foundation. C. J. L. Caudron is supported through an F.R.S-FNRS Chargé de Recherche/Université Libre de Bruxelles grant. We thank three anonymous reviewers and the Editor Fabio Florindo for their valuable reviews. In addition, we thank the respective journals and manufacturers for granting permission to reproduce some of the figures utilized in this paper. Implicit or explicit references to company names or products in this document do not imply advertisement or endorsement for the services or products provided by these companies. The data used to draw Figures 1, 16, 20, and A3 are available for academic purposes through the database of the Royal Observatory of Belgium: https://cloud-as.oma.be/index.php/s/tZrV1tye4HphHML.

References

Abbott, B. P., Abbott, R., Abbott, T. D., Abernathy, M. R., Acernese, F., Ackley, K., … LIGO Scientific Collaboration and Virgo Collaboration (2016). Observation of gravitational waves from a binary black hole merger. *Physical Review Letters*, *116*(6), 061102. https://doi.org/10.1103/PhysRevLett.116.061102

Achilli, V., Baldi, P., Casula, G., Errani, M., Focardi, S., Guerzoni, M., … Raguní, G. (1995). A calibration system for superconducting gravimeters. *Bulletin Géodésique*, *69*(2), 73–80. https://doi.org/10.1007/BF00819553

Agnew, D. (1986). Strainmeters and tiltmeters. *Reviews of Geophysics*, *24*(3), 579. https://doi.org/10.1029/RG024i003p00579

Agnew, D. (1992). The time-domain behavior of power-law noises. *Geophysical Research Letters*, *19*(4), 333–336. https://doi.org/10.1029/91GL02832

Agnew, D. (2013). *SPOTL: Some Programs for Ocean-Tide Loading* (technical report). San Diego, CA: Scripps Institution of Oceanography. Retrieved from https://igppweb.ucsd.edu/~agnew/Spotl/spotlman.pdf

Agnew, D. (2015). Earth tides. In *Treatise on Geophysics* (pp. 151–178). Amsterdam: Elsevier. https://doi.org/10.1016/B978-0-444-53802-4.00058-0

Agnew, D., & Berger, J. (1978). Vertical seismic noise at very low frequencies. *Journal of Geophysical Research*, *83*(B11), 5420. https://doi.org/10.1029/JB083iB11p05420

Agnew, D., Berger, J., Buland, R., Farrell, W., & Gilbert, F. (1976). International deployment of accelerometers: A network for very long period seismology. *Eos, Transactions American Geophysical Union*, *57*(4), 180. https://doi.org/10.1029/EO057i004p00180

Agnew, D., Berger, J., Farrell, W. E., Gilbert, J. F., Masters, G., & Miller, D. (1986). Project IDA: A decade in review. *Eos, Transactions American Geophysical Union*, *67*(16), 203. https://doi.org/10.1029/EO067i016p00203

Aki, K., & Richards, P. G. (2002). *Quantitative Seismology* (2nd ed.). Sausalito, CA: University Science Books.

Allis, R. G., Gettings, P., & Chapman, D. S. (2000). Precise gravimetry and geothermal reservoir management (pp. 179–188). Presented at the 25th Workshop on Geothermal Reservoir Engineering, Stanford University.

Alnes, H., Eiken, O., & Stenvold, T. (2008). Monitoring gas production and CO_2 injection at the Sleipner field using time-lapse gravimetry. *Geophysics*, *73*(6), WA155–WA161. https://doi.org/10.1190/1.2991119

Amalvict, M. (2010). Absolute gravimetry at BIPM, Sèvres (France), at the time of Dr. Akihiko Sakuma. *Gravity, Geoid and Earth Observation*, *135*, 83–91. https://doi.org/10.1007/978-3-642-10634-7_12

Andò, B., & Carbone, D. (2009). A LabVIEW environment to compensate temperature-driven fluctuations in the signal from continuously running spring gravimeters. *Computers & Geosciences*, *35*(10), 2129–2136. https://doi.org/10.1016/j.cageo.2008.12.007

Arnet, F., Kahle, H.-G., Klingelé, E., Smith, R. B., Meertens, C. M., & Dzurisin, D. (1997). Temporal gravity and height changes of the Yellowstone Caldera, 1977–1994. *Geophysical Research Letters*, *24*(22), 2741–2744. https://doi.org/10.1029/97GL02801

Atzbacher, K., & Gerstenecker, C. (1993). Secular gravity variations: Recent crustal movements or scale factor changes? *Journal of Geodynamics*, *18*(1–4), 107–121. https://doi.org/10.1016/0264-3707(93)90033-3

Audet, P., Bostock, M. G., Boyarko, D. C., Brudzinski, M. R., & Allen, R. M. (2010). Slab morphology in the Cascadia fore arc and its relation to episodic tremor and slip. *Journal of Geophysical Research*, *115*, B00A16. https://doi.org/10.1029/2008JB006053

Audet, P., Bostock, M. G., Christensen, N. I., & Peacock, S. M. (2009). Seismic evidence for overpressured subducted oceanic crust and megathrust fault sealing. *Nature*, *457*(7225), 76–78. https://doi.org/10.1038/nature07650

Azúa, B. M., DeMets, C., & Masterlark, T. (2002). Strong interseismic coupling, fault afterslip, and viscoelastic flow before and after the Oct. 9, 1995 Colima-Jalisco earthquake: Continuous GPS measurements from Colima, Mexico. *Geophysical Research Letters*, *29*(8), 122-1–122-4. https://doi.org/10.1029/2002GL014702

Bagnardi, M., Poland, M., Carbone, D., Baker, S., Battaglia, M., & Amelung, F. (2014). Gravity changes and deformation at Kīlauea Volcano, Hawaii, associated with summit eruptive activity, 2009–2012: Gravity changes at Kīlauea Volcano. *Journal of Geophysical Research: Solid Earth*, *119*, 7288–7305. https://doi.org/10.1002/2014JB011506

Baker, T. F., & Bos, M. (2003). Validating Earth and ocean tide models using tidal gravity measurements. *Geophysical Journal International*, *152*(2), 468–485. https://doi.org/10.1046/j.1365-246X.2003.01863.x

Banka, D., & Crossley, D. (1999). Noise levels of superconducting gravimeters at seismic frequencies. *Geophysical Journal International*, *139*(1), 87–97. https://doi.org/10.1046/j.1365-246X.1999.00913.x

Barbot, S., & Fialko, Y. (2010). A unified continuum representation of post-seismic relaxation mechanisms: Semi-analytic models of afterslip, poroelastic rebound and viscoelastic flow: Semi-analytic models of postseismic transient. *Geophysical Journal International*, *182*(3), 1124–1140. https://doi.org/10.1111/j.1365-246X.2010.04678.x

Battaglia, M. (1999). Magma intrusion beneath Long Valley Caldera confirmed by temporal changes in gravity. *Science*, *285*(5436), 2119–2122. https://doi.org/10.1126/science.285.5436.2119

Battaglia, M., Gottsmann, J., Carbone, D., & Fernández, J. (2008). 4D volcano gravimetry. *Geophysics*, *73*(6), WA3–WA18. https://doi.org/10.1190/1.2977792

Battaglia, M., Segall, P., & Roberts, C. (2003). The mechanics of unrest at Long Valley Caldera, California. 2. Constraining the nature of the source using geodetic and micro-gravity data. *Journal of Volcanology and Geothermal Research*, *127*(3–4), 219–245. https://doi.org/10.1016/S0377-0273(03)00171-9

Battaglia, M., Troise, C., Obrizzo, F., Pingue, F., & De Natale, G. (2006). Evidence for fluid migration as the source of deformation at Campi Flegrei caldera (Italy). *Geophysical Research Letters*, *33*, L01307. https://doi.org/10.1029/2005GL024904

Bear, J., & Corapcioglu, M. Y. (1981). Mathematical model for regional land subsidence due to pumping: 1. Integrated aquifer subsidence equations based on vertical displacement only. *Water Resources Research*, *17*(4), 937–946. https://doi.org/10.1029/WR017i004p00937

Beauduin, R., Lognonné, P., Montagner, J.-P., Cacho, S., Karczewski, J. F., & Morand, M. (1996). The effects of the atmospheric pressure changes on seismic signals or how to improve the quality of a station. *Bulletin of the Seismological Society of America*, *86*(6), 1760–1769.

Beavan, J., Wallace, L., Fletcher, H., & Douglas, A. (2007). Slow slip events on the Hikurangi subduction interface, New Zealand. In P. Tregoning & C. Rizos (Eds.), *Dynamic Planet* (Vol. 130, pp. 438–444). Berlin, Heidelberg: Springer Berlin Heidelberg. https://doi.org/10.1007/978-3-540-49350-1_64

Bedford, J., Moreno, M., Li, S., Oncken, O., Baez, J. C., Bevis, M., … Lange, D. (2016). Separating rapid relocking, afterslip, and viscoelastic relaxation: An application of the postseismic straightening method to the Maule 2010 cGPS. *Journal of Geophysical Research: Solid Earth*, *121*, 7618–7638. https://doi.org/10.1002/2016JB013093

Bent, A. (2013). Global Seismograph Network (GSN). In P. T. Bobrowsky (Ed.), *Encyclopedia of Natural Hazards* (pp. 417–418). Dordrecht, Netherlands: Springer. https://doi.org/10.1007/978-1-4020-4399-4_161

Beroza, G. C., & Jordan, T. H. (1990). Searching for slow and silent earthquakes using free oscillations. *Journal of Geophysical Research*, *95*(B3), 2485. https://doi.org/10.1029/JB095iB03p02485

Biolcati, E., Svitlov, S., & Germak, A. (2012). Self-attraction effect and correction on three absolute gravimeters. *Metrologia*, *49*(4), 560–566. https://doi.org/10.1088/0026-1394/49/4/560

Bizouard, C., Remus, F., Lambert, S. B., Seoane, L., & Gambis, D. (2011). The Earth's variable Chandler wobble. *Astronomy & Astrophysics*, *526*, A106. https://doi.org/10.1051/0004-6361/201015894

Blair, D., Ju, L., Zhao, C., Wen, L., Chu, Q., Fang, Q., … Ni, W.-T. (2015). Gravitational wave astronomy: The current status. *Science China - Physics Mechanics & Astronomy*, *58*(12). https://doi.org/10.1007/s11433-015-5748-6

Block, B., & Moore, R. D. (1966). Measurements in the Earth mode frequency range by an electrostatic sensing and feedback gravimeter. *Journal of Geophysical Research*, *71*(18), 4361–4375. https://doi.org/10.1029/JZ071i018p04361

Boerez, J., Hinderer, J., Jones, M. A., & Rivera, L. (2012). Analysis and filtering of the effect of tides on the hydrostatic levelling systems at CERN. *Survey Review*, *44*(327), 256–264. https://doi.org/10.1179/1752270611Y.0000000031

Bonvalot, S., Diament, M., & Gabalda, G. (1998). Continuous gravity recording with Scintrex CG-3M meters: A promising tool for monitoring active zones. *Geophysical Journal International*, *135*(2), 470–494. https://doi.org/10.1046/j.1365-246X.1998.00653.x

Bonvalot, S., Remy, D., Deplus, C., Diament, M., & Gabalda, G. (2008). Insights on the March 1998 eruption at Piton de la Fournaise volcano (La Réunion) from microgravity monitoring. *Journal of Geophysical Research*, *113*, B05407. https://doi.org/10.1029/2007JB005084

Bos, M., & Baker, T. F. (2005). An estimate of the errors in gravity ocean tide loading computations. *Journal of Geodesy*, *79*(1–3), 50–63. https://doi.org/10.1007/s00190-005-0442-5

Bos, M., & Scherneck, H.-G. (2017). Free ocean tide loading provider. Retrieved from http://holt.oso.chalmers.se/loading/

Bouguer, P. (1749). *La Figure De La Terre*. Paris: Jombert. Retrieved from http://echo.mpiwg-berlin.mpg.de/ECHOdocuView?url=/permanent/library/W9U4D55Q/pageimg&viewMode=index&mode=imagepath

Boy, J.-P. (2005). Precise evaluation of atmospheric loading effects on Earth's time-variable gravity field. *Journal of Geophysical Research*, *110*, B08412. https://doi.org/10.1029/2002JB002333

Boy, J.-P., Gegout, P., & Hinderer, J. (2002). Reduction of surface gravity data from global atmospheric pressure loading. *Geophysical Journal International*, *149*(2), 534–545. https://doi.org/10.1046/j.1365-246X.2002.01667.x

Boy, J.-P., & Hinderer, J. (2006). Study of the seasonal gravity signal in superconducting gravimeter data. *Journal of Geodynamics*, *41*(1–3), 227–233. https://doi.org/10.1016/j.jog.2005.08.035

Boy, J.-P., Longuevergne, L., Boudin, F., Jacob, T., Lyard, F., Llubes, M., … Esnoult, M.-F. (2009). Modelling atmospheric and induced non-tidal oceanic loading contributions to surface gravity and tilt measurements. *Journal of Geodynamics*, *48*(3–5), 182–188. https://doi.org/10.1016/j.jog.2009.09.022

Boyarko, D. C., & Brudzinski, M. R. (2010). Spatial and temporal patterns of nonvolcanic tremor along the southern Cascadia subduction zone. *Journal of Geophysical Research*, *115,* B00A22. https://doi.org/10.1029/2008JB006064

Brady, J. L., Hare, J. L., Ferguson, J. F., Seibert, J. E., Klopping, F. J., Chen, T., & Niebauer, T. (2010). Results of the world's first 4D microgravity surveillance of a waterflood—Prudhoe Bay, Alaska. *Methods and Applications in Reservoir Geophysics*, *15*, 475–481.

Branca, S., Carbone, D., & Greco, F. (2003). Intrusive mechanism of the 2002 NE-rift eruption at Mt. Etna (Italy) inferred through continuous microgravity data and volcanological evidences. *Geophysical Research Letters*, *30*(20), 2077. https://doi.org/10.1029/2003GL018250

Broerse, T., Riva, R., Simons, W., Govers, R., & Vermeersen, B. (2015). Postseismic GRACE and GPS observations indicate a rheology contrast above and below the Sumatra slab. *Journal of Geophysical Research: Solid Earth*, *120*, 5343–5361. https://doi.org/10.1002/2015JB011951

Broerse, T., Vermeersen, B., Riva, R. E. M., & van der Wal, W. (2011). Ocean contribution to co-seismic crustal deformation and geoid anomalies: Application to the 2004 December 26 Sumatra–Andaman earthquake. *Earth and Planetary Science Letters*, *305*(3–4), 341–349. https://doi.org/10.1016/j.epsl.2011.03.011

Camelbeeck, T., Van Camp, M., Jongmans, D., Francis, O., & van Dam, T. (2002). Comment on "Nature of the recent vertical ground movements inferred from high-precision leveling data in an intraplate setting: NE Ardenne, Belgium" by A. Demoulin and A. Collignon. *Journal of Geophysical Research*, *107*(B11), ETG 6-1–ETG 6-6. https://doi.org/10.1029/2001JB000397

Camelbeeck, T., Vanneste, K., Alexandre, P., Verbeeck, K., Petermans, T., Rosset, P., … Van Camp, M. (2007). Relevance of active faulting and seismicity studies to assessments of long-term earthquake activity and maximum magnitude in intraplate northwest Europe, between the Lower Rhine Embayment and the North Sea. *Geological Society of America Special Papers*, *425*, 193–224.

Carbone, D. (2003). Bulk processes prior to the 2001 Mount Etna eruption, highlighted through microgravity studies. *Journal of Geophysical Research*, *108*(B12), 2556. https://doi.org/10.1029/2003JB002542

Carbone, D., Budetta, G., Greco, F., & Zuccarello, L. (2007). A data sequence acquired at Mt. Etna during the 2002–2003 eruption highlights the potential of continuous gravity observations as a tool to monitor and study active volcanoes. *Journal of Geodynamics*, *43*(2), 320–329. https://doi.org/10.1016/j.jog.2006.09.012

Carbone, D., D'Amico, S., Musumeci, C., & Greco, F. (2009). Comparison between the 1994–2006 seismic and gravity data from Mt. Etna: New insight into the long-term behavior of a complex volcano. *Earth and Planetary Science Letters*, *279*(3–4), 282–292. https://doi.org/10.1016/j.epsl.2009.01.007

Carbone, D., & Greco, F. (2007). Review of microgravity observations at Mt. Etna: A powerful tool to monitor and study active volcanoes. *Pure and Applied Geophysics*, *164*(4), 769–790. https://doi.org/10.1007/s00024-007-0194-7

Carbone, D., Poland, M., Diament, M., & Greco, F. (2017). The added value of time-variable microgravimetry to the understanding of how volcanoes work. *Earth-Science Reviews*, *169*, 146–179. https://doi.org/10.1016/j.earscirev.2017.04.014

Carbone, D., Zuccarello, L., Saccorotti, G., & Greco, F. (2006). Analysis of simultaneous gravity and tremor anomalies observed during the 2002–2003 Etna eruption. *Earth and Planetary Science Letters*, *245*(3–4), 616–629. https://doi.org/10.1016/j.epsl.2006.03.055

Cashman, K. V., Sparks, R. S. J., & Blundy, J. D. (2017). Vertically extensive and unstable magmatic systems: A unified view of igneous processes. *Science*, *355*(6331), eaag3055. https://doi.org/10.1126/science.aag3055

Castelvecchi, D. (2016). Gravitational waves: 6 cosmic questions they can tackle. *Nature*. https://doi.org/10.1038/nature.2016.19337

Chapman, D. S., Sahm, E., & Gettings, P. (2008). Monitoring aquifer recharge using repeated high-precision gravity measurements: A pilot study in South Weber, Utah. *Geophysics*, *73*(6), WA83–WA93. https://doi.org/10.1190/1.2992507

Chen, S., Liu, M., Xing, L., Xu, W., Wang, W., Zhu, Y., & Li, H. (2016). Gravity increase before the 2015 M_w 7.8 Nepal earthquake: Gravity change before earthquake. *Geophysical Research Letters*, *43*, 111–117. https://doi.org/10.1002/2015GL066595

Chen, X., Kroner, C., Sun, H., Abe, M., Zhou, J., Yan, H., & Wziontek, H. (2009). Determination of gravimetric parameters of the gravity pole tide using observations recorded with superconducting gravimeters. *Journal of Geodynamics*, *48*(3–5), 348–353. https://doi.org/10.1016/j.jog.2009.09.020

Chin, E. J., Lee, K. T., Winterflood, J., Ju, L., & Blair, D. G. (2005). Low frequency vertical geometric anti-spring vibration isolators. *Physics Letters A*, *336*(2–3), 97–105. https://doi.org/10.1016/j.physleta.2005.01.013

Christiansen, L., Binning, P. J., Rosbjerg, D., Andersen, O. B., & Bauer-Gottwein, P. (2011). Using time-lapse gravity for groundwater model calibration: An application to alluvial aquifer storage. *Water Resources Research*, *47*, W06503. https://doi.org/10.1029/2010WR009859

Christiansen, L., Lund, S., Andersen, O. B., Binning, P. J., Rosbjerg, D., & Bauer-Gottwein, P. (2011). Measuring gravity change caused by water storage variations: Performance assessment under controlled conditions. *Journal of Hydrology*, *402*(1–2), 60–70. https://doi.org/10.1016/j.jhydrol.2011.03.004

Christopher, T. E., Blundy, J., Cashman, K., Cole, P., Edmonds, M., Smith, P. J., … Stinton, A. (2015). Crustal-scale degassing due to magma system destabilization and magma-gas decoupling at Soufrière Hills Volcano, Montserrat. *Geochemistry, Geophysics, Geosystems*, *16*, 2797–2811. https://doi.org/10.1002/2015GC005791

Cook, A. H. (1965a). A new absolute determination of the acceleration due to gravity at the National Physical Laboratory. *Nature*, *208*(5007), 279–279. https://doi.org/10.1038/208279a0

Cook, A. H. (1965b). The absolute determination of the acceleration due to gravity. *Metrologia*, *1*(3), 84–114. https://doi.org/10.1088/0026-1394/1/3/003

Coughlin, M., Mukund, N., Harms, J., Driggers, J., Adhikari, R., & Mitra, S. (2016). Towards a first design of a Newtonian-noise cancellation system for advanced LIGO. *Classical and Quantum Gravity*, *33*(24), 244001. https://doi.org/10.1088/0264-9381/33/24/244001

Creutzfeldt, B., Güntner, A., Klügel, T., & Wziontek, H. (2008). Simulating the influence of water storage changes on the superconducting gravimeter of the Geodetic Observatory Wettzell, Germany. *Geophysics*, *73*(6), WA95–WA104. https://doi.org/10.1190/1.2992508

Creutzfeldt, B., Güntner, A., Thoss, H., Merz, B., & Wziontek, H. (2010). Measuring the effect of local water storage changes on in situ gravity observations: Case study of the Geodetic Observatory Wettzell, Germany. *Water Resources Research*, *46*, W08531. https://doi.org/10.1029/2009WR008359

Creutzfeldt, B., Güntner, A., Wziontek, H., & Merz, B. (2010). Reducing local hydrology from high-precision gravity measurements: A lysimeter-based approach. *Geophysical Journal International*, *183*(1), 178–187. https://doi.org/10.1111/j.1365-246X.2010.04742.x

Creutzfeldt, B., Troch, P. A., Güntner, A., Ferré, T. P. A., Graeff, T., & Merz, B. (2014). Storage-discharge relationships at different catchment scales based on local high-precision gravimetry. *Hydrological Processes*, *28*(3), 1465–1475. https://doi.org/10.1002/hyp.9689

Crossley, D., & Hinderer, J. (2009). A review of the GGP network and scientific challenges. *Journal of Geodynamics*, *48*(3–5), 299–304. https://doi.org/10.1016/j.jog.2009.09.019

Crossley, D., Hinderer, J., & Riccardi, U. (2013). The measurement of surface gravity. *Reports on Progress in Physics*, *76*(4), 046101. https://doi.org/10.1088/0034-4885/76/4/046101

D'Agostino, G., Desogus, S., Germak, A., Origlia, C., Quagliotti, D., Berrino, G., … Ricciardi, G. (2008). The new IMGC-02 transportable absolute gravimeter: Measurement apparatus and applications in geophysics and volcanology. *Annals of Geophysics*, *51*(1), 39–49. Retrieved from http://www.earth-prints.org/handle/2122/4981

Dang, V. K., Doubre, C., Weber, C., Gourmelen, N., & Masson, F. (2014). Recent land subsidence caused by the rapid urban development in the Hanoi region (Vietnam) using ALOS InSAR data. *Natural Hazards and Earth System Sciences*, *14*(3), 657–674. https://doi.org/10.5194/nhess-14-657-2014

Davis, K., Li, Y., & Batzle, M. (2008). Time-lapse gravity monitoring: A systematic 4D approach with application to aquifer storage and recovery. *Geophysics*, *73*(6), WA61–WA69. https://doi.org/10.1190/1.2987376

Davis, P., & Berger, J. (2007). Calibration of the Global Seismographic Network using tides. *Seismological Research Letters*, *78*(4), 454–459. https://doi.org/10.1785/gssrl.78.4.454

De Linage, C., Hinderer, J., & Rogister, Y. (2007). A search for the ratio between gravity variation and vertical displacement due to a surface load: Ratio between gravity variation and vertical displacement due to a surface load. *Geophysical Journal International*, *171*(3), 986–994. https://doi.org/10.1111/j.1365-246X.2007.03613.x

de Viron, O., Panet, I., Mikhailov, V., Van Camp, M., & Diament, M. (2008). Retrieving earthquake signature in grace gravity solutions. *Geophysical Journal International*, *174*(1), 14–20. https://doi.org/10.1111/j.1365-246X.2008.03807.x

Debeglia, N., & Dupont, F. (2002). Some critical factors for engineering and environmental microgravity investigations. *Journal of Applied Geophysics*, *50*(4), 435–454. https://doi.org/10.1016/S0926-9851(02)00194-5

Debs, J. E., Hardman, K. S., Altin, P. A., McDonald, G., Close, J. D., & Robins, N. P. (2013). From apples to atoms: Measuring gravity with ultra cold atomic test masses. *Preview*, *2013*(164), 30–33.

Dehant, V., Defraigne, P., & Wahr, J. (1999). Tides for a convective Earth. *Journal of Geophysical Research*, *104*(B1), 1035–1058. https://doi.org/10.1029/1998JB900051

Deichmann, N., & Giardini, D. (2009). Earthquakes induced by the stimulation of an enhanced geothermal system below Basel (Switzerland). *Seismological Research Letters*, *80*(5), 784–798. https://doi.org/10.1785/gssrl.80.5.784

Deville, S. (2013). *Caractérisation de la zone non saturée des karsts par la gravimétrie et l'hydrogéologie* (PhD thesis). Université Montpellier II-Sciences et Techniques du Languedoc. Retrieved from https://tel.archives-ouvertes.fr/tel-00829346/

Deville, S., Jacob, T., Chery, J., & Champollion, C. (2013). On the impact of topography and building mask on time varying gravity due to local hydrology. *Geophysical Journal International*, *192*(1), 82–93. https://doi.org/10.1093/gji/ggs007

Ding, H., & Shen, W.-B. (2013). Search for the Slichter modes based on a new method: Optimal sequence estimation. *Journal of Geophysical Research: Solid Earth*, *118*, 5018–5029. https://doi.org/10.1002/jgrb.50344

Dixon, T. H., Amelung, F., Ferretti, A., Novali, F., Rocca, F., Dokka, R., … Whitman, D. (2006). Space geodesy: Subsidence and flooding in New Orleans. *Nature*, *441*(7093), 587–588. https://doi.org/10.1038/441587a

Djamour, Y., Vernant, P., Bayer, R., Nankali, H. R., Ritz, J.-F., Hinderer, J., … Khorrami, F. (2010). GPS and gravity constraints on continental deformation in the Alborz mountain range, Iran: GPS and gravity measurements in Alborz. *Geophysical Journal International*, *183*(3), 1287–1301. https://doi.org/10.1111/j.1365-246X.2010.04811.x

Dong, S., Samsonov, S., Yin, H., Ye, S., & Cao, Y. (2014). Time-series analysis of subsidence associated with rapid urbanization in Shanghai, China measured with SBAS InSAR method. *Environmental Earth Sciences*, *72*(3), 677–691. https://doi.org/10.1007/s12665-013-2990-y

Doornhof, D., Kristiansen, T. G., Nagel, N. B., Pattillo, P. D., & Sayers, C. (2006). Compaction and subsidence. *Oilfield Review*, *18*(3), 50–68.

Dragert, H., Wang, K., & Rogers, G. (2004). Geodetic and seismic signatures of episodic tremor and slip in the northern Cascadia subduction zone. *Earth, Planets and Space*, *56*(12), 1143–1150.

Ducarme, B. (2009). Limitations of high precision tidal predictions. *Bulletin d'Information Marées Terrestres*, *145*, 11,663–11,677.

Ducarme, B., Pálinkáš, V., Meurers, B., Xiaoming, C., & Vaľko, M. (2014). On the comparison of tidal gravity parameters with tidal models in central Europe. *Journal of Geodynamics*, *80*, 12–19. https://doi.org/10.1016/j.jog.2014.02.011

Ducarme, B., & Somerhausen, A. (1997). Tidal gravity recording at Brussels with a SCINTREX CG-3M gravity meter. *Bulletin d'Information Marées Terrestres*, *126*, 9611–9634.

Dykowski, P., Krynski, J., & Sekowski, M. (2014). Testing the suitability of the A10-020 absolute gravimeter for the establishment of new gravity control in Poland. In U. Marti (Ed.), *Gravity, Geoid and Height Systems* (Vol. 141, pp. 11–17). Cham: Springer International Publishing. https://doi.org/10.1007/978-3-319-10837-7_2

Dziewonski, A. (1971). Overtones of free oscillations and the structure of the Earth's interior. *Science*, *172*(3990), 1336–1338. https://doi.org/10.1126/science.172.3990.1336

Dziewonski, A., & Anderson, D. L. (1981). Preliminary reference Earth model. *Physics of the Earth and Planetary Interiors*, *25*(4), 297–356. https://doi.org/10.1016/0031-9201(81)90046-7

Dzurisin, D. (2003). A comprehensive approach to monitoring volcano deformation as a window on the eruption cycle. *Reviews of Geophysics*, *41*(1), 1001. https://doi.org/10.1029/2001RG000107

Einarsson, P., & Brandsdottir, B. (1978). *Seismological evidence for lateral magma intrusion during the July 1978 deflation of the Krafla volcano in NE-Iceland* (Technical Report No. UI-79-9-7, 890964) (p. 14). Reykjavik: University of Iceland. https://doi.org/10.2172/890964

Ergintav, S., Doğan, U., Gerstenecker, C., Çakmak, R., Belgen, A., Demirel, H., … Reilinger, R. (2007). A snapshot (2003–2005) of the 3D postseismic deformation for the 1999, M_w = 7.4 İzmit earthquake in the Marmara Region, Turkey, by first results of joint gravity and GPS monitoring. *Journal of Geodynamics*, *44*(1–2), 1–18. https://doi.org/10.1016/j.jog.2006.12.005

Faller, J. (1965). Results of an absolute determination of the acceleration of gravity. *Journal of Geophysical Research*, *70*(16), 4035–4038. https://doi.org/10.1029/JZ070i016p04035

Faller, J. (1967). Precision measurement of the acceleration of gravity: Measurements of *g* have always made maximum use of the available technology in measurement of length and time. *Science*, *158*(3797), 60–67. https://doi.org/10.1126/science.158.3797.60

Faller, J., & Marson, I. (1988). Ballistic methods of measuring *g*—The direct free-fall and symmetrical rise-and-fall methods compared. *Metrologia*, *25*(1), 49–55. https://doi.org/10.1088/0026-1394/25/1/008

Ferguson, J. F., Klopping, F. J., Chen, T., Seibert, J. E., Hare, J. L., & Brady, J. L. (2008). The 4D microgravity method for waterflood surveillance: Part 3—4D absolute microgravity surveys at Prudhoe Bay, Alaska. *Geophysics*, *73*(6), WA163–WA171. https://doi.org/10.1190/1.2992510

Ferré, T., Bentley, L., Binley, A., Linde, N., Kemna, A., Singha, K., … Minsley, B. (2009). Critical steps for the continuing advancement of hydrogeophysics. *Eos, Transactions American Geophysical Union*, *90*(23), 200. https://doi.org/10.1029/2009EO230004

Fischer, J., & Ullrich, J. (2016). The new system of units. *Nature Physics*, *12*(1), 4–7. https://doi.org/10.1038/nphys3612

Fleming, K., Martinec, Z., & Hagedoorn, J. (2004). Geoid displacement about Greenland resulting from past and present-day mass changes in the Greenland Ice Sheet. *Geophysical Research Letters*, *31*, L06617. https://doi.org/10.1029/2004GL019469

Flury, J., Peters, T., Schmeer, M., Timmen, L., Wilmes, H., & Falk, R. (2007). Precision gravimetry in the new Zugspitze gravity meter calibration system. *Harita Dergisi*, *18*, 401–406.

Fores, B., Champollion, C., Le Moigne, N., Bayer, R., & Chéry, J. (2017). Assessing the precision of the iGrav superconducting gravimeter for hydrological models and karstic hydrological process identification. *Geophysical Journal International*, *208*(1), 269–280. https://doi.org/10.1093/gji/ggw396

Fores, B., Champollion, C., Moigne, N. L., & Chery, J. (2016). Impact of ambient temperature on spring-based relative gravimeter measurements. *Journal of Geodesy*, *91*(3), 269–277. https://doi.org/10.1007/s00190-016-0961-2

Förste, C., Bruinsma, S., Abrikosov, O., Flechtner, F., Marty, J.-C., Lemoine, J.-M., … Biancale, R. (2014). EIGEN-6C4—The latest combined global gravity field model including GOCE data up to degree and order 1949 of GFZ Potsdam and GRGS Toulouse. In *EGU General Assembly Conference Abstracts* (Vol. 16, p. 3707). Retrieved from http://adsabs.harvard.edu/abs/2014EGUGA..16.3707F

Francis, O., Baumann, H., Ullrich, C., Castelein, S., Van Camp, M., Sousa, M. A. D., … Ellis, B. (2015). CCM. G-K2 key comparison. *Metrologia*, *52*(1A), 07009.

Francis, O., Baumann, H., Volarik, T., Rothleitner, C., Klein, G., Seil, M., … Billson, R. (2013). The European comparison af gbsolute Gravimeters 2011 (ECAG-2011) in Walferdange, Luxembourg: Results and recommendations. *Metrologia*, *50*(3), 257–268. https://doi.org/10.1088/0026-1394/50/3/257

Francis, O., & Hendrickx, M. (2001). Calibration of the LaCoste-Romberg 906 by comparison with the Superconducting Gavimeter C021 in Membach (Belgium). *Journal of Geological Society of Japan*, *47*(1), 16–21.

Francis, O., Niebauer, T., Sasagawa, G., Klopping, F., & Gschwind, J. (1998). Calibration of a superconducting gravimeter by comparison with an absolute gravimeter FG5 in Boulder. *Geophysical Research Letters*, *25*(7), 1075–1078. https://doi.org/10.1029/98GL00712

Francis, O., Rothleitner, C., & Jiang, Z. (2014). Accurate determination of the Earth tidal parameters at the BIPM to support the Watt Balance Project. In C. Rizos & P. Willis (Eds.), *Earth on the Edge: Science for a Sustainable Planet* (Vol. 139, pp. 319–324). Berlin, Heidelberg: Springer Berlin Heidelberg. https://doi.org/10.1007/978-3-642-37222-3_42

Francis, O., & van Dam, T. (2002). Evaluation of the precision of using absolute gravimeters to calibrate superconducting gravimeters. *Metrologia*, *39*(5), 485.

Francis, O., van Dam, T., Amalvict, M., de Andrade Sousa, M., Bilker, M., Billson, R., … Wilmes, H. (2005). Results of the international comparison of absolute gravimeters in Walferdange (Luxembourg) of November 2003. In *Gravity, Geoid and Space Missions* (pp. 272–275). Berlin, Heidelberg: Springer. Retrieved from http://link.springer.com/chapter/10.1007/3-540-26932-0_47

Francis, O., van Dam, T., Germak, A., Amalvict, M., Bayer, R., Bilker-Koivula, M., … Xing, L. (2010). Results of the European comparison of absolute gravimeters in Walferdange (Luxembourg) of November 2007. In *Gravity, Geoid and Earth Observation* (pp. 31–35). Berlin, Heidelberg: Springer. Retrieved from http://link.springer.com/chapter/10.1007/978-3-642-10634-7_5

Fratepietro, F., Baker, T. F., Williams, S. D. P., & Van Camp, M. (2006). Ocean loading deformations caused by storm surges on the northwest European shelf. *Geophysical Research Letters*, *33*, L06317. https://doi.org/10.1029/2005GL025475

Freier, C., Hauth, M., Schkolnik, V., Leykauf, B., Schilling, M., Wziontek, H., … Peters, A. (2016). Mobile quantum gravity sensor with unprecedented stability. *Journal of Physics: Conference Series*, *723*, 012050. https://doi.org/10.1088/1742-6596/723/1/012050

Fuchs, M. J., Bouman, J., Broerse, T., Visser, P., & Vermeersen, B. (2013). Observing coseismic gravity change from the Japan Tohoku-Oki 2011 earthquake with GOCE gravity gradiometry. *Journal of Geophysical Research: Solid Earth*, *118*, 5712–5721. https://doi.org/10.1002/jgrb.50381

Fulton, P. M., & Brodsky, E. E. (2016). In situ observations of earthquake-driven fluid pulses within the Japan Trench plate boundary fault zone. *Geology*, *44*(10), 851–854. https://doi.org/10.1130/G38034.1

Furuya, M., Okubo, S., Sun, W., Tanaka, Y., Oikawa, J., Watanabe, H., & Maekawa, T. (2003). Spatiotemporal gravity changes at Miyakejima Volcano, Japan: Caldera collapse, explosive eruptions and magma movement. *Journal of Geophysical Research*, *108*(B4), 2219. https://doi.org/10.1029/2002JB001989

Gambolati, G., & Teatini, P. (2015). Geomechanics of subsurface water withdrawal and injection. *Water Resources Research*, *51*, 3922–3955. https://doi.org/10.1002/2014WR016841

Gasperikova, E., & Hoversten, G. M. (2008). Gravity monitoring of CO_2 movement during sequestration: Model studies. *Geophysics*, *73*(6), WA105–WA112. https://doi.org/10.1190/1.2985823

Geng, J., Williams, S. D. P., Teferle, F. N., & Dodson, A. H. (2012). Detecting storm surge loading deformations around the southern North Sea using subdaily GPS: *Storm surge loading*. *Geophysical Journal International*, *191*(2), 569–578. https://doi.org/10.1111/j.1365-246X.2012.05656.x

Gettings, P., Chapman, D. S., & Allis, R. (2008). Techniques, analysis, and noise in a Salt Lake Valley 4D gravity experiment. *Geophysics*, *73*(6), WA71–WA82. https://doi.org/10.1190/1.2996303

Ghosh, A., Vidale, J. E., Sweet, J. R., Creager, K. C., & Wech, A. G. (2009). Tremor patches in Cascadia revealed by seismic array analysis. *Geophysical Research Letters*, *36*, L17316. https://doi.org/10.1029/2009GL039080

Giacomo, P. (1984). News from the BIPM. *Metrologia*, *20*(1), 25. https://doi.org/10.1088/0026-1394/20/1/005

Gillot, P., Francis, O., Landragin, A., Pereira Dos Santos, F., & Merlet, S. (2014). Stability comparison of two absolute gravimeters: Optical versus atomic interferometers. *Metrologia*, *51*(5), L15. https://doi.org/10.1088/0026-1394/51/5/L15

Goodkind, J. M. (1999). The superconducting gravimeter. *Review of Scientific Instruments*, *70*(11), 4131–4152. https://doi.org/10.1063/1.1150092

Gottsmann, J., Carniel, R., Coppo, N., Wooller, L., Hautmann, S., & Rymer, H. (2007). Oscillations in hydrothermal systems as a source of periodic unrest at caldera volcanoes: Multiparameter insights from Nisyros, Greece. *Geophysical Research Letters*, *34*, L07307. https://doi.org/10.1029/2007GL029594

Gottsmann, J., De Angelis, S., Fournier, N., Van Camp, M., Sacks, S., Linde, A., & Ripepe, M. (2011). On the geophysical fingerprint of vulcanian explosions. *Earth and Planetary Science Letters*, *306*(1–2), 98–104. https://doi.org/10.1016/j.epsl.2011.03.035

Gottsmann, J., Rymer, H., & Wooller, L. K. (2005). On the interpretation of gravity variations in the presence of active hydrothermal systems: Insights from the Nisyros Caldera, Greece. *Geophysical Research Letters*, *32*, L23310. https://doi.org/10.1029/2005GL024061

Greco, F., Currenti, G., Del Negro, C., Napoli, R., Budetta, G., Fedi, M., & Boschi, E. (2010). Spatiotemporal gravity variations to look deep into the southern flank of Etna volcano. *Journal of Geophysical Research*, *115*, B11411. https://doi.org/10.1029/2009JB006835

Greff-Lefftz, M., & Legros, H. (1999). Core rotational dynamics and geological events. *Science*, *286*(5445), 1707–1709. https://doi.org/10.1126/science.286.5445.1707

Gross, R. (2007). Earth rotation variations—Long period. In *Volume 3: Geodesy* (Vol. 3, pp. 239–294). Amsterdam: Elsevier. https://doi.org/10.1016/B978-044452748-6/00057-2

Gubbins, D., & Herrero-Bervera, E. (Eds.) (2007). *Encyclopedia of Geomagnetism and Paleomagnetism*. Dordrecht: Springer.

Gudmundsson, A. (1995). Infrastructure and mechanics of volcanic systems in Iceland. *Journal of Volcanology and Geothermal Research*, *64*(1–2), 1–22. https://doi.org/10.1016/0377-0273(95)92782-Q

Gudmundsson, A. (1998). Magma chambers modeled as cavities explain the formation of rift zone central volcanoes and their eruption and intrusion statistics. *Journal of Geophysical Research*, *103*(B4), 7401–7412. https://doi.org/10.1029/97JB03747

Gudmundsson, M., Jónsdóttir, K., Hooper, A., Holohan, E. P., Halldórsson, S. A., Ófeigsson, B. G., … Aiuppa, A. (2016). Gradual caldera collapse at Bárdarbunga volcano, Iceland, regulated by lateral magma outflow. *Science*, *353*(6296), aaf8988. https://doi.org/10.1126/science.aaf8988

Güntner, A., Reich, M., Mikolaj, M., Creutzfeldt, B., Schroeder, S., & Wziontek, H. (2017). Landscape-scale water balance monitoring with an iGrav superconducting gravimeter in a field enclosure. *Hydrology and Earth System Sciences Discussions*, *21*, 1–28. https://doi.org/10.5194/hess-2017-103

Han, S.-C. (2006). Crustal dilatation observed by GRACE after the 2004 Sumatra-Andaman earthquake. *Science*, *313*(5787), 658–662. https://doi.org/10.1126/science.1128661

Han, S.-C., Sauber, J., & Pollitz, F. (2016). Postseismic gravity change after the 2006–2007 great earthquake doublet and constraints on the asthenosphere structure in the central Kuril Islands: Gravity change of the Kuril earthquakes. *Geophysical Research Letters*, *43*, 3169–3177. https://doi.org/10.1002/2016GL068167

Harms, J., & Venkateswara, K. (2016). Newtonian-noise cancellation in large-scale interferometric GW detectors using seismic tiltmeters. *Classical and Quantum Gravity*, *33*(23), 234001.

Harpalani, S., & Mitra, A. (2010). Impact of CO_2 injection on flow behavior of coalbed methane reservoirs. *Transport in Porous Media*, *82*(1), 141–156. https://doi.org/10.1007/s11242-009-9475-1

Hartmann, T., & Wenzel, H.-G. (1995). The HW95 tidal potential catalogue. *Geophysical Research Letters*, *22*(24), 3553–3556. https://doi.org/10.1029/95GL03324

Hauth, M., Freier, C., Schkolnik, V., Senger, A., Schmidt, M., & Peters, A. (2013). First gravity measurements using the mobile atom interferometer GAIN. *Applied Physics B*, *113*(1), 49–55. https://doi.org/10.1007/s00340-013-5413-6

Hautmann, S., Gottsmann, J., Camacho, A. G., Van Camp, M., & Fournier, N. (2014). Chapter 14 continuous and campaign-style gravimetric investigations on Montserrat 2006 to 2009. *Geological Society, London, Memoirs*, *39*(1), 241–251. https://doi.org/10.1144/M39.14

Hector, B., & Hinderer, J. (2016). pyGrav, a Python-based program for handling and processing relative gravity data. *Computers & Geosciences*, *91*, 90–97. https://doi.org/10.1016/j.cageo.2016.03.010

Hector, B., Séguis, L., Hinderer, J., Cohard, J.-M., Wubda, M., Descloitres, M., … Boy, J.-P. (2015). Water storage changes as a marker for base flow generation processes in a tropical humid basement catchment (Benin): Insights from hybrid gravimetry. *Water Resources Research*, *51*, 8331–8361. https://doi.org/10.1002/2014WR015773

Hemmings, B., Gottsmann, J., Whitaker, F., & Coco, A. (2016). Investigating hydrological contributions to volcano monitoring signals: A time-lapse gravity example. *Geophysical Journal International*, *207*(1), 259–273.

Hensley, J. M., Peters, A., & Chu, S. (1999). Active low frequency vertical vibration isolation. *Review of Scientific Instruments*, *70*(6), 2735–2741. https://doi.org/10.1063/1.1149838

Herring, T. A., Melbourne, T. I., Murray, M. H., Floyd, M. A., Szeliga, W. M., King, R. W., … Wang, L. (2016). Plate boundary observatory and related networks: GPS data analysis methods and geodetic products: PBO data analysis methods and products. *Reviews of Geophysics*, *54*(4), 759–808. https://doi.org/10.1002/2016RG000529

Hinderer, J., Crossley, D., & Warburton, R. J. (2015). Superconducting gravimetry. In *Treatise on Geophysics* (pp. 59–115). Amsterdam: Elsevier. https://doi.org/10.1016/B978-0-444-53802-4.00062-2

Hinderer, J., Hector, B., Boy, J.-P., Riccardi, U., Rosat, S., Calvo, M., & Littel, F. (2014). A search for atmospheric effects on gravity at different time and space scales. *Journal of Geodynamics*, *80*, 50–57. https://doi.org/10.1016/j.jog.2014.02.001

Hinderer, J., Hector, B., Mémin, A., & Calvo, M. (2016). *Hybrid Gravimetry as a tool to Monitor Surface and Underground Mass Changes* (pp. 1–8). Berlin, Heidelberg: Springer. https://doi.org/10.1007/1345_2016_253

Hinze, W. J., Von Frese, R., & Saad, A. H. (2013). *Gravity and Magnetic Exploration: Principles, Practices, and Applications*. New York: Cambridge University Press.

Holland, A. A. (2013). Earthquakes triggered by hydraulic fracturing in south-central Oklahoma. *Bulletin of the Seismological Society of America*, *103*(3), 1784–1792. https://doi.org/10.1785/0120120109

Hu, X.-G., Liu, L.-T., Ducarme, B., Xu, H. J., & Sun, H.-P. (2007). Estimation of the pole tide gravimetric factor at the chandler period through wavelet filtering. *Geophysical Journal International*, *169*(3), 821–829. https://doi.org/10.1111/j.1365-246X.2007.03330.x

Hu, Y., Bürgmann, R., Banerjee, P., Feng, L., Hill, E. M., Ito, T., … Wang, K. (2016). Asthenosphere rheology inferred from observations of the 2012 Indian Ocean earthquake. *Nature*, *538*(7625), 368–372.

Hu, Y., Bürgmann, R., Freymueller, J. T., Banerjee, P., & Wang, K. (2014). Contributions of poroelastic rebound and a weak volcanic arc to the postseismic deformation of the 2011 Tohoku earthquake. *Earth, Planets and Space*, *66*(1), 106. https://doi.org/10.1186/1880-5981-66-106

Hui, L., Chongyang, S., Shaoan, S., Xiaoquan, W., Aimin, X., & Shaoming, L. (2011). Recent gravity changes in China Mainland. *Geodesy and Geodynamics*, *2*(1), 1–12. https://doi.org/10.3724/SP.J.1246.2011.00001

Hunt, T. (1995). Microgravity measurements at Wairakei Geothermal Field, New Zealand; a review of 30 years of data (1961–1991). In *Presented at the World Geothermal Congress 1995* (pp. 863–868). Antalya, Turkey: Water Resources Publications.

Hunt, T., & Bowyer, D. (2007). Reinjection and gravity changes at Rotokawa geothermal field, New Zealand. *Geothermics*, *36*(5), 421–435. https://doi.org/10.1016/j.geothermics.2007.07.004

Hutcheon, J. A., Chiolero, A., & Hanley, J. A. (2010). Random measurement error and regression dilution bias. *BMJ*, *340*(jun23 2), c2289–c2289. https://doi.org/10.1136/bmj.c2289

Ide, S., Beroza, G. C., Shelly, D. R., & Uchide, T. (2007). A scaling law for slow earthquakes. *Nature*, *447*(7140), 76–79. https://doi.org/10.1038/nature05780

Imanishi, Y. (2004). A network of superconducting gravimeters detects submicrogal coseismic gravity changes. *Science*, *306*(5695), 476–478. https://doi.org/10.1126/science.1101875

Imanishi, Y., Kokubo, K., & Tatehata, H. (2006). Effect of underground water on gravity observation at Matsushiro, Japan. *Journal of Geodynamics*, *41*(1–3), 221–226. https://doi.org/10.1016/j.jog.2005.08.031

Imanishi, Y., Nawa, K., & Takayama, H. (2013). Local hydrological processes in a fractured bedrock and the short-term effect on gravity at Matsushiro, Japan. *Journal of Geodynamics*, *63*, 62–68. https://doi.org/10.1016/j.jog.2012.10.001

Ishido, T., Sugihara, M., Pritchett, W., & Ariki, K. (1995). Feasibility study of reservoir monitoring using repeat precision gravity measurements at the Sumikawa geothermal field (pp. 853–858). Presented at the World Geothermal Congress, Firenze, Italy. Retrieved from https://www.geothermal-energy.org/pdf/IGAstandard/WGC/1995/2-Ishido.pdf

Ivins, E. R., James, T. S., Wahr, J. O., Schrama, E. J., Landerer, F. W., & Simon, K. M. (2013). Antarctic contribution to sea level rise observed by GRACE with improved GIA correction. *Journal of Geophysical Research: Solid Earth*, *118*, 3126–3141. https://doi.org/10.1002/jgrb.50208

Jacob, T., Bayer, R., Chery, J., Jourde, H., Moigne, N. L., Boy, J.-P., … Brunet, P. (2008). Absolute gravity monitoring of water storage variation in a karst aquifer on the larzac plateau (Southern France). *Journal of Hydrology*, *359*(1–2), 105–117. https://doi.org/10.1016/j.jhydrol.2008.06.020

Jacob, T., Bayer, R., Chery, J., & Le Moigne, N. (2010). Time-lapse microgravity surveys reveal water storage heterogeneity of a karst aquifer. *Journal of Geophysical Research*, *115*, B06402. https://doi.org/10.1029/2009JB006616

Jacob, T., Chery, J., Bayer, R., Le Moigne, N., Boy, J.-P., Vernant, P., & Boudin, F. (2009). Time-lapse surface to depth gravity measurements on a karst system reveal the dominant role of the epikarst as a water storage entity. *Geophysical Journal International*, *177*(2), 347–360. https://doi.org/10.1111/j.1365-246X.2009.04118.x

Joint Committee for Guides in Metrology (2012). *International vocabulary of metrology—Basic and general concepts and associated terms (VIM)* (No. JCGM 200:2012). Joint Committee for Guides in Metrology. Retrieved from http://www.bipm.org/jsp/fr/ViewCGPMResolution.jsp?CGPM=17&RES=1

Jentzsch, G. (2008). The automated Burris gravity meter—A new instrument using an old principle. In *Terrestrial Gravimetry: Static and Mobile Measurements (TG-SMM2007). Proceedings of the International Symposium. Elektropribor, St. Petersburg* (pp. 21–28). Retrieved from https://www.researchgate.net/profile/Gerhard_Jentzsch/publication/283095114_A_well-known_principle_in_a_new_gravimeter_The_automated_Burris_Gravity_Meter/links/56583e8508aeafc2aac2c051.pdf

Jiang, Y., Wdowinski, S., Dixon, T. H., Hackl, M., Protti, M., & Gonzalez, V. (2012). Slow slip events in Costa Rica detected by continuous GPS observations, 2002–2011. *Geochemistry, Geophysics, Geosystems*, *13*, Q04006. https://doi.org/10.1029/2012GC004058

Jiang, Z., Francis, O., Vitushkin, L., Palinkas, V., Germak, A., Becker, M., … Wilmes, H. (2011). Final report on the Seventh International Comparison of Absolute Gravimeters (ICAG 2005). *Metrologia*, *48*(5), 246–260. https://doi.org/10.1088/0026-1394/48/5/003

Jiang, Z., Pálinkáš, V., Arias, F. E., Liard, J., Merlet, S., Wilmes, H., … Robinson, I. (2012). The 8th International Comparison of Absolute Gravimeters 2009: The first key comparison (CCM.G-K1) in the field of absolute gravimetry. *Metrologia*, *49*(6), 666–684. https://doi.org/10.1088/0026-1394/49/6/666

Johnson, J. B. (1925). The Schottky effect in low frequency circuits. *Physical Review*, *26*(1), 71–85. https://doi.org/10.1103/PhysRev.26.71

Jones, C. E., An, K., Blom, R. G., Kent, J. D., Ivins, E. R., & Bekaert, D. (2016). Anthropogenic and geologic influences on subsidence in the vicinity of New Orleans, Louisiana: Subsidence of New Orleans. *Journal of Geophysical Research: Solid Earth*, *121*, 3867–3887. https://doi.org/10.1002/2015JB012636

Jónsson, S., Segall, P., Pedersen, R., & Björnsson, G. (2003). Post-earthquake ground movements correlated to pore-pressure transients. *Nature*, *424*(6945), 179–183. https://doi.org/10.1038/nature01776

Jousset, P., Dwipa, S., Beauducel, F., Duquesnoy, T., & Diament, M. (2000). Temporal gravity at Merapi during the 1993–1995 crisis: An insight into the dynamical behaviour of volcanoes. *Journal of Volcanology and Geothermal Research*, *100*(1), 289–320.

Karbon, M., Böhm, J., Meurers, B., & Schuh, H. (2014). Atmospheric corrections for superconducting gravimeters using operational weather models. In C. Rizos & P. Willis (Eds.), *Earth on the Edge: Science for a Sustainable Planet* (Vol. 139, pp. 421–427). Berlin, Heidelberg: Springer Berlin Heidelberg. https://doi.org/10.1007/978-3-642-37222-3_56

Kazama, T., Hayakawa, H., Higashi, T., Ohsono, S., Iwanami, S., Hanyu, T., … Shibuya, K. (2013). Gravity measurements with a portable absolute gravimeter A10 in Syowa Station and Langhovde, East Antarctica. *Polar Science*, *7*(3–4), 260–277. https://doi.org/10.1016/j.polar.2013.07.001

Kazama, T., & Okubo, S. (2009). Hydrological modeling of groundwater disturbances to observed gravity: Theory and application to Asama Volcano, Central Japan. *Journal of Geophysical Research*, *114*, B08402. https://doi.org/10.1029/2009JB006391

Kazama, T., Tamura, Y., Asari, K., Manabe, S., & Okubo, S. (2012). Gravity changes associated with variations in local land-water distributions: Observations and hydrological modeling at Isawa Fan, northern Japan. *Earth, Planets and Space*, *64*(4), 309–331. https://doi.org/10.5047/eps.2011.11.003

Kedar, S., Longuet-Higgins, M., Webb, F., Graham, N., Clayton, R., & Jones, C. (2008). The origin of deep ocean microseisms in the North Atlantic Ocean. *Proceedings of the Royal Society A: Mathematical, Physical and Engineering Sciences*, *464*(2091), 777–793. https://doi.org/10.1098/rspa.2007.0277

Kennedy, J., Ferré, T. P. A., & Creutzfeldt, B. (2016). Time-lapse gravity data for monitoring and modeling artificial recharge through a thick unsaturated zone. *Water Resources Research*, *52*, 7244–7261. https://doi.org/10.1002/2016WR018770

Kennedy, J., Ferré, T. P. A., Güntner, A., Abe, M., & Creutzfeldt, B. (2014). Direct measurement of subsurface mass change using the variable baseline gravity gradient method: Kennedy et al.: Variable-baseline gradients. *Geophysical Research Letters*, *41*, 2827–2834. https://doi.org/10.1002/2014GL059673

Kibble, B. P. (1976). A measurement of the gyromagnetic ratio of the proton by the strong field method. In J. H. Sanders & A. H. Wapstra (Eds.), *Atomic Masses and Fundamental Constants 5* (pp. 545–551). Boston, MA: Springer US. https://doi.org/10.1007/978-1-4684-2682-3_80

Klügel, T., & Wziontek, H. (2009). Correcting gravimeters and tiltmeters for atmospheric mass attraction using operational weather models. *Journal of Geodynamics*, *48*(3), 204–210.

Kroner, C., Dierks, O., Neumeyer, J., & Wilmes, H. (2005). Analysis of observations with dual sensor superconducting gravimeters. *Physics of the Earth and Planetary Interiors*, *153*(4), 210–219. https://doi.org/10.1016/j.pepi.2005.07.002

Lambert, A., Courtier, N., & James, T. S. (2006). Long-term monitoring by absolute gravimetry: Tides to postglacial rebound. *Journal of Geodynamics*, *41*(1–3), 307–317. https://doi.org/10.1016/j.jog.2005.08.032

Lambert, A., Henton, J., Mazzotti, S., Huang, J., James, T. S., Courtier, N., & van der Kamp, G. (2013). *Postglacial rebound and total water storage variations in the Nelson River drainage basin: A gravity-GPS study* (No. 7317). https://doi.org/10.4095/292189

Lambert, A., Huang, J., van der Kamp, G., Henton, J., Mazzotti, S., James, T. S., … Barr, A. G. (2013). Measuring water accumulation rates using GRACE data in areas experiencing glacial isostatic adjustment: The Nelson River basin. *Geophysical Research Letters*, *40*, 6118–6122. https://doi.org/10.1002/2013GL057973

Lampitelli, C., & Francis, O. (2010). Hydrological effects on gravity and correlations between gravitational variations and level of the Alzette River at the station of Walferdange, Luxembourg. *Journal of Geodynamics*, *49*(1), 31–38. https://doi.org/10.1016/j.jog.2009.08.003

Larson, K., & van Dam, T. (2000). Measuring postglacial rebound with GPS and absolute gravity. *Geophysical Research Letters*, *27*(23), 3925–3928. https://doi.org/10.1029/2000GL011946

Laske, G., & Widmer-Schnidrig, R. (2015). Theory and observations: Normal mode and surface wave observations. In *Treatise on Geophysics* (pp. 117–167). Amsterdam: Elsevier. https://doi.org/10.1016/B978-0-444-53802-4.00003-8

Le Gouët, J., Mehlstäubler, T. E., Kim, J., Merlet, S., Clairon, A., Landragin, A., & Pereira Dos Santos, F. (2008). Limits to the sensitivity of a low noise compact atomic gravimeter. *Applied Physics B*, *92*(2), 133–144. https://doi.org/10.1007/s00340-008-3088-1

Levine, J., Harrison, J. C., & Dewhurst, W. (1986). Gravity tide measurements with a feedback gravity meter. *Journal of Geophysical Research*, *91*(B12), 12,835–12,841. https://doi.org/10.1029/JB091iB12p12835

Li, S., Moreno, M., Bedford, J., Rosenau, M., Heidbach, O., Melnick, D., & Oncken, O. (2017). Postseismic uplift of the Andes following the 2010 Maule earthquake: Implications for mantle rheology: Postseismic deformation of Maule EQ. *Geophysical Research Letters*, *44*, 1768–1776. https://doi.org/10.1002/2016GL071995

Longman, I. M. (1959). Formulas for computing the tidal accelerations due to the Moon and the Sun. *Journal of Geophysical Research*, *64*(12), 2351–2355. https://doi.org/10.1029/JZ064i012p02351

Loyer, S., Hinderer, J., & Boy, J.-P. (1999). Determination of the gravimetric factor at the Chandler period from Earth orientation data and superconducting gravimetry observations. *Geophysical Journal International*, *136*(1), 1–7. https://doi.org/10.1046/j.1365-246X.1999.00646.x

Makinen, A. M., & Deuss, A. (2013). Normal mode splitting function measurements of anelasticity and attenuation in the Earth's inner core. *Geophysical Journal International*, *194*(1), 401–416. https://doi.org/10.1093/gji/ggt092

Mäkinen, J., Engfeldt, A., Harsson, B. G., Ruotsalainen, H., Strykowski, G., Oja, T., & Wolf, D. (2005). The Fennoscandian land uplift gravity lines 1966–2003. In C. Jekeli, L. Bastos, & J. Fernandes (Eds.), *Gravity, Geoid and Space Missions* (Vol. 129, pp. 328–332). Berlin/Heidelberg: Springer-Verlag. https://doi.org/10.1007/3-540-26932-0_57

Mandelbrot, B. B., & Van Ness, J. W. (1968). Fractional Brownian motions, fractional noises and applications. *SIAM Review*, *10*(4), 422–437. https://doi.org/10.1137/1010093

Marone, C. J., Scholtz, C. H., & Bilham, R. (1991). On the mechanics of earthquake afterslip. *Journal of Geophysical Research*, *96*(B5), 8441. https://doi.org/10.1029/91JB00275

Marson, I. (2012). A short walk along the gravimeters path. *International Journal of Geophysics*, *2012*, 1–9. https://doi.org/10.1155/2012/687813

Masterlark, T., & Wang, H. (2000). Poroelastic coupling between the 1992 Landers and Big Bear earthquakes. *Geophysical Research Letters*, *27*(22), 3647–3650. https://doi.org/10.1029/2000GL011472

Masters, G. (1979). Observational constraints on the chemical and thermal structure of the Earth's deep interior. *Geophysical Journal International*, *57*(2), 507–534. https://doi.org/10.1111/j.1365-246X.1979.tb04791.x

Mazzotti, S., Lambert, A., Courtier, N., Nykolaishen, L., & Dragert, H. (2007). Crustal uplift and sea level rise in northern Cascadia from GPS, absolute gravity, and tide gauge data. *Geophysical Research Letters*, *34*, L15306. https://doi.org/10.1029/2007GL030283

Mazzotti, S., Lambert, A., Henton, J., James, T. S., & Courtier, N. (2011). Absolute gravity calibration of GPS velocities and glacial isostatic adjustment in mid-continent North America. *Geophysical Research Letters*, *38*, L24311. https://doi.org/10.1029/2011GL049846

McClure, M. W. (2015). Generation of large postinjection-induced seismic events by backflow from dead-end faults and fractures. *Geophysical Research Letters*, *42*, 6647–6654. https://doi.org/10.1002/2015GL065028

Melchior, P., & Ducarme, B. (1986). Detection of inertial gravity oscillations in the Earth's core with a superconducting gravimeter at Brussels. *Physics of the Earth and Planetary Interiors*, *42*(3), 129–134. https://doi.org/10.1016/0031-9201(86)90085-3

Meltzner, A. J., Sieh, K., Abrams, M., Agnew, D., Hudnut, K. W., Avouac, J.-P., & Natawidjaja, D. H. (2006). Uplift and subsidence associated with the great Aceh-Andaman earthquake of 2004. *Journal of Geophysical Research*, *111*, B02407. https://doi.org/10.1029/2005JB003891

Mémin, A., Rogister, Y., Hinderer, J., Omang, O. C., & Luck, B. (2011). Secular gravity variation at Svalbard (Norway) from ground observations and GRACE satellite data: Secular gravity variation at Svalbard. *Geophysical Journal International*, *184*(3), 1119–1130. https://doi.org/10.1111/j.1365-246X.2010.04922.x

Merlet, S., Kopaev, A., Diament, M., Geneves, G., Landragin, A., & Pereira Dos Santos, F. (2008). Micro-gravity investigations for the LNE watt balance project. *Metrologia*, *45*(3), 265–274. https://doi.org/10.1088/0026-1394/45/3/002

Merriam, J. B. (1992). Atmospheric pressure and gravity. *Geophysical Journal International*, *109*(3), 488–500. https://doi.org/10.1111/j.1365-246X.1992.tb00112.x

Métivier, L., & Conrad, C. P. (2008). Body tides of a convecting, laterally heterogeneous, and aspherical Earth. *Journal of Geophysical Research*, *113*, B11405. https://doi.org/10.1029/2007JB005448

Meurers, B. (2012). Superconducting gravimeter calibration by colocated gravity observations: Results from GWR C025. *International Journal of Geophysics*, *2012*, 1–12. https://doi.org/10.1155/2012/954271

Meurers, B. (2017). Scintrex CG5 used for superconducting gravimeter calibration. *Geodesy and Geodynamics*.. https://doi.org/10.1016/j.geog.2017.02.009

Meurers, B., Van Camp, M., Francis, O., & Pálinkáš, V. (2016). Temporal variation of tidal parameters in superconducting gravimeter time-series. *Geophysical Journal International*, *205*(1), 284–300. https://doi.org/10.1093/gji/ggw017

Meurers, B., Van Camp, M., & Petermans, T. (2007). Correcting superconducting gravity time-series using rainfall modelling at the Vienna and Membach stations and application to Earth tide analysis. *Journal of Geodesy*, *81*(11), 703–712. https://doi.org/10.1007/s00190-007-0137-1

Mickus, K. (2003). Gravity method: Environmental and engineering applications. In *3rd International Conference on Applied Geophysics, Hotel Royal Plaza, Orlando, FL*. Retrieved from http://www.academia.edu/download/31892491/soteloct.pdf

Middlemiss, R. P., Samarelli, A., Paul, D. J., Hough, J., Rowan, S., & Hammond, G. D. (2016). Measurement of the Earth tides with a MEMS gravimeter. *Nature*, *531*(7596), 614–617. https://doi.org/10.1038/nature17397

Mikolaj, M., Meurers, B., & Mojzeš, M. (2015). The reduction of hydrology-induced gravity variations at sites with insufficient hydrological instrumentation. *Studia Geophysica et Geodaetica*, *59*(3), 424–437. https://doi.org/10.1007/s11200-014-0232-8

Mogi, K. (1958). Relations between the eruptions of various volcanoes and the deformations of the ground surfaces around them. *Bulletin of the Earthquake Research Institute*, *36*, 99–134.

Montagner, J.-P., Juhel, K., Barsuglia, M., Ampuero, J. P., Chassande-Mottin, E., Harms, J., … Lognonné, P. (2016). Prompt gravity signal induced by the 2011 Tohoku-Oki earthquake. *Nature Communications*, *7*, 13349. https://doi.org/10.1038/ncomms13349

Montgomery, E. L. (1971, November 30). *Determination of coefficient of storage by use of gravity measurements*. (PhD thesis). U. Arizona. Retrieved from http://arizona.openrepository.com/arizona/handle/10150/190978

Mouyen, M., Chao, B. F., Hwang, C., & Hsieh, W.-C. (2016). Gravity monitoring of Tatun Volcanic Group activities and inference for underground fluid circulations. *Journal of Volcanology and Geothermal Research*, *328*, 45–58. https://doi.org/10.1016/j.jvolgeores.2016.10.001

Mouyen, M., Masson, F., Hwang, C., Cheng, C.-C., Le Moigne, N., Lee, C. W., … Hsieh, W.-C. (2013). Erosion effects assessed by repeated gravity measurements in southern Taiwan. *Geophysical Journal International*, *192*(1), 113–136. https://doi.org/10.1093/gji/ggs019

Mouyen, M., Simoes, M., Mouthereau, F., Masson, F., Hwang, C., & Cheng, C.-C. (2014). Investigating possible gravity change rates expected from long-term deep crustal processes in Taiwan. *Geophysical Journal International*, *198*(1), 187–197. https://doi.org/10.1093/gji/ggu133

Mukuhira, Y., Dinske, C., Asanuma, H., Ito, T., & Häring, M. O. (2016). Pore pressure behavior at the shut-in phase and causality of large induced seismicity at Basel, Switzerland: Large induced events at shut-in phase. *Journal of Geophysical Research: Solid Earth*, *122*, 411–435. https://doi.org/10.1002/2016JB013338

Munk, W. H., & Cartwright, D. E. (1966). Tidal spectroscopy and prediction. *Philosophical Transactions of the Royal Society A: Mathematical, Physical and Engineering Sciences*, *259*(1105), 533–581. https://doi.org/10.1098/rsta.1966.0024

Nagy, D. (1966). The gravitational attraction of a right rectangular prism. *Geophysics*, *31*(2), 362–371. https://doi.org/10.1190/1.1439779

Naujoks, M., Weise, A., Kroner, C., & Jahr, T. (2008). Detection of small hydrological variations in gravity by repeated observations with relative gravimeters. *Journal of Geodesy*, *82*(9), 543–553. https://doi.org/10.1007/s00190-007-0202-9

Nawa, K., Suda, N., Fukao, Y., Sato, T., Aoyama, Y., & Shibuya, K. (1998). Incessant excitation of the Earth's free oscillations. *Earth, Planets and Space*, *50*(1), 3–8. https://doi.org/10.1186/BF03352080

Neumeyer, J. (2010). Superconducting gravimetry. In G. Xu (Ed.), *Sciences of Geodesy—I: Advances and Future Directions* (pp. 339–413). Berlin, Heidelberg: Springer Berlin Heidelberg. https://doi.org/10.1007/978-3-642-11741-1_10

Niebauer, T. (2015). Gravimetric methods—Absolute and relative gravity meter: Instruments concepts and implementation. In *Treatise on Geophysics* (pp. 37–57). Amsterdam: Elsevier.

Niebauer, T., Billson, R., Schiel, A., van Westrum, D., & Klopping, F. (2013). The self-attraction correction for the FG5X absolute gravity meter. *Metrologia*, *50*(1), 1–8. https://doi.org/10.1088/0026-1394/50/1/1

Niebauer, T., McHugh, M. P., & Faller, J. (1987). Galilean test for the fifth force. *Physical Review Letters*, *59*(6), 609–612. https://doi.org/10.1103/PhysRevLett.59.609

Niebauer, T., Sasagawa, G., Faller, J., Hilt, R., & Klopping, F. (1995). A new generation of absolute gravimeters. *Metrologia*, *32*(3), 159–180. https://doi.org/10.1088/0026-1394/32/3/004

Nielsen, J. E., Forsberg, R., & Strykowski, G. (2014). Measured and modelled absolute gravity changes in Greenland. *Journal of Geodynamics*, *73*, 53–59. https://doi.org/10.1016/j.jog.2013.09.003

Nishida, K. (2013). Earth's background free oscillations. *Annual Review of Earth and Planetary Sciences*, *41*(1), 719–740. https://doi.org/10.1146/annurev-earth-050212-124020

Nishijima, J., Umeda, C., Fujimitsu, Y., Takayama, J., Hiraga, N., & Higuchi, S. (2016). Repeat absolute and relative gravity measurements for geothermal reservoir monitoring in the Ogiri Geothermal Field, Southern Kyushu, Japan. *IOP Conference Series: Earth and Environmental Science*, *42*, 012004. https://doi.org/10.1088/1755-1315/42/1/012004

Nooner, S. L., Eiken, O., Hermanrud, C., Sasagawa, G., Stenvold, T., & Zumberge, M. (2007). Constraints on the in situ density of CO_2 within the Utsira formation from time-lapse seafloor gravity measurements. *International Journal of Greenhouse Gas Control*, *1*(2), 198–214. https://doi.org/10.1016/S1750-5836(07)00018-7

Nordman, M., Virtanen, H., Nyberg, S., & Mäkinen, J. (2015). Non-tidal loading by the Baltic Sea: Comparison of modelled deformation with GNSS time series. *GeoResJ*, *7*, 14–21. https://doi.org/10.1016/j.grj.2015.03.002

Nordquist, G., Protacio, J. A. P., & Acuña, J. A. (2004). Precision gravity monitoring of the Bulalo geothermal field, Philippines: Independent checks and constraints on numerical simulation. *Geothermics*, *33*(1–2), 37–56. https://doi.org/10.1016/j.geothermics.2003.03.001

Nur, A., & Booker, J. R. (1972). Aftershocks caused by pore fluid flow? *Science*, *175*(4024), 885–887. https://doi.org/10.1126/science.175.4024.885

Obara, K. (2002). Nonvolcanic deep tremor associated with subduction in Southwest Japan. *Science*, *296*(5573), 1679–1681. https://doi.org/10.1126/science.1070378

Ogawa, R., & Heki, K. (2007). Slow postseismic recovery of geoid depression formed by the 2004 Sumatra-Andaman earthquake by mantle water diffusion. *Geophysical Research Letters*, *34*, L06313. https://doi.org/10.1029/2007GL029340

Okal, E. A. (1996). Radial modes from the great 1994 Bolivian earthquake: No evidence for an isotropic component to the source. *Geophysical Research Letters*, *23*(5), 431–434. https://doi.org/10.1029/96GL00375

Okiwelu, A. A., Okwueze, E. E., & Osazuwa, I. B. (2011). Strategies for accurate determination of drift characteristics of unstable gravimeter in tropical, coastal environment. *Applied Physics Research*, *3*(2), 190.

Olsson, P.-A., Scherneck, H.-G., & Ågren, J. (2009). Effects on gravity from non-tidal sea level variations in the Baltic Sea. *Journal of Geodynamics*, *48*(3–5), 151–156. https://doi.org/10.1016/j.jog.2009.09.002

Omang, O. C. D., & Kierulf, H. P. (2011). Past and present-day ice mass variation on Svalbard revealed by superconducting gravimeter and GPS measurements. *Geophysical Research Letters*, *38*, L22304. https://doi.org/10.1029/2011GL049266

Ophaug, V., Breili, K., Gerlach, C., Omholt Gjevestad, J. G., Lysaker, D. I., Dahl Omang, O. C., & Pettersen, B. R. (2016). Absolute gravity observations in Norway (1993–2014) for glacial isostatic adjustment studies: The influence of gravitational loading effects on secular gravity trends. *Journal of Geodynamics*, *102*, 83–94. https://doi.org/10.1016/j.jog.2016.09.001

Pail, R., Bruinsma, S., Migliaccio, F., Förste, C., Goiginger, H., Schuh, W.-D., … Tscherning, C. C. (2011). First GOCE gravity field models derived by three different approaches. *Journal of Geodesy*, *85*(11), 819–843. https://doi.org/10.1007/s00190-011-0467-x

Pálinkáš, V., Francis, O., Val'ko, M., Kostelecký, J., Van Camp, M., Castelein, S., … Lucero, B. (2017). Regional comparison of absolute gravimeters, EURAMET.M.G-K2 key comparison. *Metrologia*, *54*(1A), 07012–07012. https://doi.org/10.1088/0026-1394/54/1A/07012

Pálinkáš, V., Lederer, M., Kostelecký, J., Šimek, J., Mojzeš, M., Ferianc, D., & Csapó, G. (2013). Analysis of the repeated absolute gravity measurements in the Czech Republic, Slovakia and Hungary from the period 1991–2010 considering instrumental and hydrological effects. *Journal of Geodesy*, *87*(1), 29–42. https://doi.org/10.1007/s00190-012-0576-1

Panet, I., Pollitz, F., Mikhailov, V., Diament, M., Banerjee, P., & Grijalva, K. (2010). Upper mantle rheology from GRACE and GPS postseismic deformation after the 2004 Sumatra-Andaman earthquake. *Geochemistry, Geophysics, Geosystems*, *11*, Q06008. https://doi.org/10.1029/2009GC002905

Park, J., Butler, R., Anderson, K., Berger, J., Davis, P., Benz, H., … Aster, R. (2005). Performance review of the global seismographic network for the Sumatra-Andaman megathrust earthquake. *Seismological Research Letters*, *76*(3), 331–343. https://doi.org/10.1785/gssrl.76.3.331

Park, J., Song, T.-R. A., Tromp, J., Okal, E. A., Stein, S., Roul, G., … Van Camp, M. (2005). Earth's free oscillations excited by the 26 December 2004 Sumatra-Andaman earthquake. *Science*, *308*(5725), 1139–1144. https://doi.org/10.1126/science.1112305

Parseliunas, E., Petroskevivius, P., Birvydiene, R., & Obuchovski, R. (2011). In Environmental Engineering, D. Cygas, K. D. Froehner, & A. Breznikar (Eds.), *Environmental Engineering: Selected Papers. Vol. 3*. Vilnius: Vilnius Gediminas Technical University Press "Technika.".

Peng, J., Loew, A., Merlin, O., & Verhoest, N. E. C. (2017). A review of spatial downscaling of satellite remotely-sensed soil moisture: Downscale satellite-based soil moisture. *Reviews of Geophysics*, *55*(2), 341–366. https://doi.org/10.1002/2016RG000543

Perfettini, H., & Avouac, J.-P. (2004). Postseismic relaxation driven by brittle creep: A possible mechanism to reconcile geodetic measurements and the decay rate of aftershocks, application to the Chi-Chi earthquake, Taiwan. *Journal of Geophysical Research*, *109*, B02304. https://doi.org/10.1029/2003JB002488

Peters, A., Chung, K. Y., & Chu, S. (1999). Measurement of gravitational acceleration by dropping atoms. *Nature*, *400*(6747), 849–852. https://doi.org/10.1038/23655

Peters, A., Chung, K. Y., & Chu, S. (2001). High-precision gravity measurements using atom interferometry. *Metrologia*, *38*(1), 25–61. https://doi.org/10.1088/0026-1394/38/1/4

Peterson, J. (1993). *Observations and modeling of seismic background noise* (USGS Open-File No. 93–322) (pp. 1–94). U.S. Department of Interior Geological Survey. Retrieved from https://pubs.usgs.gov/of/1993/0322/report.pdf

Phillips, W. D., & Metcalf, H. J. (1987). Cooling and trapping atoms. *Scientific American*, *256*(3), 50–56. https://doi.org/10.1038/scientificamerican0387-50

Plag, H.-P. (1997). Chandler wobble and pole tide in relation to interannual atmosphere-ocean dynamics. In H. Wilhelm, W. Zürn, & H.-G. Wenzel (Eds.), *Tidal Phenomena* (Vol. 66, pp. 183–218). Berlin/Heidelberg: Springer-Verlag. https://doi.org/10.1007/BFb0011463

Plag, H.-P., & Pearlman, M. (Eds.) (2009). *Global Geodetic Observing System: Meeting the requirements of a global society on a changing planet in 2020*. Berlin: Springer.

Poland, M., & Carbone, D. (2016). Insights into shallow magmatic processes at Kīlauea Volcano, Hawai'i, from a multiyear continuous gravity time series: Continuous gravity at Kīlauea. *Journal of Geophysical Research: Solid Earth*, *121*, 5477–5492. https://doi.org/10.1002/2016JB013057

Pollitz, F. (1997). Gravitational viscoelastic postseismic relaxation on a layered spherical Earth. *Journal of Geophysical Research*, *102*(B8), 17,921–17,941. https://doi.org/10.1029/97JB01277

Pollitz, F. (2001). Mantle flow beneath a continental strike-slip fault: Postseismic deformation after the 1999 Hector Mine earthquake. *Science*, *293*(5536), 1814–1818. https://doi.org/10.1126/science.1061361

Pollitz, F., Banerjee, P., Grijalva, K., Nagarajan, B., & Bürgmann, R. (2008). Effect of 3-D viscoelastic structure on post-seismic relaxation from the 2004 M = 9.2 Sumatra earthquake. *Geophysical Journal International*, *173*(1), 189–204. https://doi.org/10.1111/j.1365-246X.2007.03666.x

Pool, D. R. (2008). The utility of gravity and water-level monitoring at alluvial aquifer wells in southern Arizona. *Geophysics*, *73*(6), WA49–WA59. https://doi.org/10.1190/1.2980395

Pool, D. R., & Eychaner, J. H. (1995). Measurements of aquifer-storage change and specific yield using gravity surveys. *Ground Water*, *33*(3), 425–432. https://doi.org/10.1111/j.1745-6584.1995.tb00299.x

Preston-Thomas, H., Turnbull, L. G., Green, E., Dauphinee, T. M., & Kalra, S. N. (1960). An absolute measurement of the acceleration due to gravity at Ottawa. *Canadian Journal of Physics*, *38*(6), 824–852. https://doi.org/10.1139/p60-088

Prothero, W. A., & Goodkind, J. M. (1968). A superconducting gravimeter. *Review of Scientific Instruments*, *39*(9), 1257–1262. https://doi.org/10.1063/1.1683645

Radiguet, M., Perfettini, H., Cotte, N., Gualandi, A., Valette, B., Kostoglodov, V., … Campillo, M. (2016). Triggering of the 2014 M_w7.3 Papanoa earthquake by a slow slip event in Guerrero, Mexico. *Nature Geoscience*, *9*(11), 829–833. https://doi.org/10.1038/ngeo2817

Reigber, C., Balmino, G., Schwintzer, P., Biancale, R., Bode, A., Lemoine, J.-M., … Zhu, S. Y. (2002). A high-quality global gravity field model from CHAMP GPS tracking data and accelerometry (EIGEN-1S). *Geophysical Research Letters*, *29*(14), 37-1–37–4. https://doi.org/10.1029/2002GL015064

Remy, D., Perfettini, H., Cotte, N., Avouac, J.-P., Chlieh, M., Bondoux, F., … Socquet, A. (2016). Postseismic relocking of the subduction megathrust following the 2007 Pisco, Peru, earthquake. *Journal of Geophysical Research: Solid Earth*, *121*, 3978–3995. https://doi.org/10.1002/2015JB012417

Reynolds, J. M. (2011). *An Introduction to Applied and Environmental Geophysics* (2nd ed.). Chichester, West Sussex ; Malden, MA: Wiley-Blackwell.

Riccardi, U., Rosat, S., & Hinderer, J. (2011). Comparison of the Micro-g LaCoste gPhone-054 spring gravimeter and the GWR-C026 superconducting gravimeter in Strasbourg (France) using a 300-day time series. *Metrologia*, *48*(1), 28–39. https://doi.org/10.1088/0026-1394/48/1/003

Richter, B., Wilmes, H., & Nowak, I. (1995). The Frankfurt calibration system for relative gravimeters. *Metrologia*, *32*(3), 217–223. https://doi.org/10.1088/0026-1394/32/3/010

Rinker, R. L. (1983). *Super Spring—A New Type of Low-Frequency Vibration Isolator*. Boulder, CO: University of Colorado. Retrieved from http://adsabs.harvard.edu/abs/1983PhDT.....60R

Rivalta, E., Taisne, B., Bunger, A. P., & Katz, R. F. (2015). A review of mechanical models of dike propagation: Schools of thought, results and future directions. *Tectonophysics*, *638*, 1–42. https://doi.org/10.1016/j.tecto.2014.10.003

Rodell, M., Houser, P. R., Jambor, U., Gottschalck, J., Mitchell, K., Meng, C.-J., … Toll, D. (2004). The global land data assimilation system. *Bulletin of the American Meteorological Society*, *85*(3), 381–394. https://doi.org/10.1175/BAMS-85-3-381

Rogers, G. (2003). Episodic tremor and slip on the Cascadia subduction zone: The chatter of silent slip. *Science*, *300*(5627), 1942–1943. https://doi.org/10.1126/science.1084783

Romanowicz, B., & Bréger, L. (2000). Anomalous splitting of free oscillations: A reevaluation of possible interpretations. *Journal of Geophysical Research*, *105*(B9), 21,559–21,578. https://doi.org/10.1029/2000JB900144

Romanowicz, B., Cao, A., Godwal, B., Wenk, R., Ventosa, S., & Jeanloz, R. (2016). Seismic anisotropy in the Earth's innermost inner core: Testing structural models against mineral physics predictions. *Geophysical Research Letters*, *43*, 93–100. https://doi.org/10.1002/2015GL066734

Roosbeek, F. (1996). RATGP95: A harmonic development of the tide-generating potential using an analytical method. *Geophysical Journal International*, *126*(1), 197–204.

Rosat, S. (2003). First observation of ${}_2S_1$ and study of the splitting of the football mode ${}_0S_2$ after the June 2001 Peru earthquake of magnitude 8.4. *Geophysical Research Letters*, *30*(21), 2111. https://doi.org/10.1029/2003GL018304

Rosat, S. (2005). High-resolution analysis of the gravest seismic normal modes after the 2004 M_w = 9 Sumatra earthquake using superconducting gravimeter data. *Geophysical Research Letters*, *32*, L13304. https://doi.org/10.1029/2005GL023128

Rosat, S. (2007). Optimal seismic source mechanisms to excite the Slichter mode. In P. Tregoning & C. Rizos (Eds.), *Dynamic Planet: Monitoring and Understanding a Dynamic Planet with Geodetic and Oceanographic Tools IAG Symposium Cairns, Australia 22–26 August, 2005* (pp. 571–577). Berlin, Heidelberg: Springer Berlin Heidelberg. https://doi.org/10.1007/978-3-540-49350-1_83

Rosat, S., & Hinderer, J. (2011). Noise levels of superconducting gravimeters: Updated comparison and time stability. *Bulletin of the Seismological Society of America*, *101*(3), 1233–1241. https://doi.org/10.1785/0120100217

Rosat, S., Hinderer, J., Crossley, D., & Rivera, L. (2003). The search for the Slichter mode: Comparison of noise levels of superconducting gravimeters and investigation of a stacking method. *Physics of the Earth and Planetary Interiors*, *140*(1–3), 183–202. https://doi.org/10.1016/j.pepi.2003.07.010

Rosat, S., Lambert, S. B., Gattano, C., & Calvo, M. (2017). Earth's core and inner-core resonances from analysis of VLBI nutation and superconducting gravimeter data. *Geophysical Journal International*, *208*(1), 211–220. https://doi.org/10.1093/gji/ggw378

Rosat, S., Rogister, Y., Crossley, D., & Hinderer, J. (2006). A search for the Slichter triplet with superconducting gravimeters: Impact of the density jump at the inner core boundary. *Journal of Geodynamics*, *41*(1–3), 296–306. https://doi.org/10.1016/j.jog.2005.08.033

Rymer, H. (1994). Microgravity change as a precursor to volcanic activity. *Journal of Volcanology and Geothermal Research*, *61*(3–4), 311–328. https://doi.org/10.1016/0377-0273(94)90011-6

Rymer, H. (2016). Applied physics: Gravity measurements on chips. *Nature*, *531*(7596), 585–586.

Rymer, H., & Brown, G. (1989). Gravity changes as a precursor to volcanic eruption at Poás volcano, Costa Rica. *Nature*, *342*(6252), 902–905. https://doi.org/10.1038/342902a0

Rymer, H., van Wyk de Vries, B., Stix, J., & Williams-Jones, G. (1998). Pit crater structure and processes governing persistent activity at Masaya Volcano, Nicaragua. *Bulletin of Volcanology*, *59*(5), 345–355.

Rymer, H., & Williams-Jones, G. (2000). Volcanic eruption prediction: Magma chamber physics from gravity and deformation measurements. *Geophysical Research Letters*, *27*(16), 2389–2392. https://doi.org/10.1029/1999GL011293

Sakuma, A. (1963). État actuel de la nouvelle détermination absolue de la pesanteur au Bureau International des Poids et Mesures. *Bulletin géodésique*, *69*(1), 249–260. https://doi.org/10.1007/BF02525900

Sasagawa, G., Crawford, W., Eiken, O., Nooner, S., Stenvold, T., & Zumberge, M. (2003). A new sea-floor gravimeter. *Geophysics*, *68*(2), 544–553. https://doi.org/10.1190/1.1567223

Sasagawa, G., Zumberge, M., & Eiken, O. (2008). Long-term seafloor tidal gravity and pressure observations in the North Sea: Testing and validation of a theoretical tidal model. *Geophysics*, *73*(6), WA143–WA148. https://doi.org/10.1190/1.2976778

Sato, T., Miura, S., Sun, W., Sugano, T., Freymueller, J. T., Larsen, C. F., … Motyka, R. J. (2012). Gravity and uplift rates observed in southeast Alaska and their comparison with GIA model predictions. *Journal of Geophysical Research*, *117*, B01401. https://doi.org/10.1029/2011JB008485

Sato, T., Okuno, J., Hinderer, J., MacMillan, D. S., Plag, H.-P., Francis, O., … Fukuda, Y. (2006). A geophysical interpretation of the secular displacement and gravity rates observed at Ny-Ålesund, Svalbard in the Arctic-effects of post-glacial rebound and present-day ice melting. *Geophysical Journal International*, *165*(3), 729–743. https://doi.org/10.1111/j.1365-246X.2006.02992.x

Schilling, M., & Gitlein, O. (2015). Accuracy estimation of the IfE gravimeters Micro-g LaCoste gPhone-98 and ZLS Burris Gravity Meter B-64. In C. Rizos & P. Willis (Eds.), *IAG 150 Years* (Vol. 143, pp. 249–256). Cham: Springer International Publishing. https://doi.org/10.1007/1345_2015_29

Schmerge, D., Francis, O., Henton, J., Ingles, D., Jones, D., Kennedy, J., … van Westrum, D. (2012). Results of the first North American comparison of absolute gravimeters, NACAG-2010. *Journal of Geodesy*, *86*(8), 591–596. https://doi.org/10.1007/s00190-011-0539-y

Schüller, K. (2015). Theoretical basis for Earth tide analysis with the new ETERNA34-ANA-V4. 0 program. *Bull. Inf. Marées Terrestres*, *149*(12), 024–012.

Schwartz, S. Y. (2015). Episodic aseismic slip at plate boundaries. In *Treatise on Geophysics* (pp. 445–465). Amsterdam: Elsevier. https://doi.org/10.1016/B978-0-444-53802-4.00084-1

Schwarz, J. P., Robertson, D. S., Niebauer, T., & Faller, J. (1998). A free-fall determination of the Newtonian constant of gravity. *Science*, *282*(5397), 2230–2234. https://doi.org/10.1126/science.282.5397.2230

Scintrex Ltd. (2017). Scintrex. Retrieved March 27, 2017. Retrieved from http://www.scintrexltd.com/internal.php?storeCategoryID=1&subcatID=9&s_page=Gravity

Seeber, G. (2003). *Satellite Geodesy* (2nd Completely Rev. and Extended ed). Berlin; New York: Walter de Gruyter.

Seigel, H. O., Brcic, I., & Mistry, P. (1993). The CG-3M—A high precision, μGal resolution, land gravimeter with worldwide range. In *A Guide to High Precision L* and Gravimeter Surveys (pp. 105–127). Concord Ontario, Canada: Seigel, H.O. Scintrex Ltd. Retrieved from http://scintrexltd.com/downloads/GRAVGUID.pdf

Shapiro, N. M. (2005). High-resolution surface-wave tomography from ambient seismic noise. *Science*, *307*(5715), 1615–1618. https://doi.org/10.1126/science.1108339

Shen, W., & Luan, W. (2015). Feasibility analysis of searching for the Slichter triplet in superconducting gravimeter records. *Geodesy and Geodynamics*, *6*(5), 307–315. https://doi.org/10.1016/j.geog.2015.05.011

Shen, W., Wang, D., & Hwang, C. (2011). Anomalous signals prior to Wenchuan earthquake detected by superconducting gravimeter and broadband seismometers records. *Journal of Earth Science*, *22*(5), 640–651. https://doi.org/10.1007/s12583-011-0215-4

Showstack, R. (2014). Scientists focus on land subsidence impacts on coastal and delta cities. *Eos, Transactions American Geophysical Union*, *95*(19), 159–159. https://doi.org/10.1002/2014EO190003

Sigmundsson, F., Hooper, A., Hreinsdóttir, S., Vogfjörd, K. S., Ófeigsson, B. G., Heimisson, E. R., … Eibl, E. P. S. (2014). Segmented lateral dyke growth in a rifting event at Bárðarbunga volcanic system, Iceland. *Nature*, *517*(7533), 191–195. https://doi.org/10.1038/nature14111

Singh, S. K. (1977). Gravitational attraction of a circular disc. *Geophysics*, *42*(1), 111–113. https://doi.org/10.1190/1.1440704

Singhal, B. B. S. (2010). Geophysical exploration. In B. B. S. Singhal & R. P. Gupta (Eds.), *Applied Hydrogeology of Fractured Rocks* (pp. 75–94). Dordrecht, Netherlands: Springer. https://doi.org/10.1007/978-90-481-8799-7_5

Smith, S. W., & Wyss, M. (1968). Displacement on the San Andreas fault subsequent to the 1966 Parkfield earthquake. *Bulletin of the Seismological Society of America*, *58*(6), 1955–1973.

Souriau, A., & Calvet, M. (2015). Deep Earth structure: The Earth's cores. In *Treatise on Geophysics* (pp. 725–757). Amsterdam: Elsevier. https://doi.org/10.1016/B978-0-444-53802-4.00020-8

Sparks, R. S. J., & Cashman, K. V. (2017). Dynamic magma systems: Implications for forecasting volcanic activity. *Elements*, *13*(1), 35–40. https://doi.org/10.2113/gselements.13.1.35

Steffen, H., Gitlein, O., Denker, H., Müller, J., & Timmen, L. (2009). Present rate of uplift in Fennoscandia from GRACE and absolute gravimetry. *Tectonophysics*, *474*(1–2), 69–77. https://doi.org/10.1016/j.tecto.2009.01.012

Steffen, H., & Wu, P. (2011). Glacial isostatic adjustment in Fennoscandia—A review of data and modeling. *Journal of Geodynamics*, *52*(3–4), 169–204. https://doi.org/10.1016/j.jog.2011.03.002

Steffen, H., Wu, P., & Wang, H. (2012). Optimal locations for absolute gravity measurements and sensitivity of GRACE observations for constraining glacial isostatic adjustment on the northern hemisphere. *Geophysical Journal International*, *190*, 1483–1494. https://doi.org/10.1111/j.1365-246X.2012.05563.x

Stein, S., & Okal, E. A. (2005). Seismology: Speed and size of the Sumatra earthquake. *Nature*, *434*(7033), 581–582. https://doi.org/10.1038/434581a

Stock, M. (2013). Watt balance experiments for the determination of the Planck constant and the redefinition of the kilogram. *Metrologia*, *50*(1), R1–R16. https://doi.org/10.1088/0026-1394/50/1/R1

Stutzmann, E. (2000). GEOSCOPE station noise levels. *Bulletin of the Seismological Society of America*, *90*(3), 690–701. https://doi.org/10.1785/0119990025

Sugihara, G., May, R., Ye, H., Hsieh, C.-H., Deyle, E., Fogarty, M., & Munch, S. (2012). Detecting causality in complex ecosystems. *Science*, *338*(6106), 496–500. https://doi.org/10.1126/science.1227079

Sugihara, M., & Ishido, T. (2008). Geothermal reservoir monitoring with a combination of absolute and relative gravimetry. *Geophysics*, *73*(6), WA37–WA47. https://doi.org/10.1190/1.2991105

Sugihara, M., & Nawa, K. (2012). Continuous gravity measurement for practical monitoring. In *Proceedings of the 37th Workshop on Geothermal Reservoir Engineering*. Stanford: Stanford University. Retrieved from https://pangea.stanford.edu/ERE/pdf/IGAstandard/SGW/2012/Sugihara.pdf

Suito, H., & Freymueller, J. T. (2009). A viscoelastic and afterslip postseismic deformation model for the 1964 Alaska earthquake. *Journal of Geophysical Research*, *114*, B11404. https://doi.org/10.1029/2008JB005954

Taguchi, E., Stammer, D., & Zahel, W. (2014). Inferring deep ocean tidal energy dissipation from the global high-resolution data-assimilative HAMTIDE model. *Journal of Geophysical Research, Oceans*, *119*, 4573–4592. https://doi.org/10.1002/2013JC009766

Tanaka, T., Miyajima, R., Asai, H., Horiuchi, Y., Kumada, K., Asai, Y., & Ishii, H. (2013). Hydrological gravity response detection using a gPhone below- and aboveground. *Earth, Planets and Space*, *65*(2), 59–66. https://doi.org/10.5047/eps.2012.06.012

Tapley, B. D. (2004). GRACE meeasurements of mass variability in the Earth system. *Science*, *305*(5683), 503–505. https://doi.org/10.1126/science.1099192

Teatini, P., Gambolati, G., Ferronato, M., & Settari, A. (Tony), & Walters, D. (2011). Land uplift due to subsurface fluid injection. *Journal of Geodynamics*, *51*(1), 1–16. https://doi.org/10.1016/j.jog.2010.06.001

Teatini, P., Tosi, L., & Strozzi, T. (2012). Comment on "Recent subsidence of the Venice Lagoon from continuous GPS and interferometric synthetic aperture radar" by Y. Bock, S. Wdowinski, A. Ferretti, F. Novali, and A. Fumagalli. *Geochemistry, Geophysics, Geosystems*, *13*, Q07008. https://doi.org/10.1029/2012GC004191

Teferle, F. N., Bingley, R. M., Orliac, E. J., Williams, S. D. P., Woodworth, P. L., McLaughlin, D., … Hansen, D. N. (2009). Crustal motions in Great Britain: Evidence from continuous GPS, absolute gravity and Holocene sea level data. *Geophysical Journal International*, *178*(1), 23–46. https://doi.org/10.1111/j.1365-246X.2009.04185.x

Teferle, F. N., Bingley, R. M., Williams, S. D. P., Baker, T. F., & Dodson, A. H. (2006). Using continuous GPS and absolute gravity to separate vertical land movements and changes in sea-level at tide-gauges in the UK. *Philosophical Transactions of the Royal Society A: Mathematical, Physical and Engineering Sciences*, *364*(1841), 917–930. https://doi.org/10.1098/rsta.2006.1746

Thatcher, W., & Pollitz, F. (2008). Temporal evolution of continental lithospheric strength in actively deforming regions. *GSA Today*, *18*(4), 4. https://doi.org/10.1130/GSAT01804-5A.1

Thulin, Å. (1958). Résultat d'une nouvelle détermination absolue de l'accélération due à la pesanteur, au Pavillon de Breteuil. *C.R. Académie des Sci*. (pp. 3322–3324).

Torge, W. (1989). *Gravimetry*. Berlin, Boston: De Gruyter. Retrieved from https://www.degruyter.com/view/product/59078

Uhrhammer, R. A., Karavas, W., & Romanowicz, B. (1998). Broadband seismic station installation guidelines. *Seismological Research Letters*, *69*(1), 15–26. https://doi.org/10.1785/gssrl.69.1.15

Uppala, S. M., KÅllberg, P. W., Simmons, A. J., Andrae, U., Bechtold, V. D. C., Fiorino, M., … Woollen, J. (2005). The ERA-40 re-analysis. *Quarterly Journal of the Royal Meteorological Society*, *131*(612), 2961–3012. https://doi.org/10.1256/qj.04.176

Vallée, M., Nocquet, J.-M., Battaglia, J., Font, Y., Segovia, M., Régnier, M., … Chlieh, M. (2013). Intense interface seismicity triggered by a shallow slow slip event in the Central Ecuador subduction zone. *Journal of Geophysical Research: Solid Earth*, *118*, 2965–2981. https://doi.org/10.1002/jgrb.50216

Valliant, H. D. (1991). Gravity meter calibration at LaCoste and Romberg. *Geophysics*, *56*(5), 705–711. https://doi.org/10.1190/1.1443089

Valty, P., de Viron, O., Panet, I., Van Camp, M., & Legrand, J. (2013). Assessing the precision in loading estimates by geodetic techniques in Southern Europe. *Geophysical Journal International*, *194*(3), 1441–1454. https://doi.org/10.1093/gji/ggt173

Van Camp, M. (1999). Measuring seismic normal modes with the GWR C021 superconducting gravimeter. *Physics of the Earth and Planetary Interiors*, *116*(1–4), 81–92. https://doi.org/10.1016/S0031-9201(99)00120-X

Van Camp, M. (2003). Efficiency of tidal corrections on absolute gravity measurements at the Membach station. In *Proceedings of the Workshop: IMG-2002: Instrumentation and Metrology in Gravimetry, October 28–30, 2002, Münsbach Castle, Münsbach, Grand-Duchy of Luxembourg, Cah. Cent. Eur. Géodyn. Séismol* (Vol. 22, pp. 99–103). Retrieved from https://www.researchgate.net/profile/Michel_Van_

Camp/publication/255179922_Efficiency_of_tidal_corrections_on_absolute_gravity_measurements_at_the_Membach_station/links/0deec5200b5427c5ac000000.pdf
van Camp, M. (2017). World record in the underground laboratory of Membach: A sphere of mass 4 grams has been levitating for 8081 days [Press release]. Retrieved from http://www.astro.oma.be/en/world-record-in-the-underground-laboratory-of-membach/
Van Camp, M., & de Viron, O. (2016). The slightness of gravimetry. *Nature Physics*, *12*(8), 816–816.
Van Camp, M., de Viron, O., & Avouac, J.-P. (2016). Separating climate-induced mass transfers and instrumental effects from tectonic signal in repeated absolute gravity measurements: Uncertainty of absolute gravity data. *Geophysical Research Letters*, *43*, 4313–4320. https://doi.org/10.1002/2016GL068648
Van Camp, M., de Viron, O., Métivier, L., Meurers, B., & Francis, O. (2014a). Reply to comment on: 'The quest for a consistent signal in ground and GRACE gravity time series', by Michel Van Camp, Olivier de Viron, Laurent Metivier, Bruno Meurers and Olivier Francis. *Geophysical Journal International*, *199*(3), 1818–1822. https://doi.org/10.1093/gji/ggu360
Van Camp, M., de Viron, O., Métivier, L., Meurers, B., & Francis, O. (2014b). The quest for a consistent signal in ground and GRACE gravity time-series. *Geophysical Journal International*, *197*(1), 192–201. https://doi.org/10.1093/gji/ggt524
Van Camp, M., de Viron, O., Pajot-Métivier, G., Casenave, F., Watlet, A., Dassargues, A., & Vanclooster, M. (2016). Direct measurement of evapotranspiration from a forest using a superconducting gravimeter. *Geophysical Research Letters*, *43*, 10,225–10,231. https://doi.org/10.1002/2016GL070534
Van Camp, M., de Viron, O., Scherneck, H.-G., Hinzen, K.-G., Williams, S. D. P., Lecocq, T., … Camelbeeck, T. (2011). Repeated absolute gravity measurements for monitoring slow intraplate vertical deformation in western Europe. *Journal of Geophysical Research*, *116*, B08402. https://doi.org/10.1029/2010JB008174
Van Camp, M., de Viron, O., & Warburton, R. J. (2013). Improving the determination of the gravity rate of change by combining superconducting with absolute gravimeter data. *Computers & Geosciences*, *51*, 49–55. https://doi.org/10.1016/j.cageo.2012.07.029
Van Camp, M., & Francis, O. (2007). Is the instrumental drift of superconducting gravimeters a linear or exponential function of time? *Journal of Geodesy*, *81*(5), 337–344. https://doi.org/10.1007/s00190-006-0110-4
Van Camp, M., Francis, O., Meus, P., Quinif, Y., Kaufmann, O., Rochez, G., … Watlet, A. (2016). Continuous gravimetric monitoring as an integrative tool for exploring hydrological processes in the Lomme Karst System (Belgium). Presented at the AGU Fall meeting 2016, San Francisco. Retrieved from https://publi2-as.oma.be/record/2962
Van Camp, M., Métivier, L., de Viron, O., Meurers, B., & Williams, S. D. P. (2010). Characterizing long-time scale hydrological effects on gravity for improved distinction of tectonic signals. *Journal of Geophysical Research*, *115*, B07407. https://doi.org/10.1029/2009JB006615
Van Camp, M., Meurers, B., de Viron, O., & Forbriger, T. (2016). Optimized strategy for the calibration of superconducting gravimeters at the one per mille level. *Journal of Geodesy*, *90*(1), 91–99. https://doi.org/10.1007/s00190-015-0856-7
Van Camp, M., Vanclooster, M., Crommen, O., Petermans, T., Verbeeck, K., Meurers, B., … Dassargues, A. (2006). Hydrogeological investigations at the Membach station, Belgium, and application to correct long periodic gravity variations. *Journal of Geophysical Research*, *111*, B10403. https://doi.org/10.1029/2006JB004405
Van Camp, M., & Vauterin, P. (2005). Tsoft: Graphical and interactive software for the analysis of time series and Earth tides. *Computers & Geosciences*, *31*(5), 631–640. https://doi.org/10.1016/j.cageo.2004.11.015
Van Camp, M., Williams, S. D. P., & Francis, O. (2005). Uncertainty of absolute gravity measurements. *Journal of Geophysical Research*, *110*, B05406 https://doi.org/10.1029/2004JB003497
van Dam, T., Francis, O., Wahr, J., Khan, S. A., Bevis, M., & van den Broeke, M. R. (2017). Using GPS and absolute gravity observations to separate the effects of present-day and Pleistocene ice-mass changes in south east Greenland. *Earth and Planetary Science Letters*, *459*, 127–135. https://doi.org/10.1016/j.epsl.2016.11.014
Vermeersen, B., & Schotman, H. H. A. (2008). High-harmonic geoid signatures related to glacial isostatic adjustment and their detectability by GOCE. *Journal of Geodynamics*, *46*(3–5), 174–181. https://doi.org/10.1016/j.jog.2008.04.003
Vidal, J., & Schaeffer, N. (2015). Quasi-geostrophic modes in the Earth's fluid core with an outer stably stratified layer. *Geophysical Journal International*, *202*(3), 2182–2193. https://doi.org/10.1093/gji/ggv282
Vigouroux, N., Williams-Jones, G., Chadwick, W., Geist, D., Ruiz, A., & Johnson, D. (2008). 4D gravity changes associated with the 2005 eruption of Sierra Negra volcano, Galápagos. *Geophysics*, *73*(6), WA29–WA35. https://doi.org/10.1190/1.2987399
Virtanen, H., & Mäkinen, J. (2003). The effect of the Baltic Sea level on gravity at the Metsähovi station. *Journal of Geodynamics*, *35*(4–5), 553–565. https://doi.org/10.1016/S0264-3707(03)00014-0
Vitushkin, L., Becker, M., Jiang, Z., Francis, O., van Dam, T., Faller, J., … Williams, S. D. P. (2002). Results of the Sixth International Comparison of Absolute Gravimeters, ICAG-2001. *Metrologia*, *39*(5), 407–424. https://doi.org/10.1088/0026-1394/39/5/2
Volet, C. (1946). Sur la mesure absolue de la gravité. *Comptes Rendus Hebdomadaires des Séances de l'Académie des Sciences*, *222*, 373–375.
Volet, C. (1952). Mesure de l'accélération due à la pesanteur, au Pavillon de Breteuil. *Comptes Rendus Hebdomadaires des Séances de l'Académie des Sciences*, *235*, 442–444.
Wahr, J. (1985). Deformation induced by polar motion. *Journal of Geophysical Research*, *90*(B11), 9363. https://doi.org/10.1029/JB090iB11p09363
Wahr, J., DaZhong, H., & Trupin, A. (1995). Predictions of vertical uplift caused by changing polar ice volumes on a viscoelastic Earth. *Geophysical Research Letters*, *22*(8), 977–980. https://doi.org/10.1029/94GL02840
Wahr, J., van Dam, T., Larson, K., & Francis, O. (2001). Geodetic measurements in Greenland and their implications. *Journal of Geophysical Research*, *106*(B8), 16,567–16,581. https://doi.org/10.1029/2001JB000211
Wake, L. M., Lecavalier, B. S., & Bevis, M. (2016). Glacial isostatic adjustment (GIA) in Greenland: A review. *Current Climate Change Reports*, *2*(3), 101–111. https://doi.org/10.1007/s40641-016-0040-z
Wallace, L. M., Webb, S. C., Ito, Y., Mochizuki, K., Hino, R., Henrys, S., … Sheehan, A. F. (2016). Slow slip near the trench at the Hikurangi subduction zone, New Zealand. *Science*, *352*(6286), 701–704. https://doi.org/10.1126/science.aaf2349
Wang, K., & Dickinson, R. E. (2012). A review of global terrestrial evapotranspiration: Observation, modeling, climatology, and climatic variability. *Reviews of Geophysics*, *50*(2). 0373. https://doi.org/10.1029/2011RG000373
Warburton, R. J., & Goodkind, J. M. (1977). The influence of barometric-pressure variations on gravity. *Geophysical Journal International*, *48*(3), 281–292. https://doi.org/10.1111/j.1365-246X.1977.tb03672.x
Webb, S. C. (2007). The Earth's 'hum' is driven by ocean waves over the continental shelves. *Nature*, *445*(7129), 754–756. https://doi.org/10.1038/nature05536
Wenzel, H.-G. (1997a). Analysis of Earth tide observations. In H. Wilhelm, W. Zürn, & H.-G. Wenzel (Eds.), *Tidal Phenomena* (pp. 59–75). Berlin, Heidelberg: Springer Berlin Heidelberg. https://doi.org/10.1007/BFb0011457

Wenzel, H.-G. (1997b). Tide-generating potential for the Earth. In H. Wilhelm, W. Zürn, & H.-G. Wenzel (Eds.), *Tidal Phenomena* (pp. 9–26). Berlin, Heidelberg: Springer Berlin Heidelberg. https://doi.org/10.1007/BFb0011455

Widmer-Schnidrig, R. (2003). What can superconducting gravimeters contribute to normal-mode seismology? *Bulletin of the Seismological Society of America*, *93*(3), 1370–1380. https://doi.org/10.1785/0120020149

Wielandt, E. (2002). 18 seismometry. In *International Geophysics* (Vol. 81, pp. 283–304). Amsterdam: Elsevier. https://doi.org/10.1016/S0074-6142(02)80221-2

Wilhelm, H., Zürn, W., & Wenzel, H.-G. (Eds.) (1997). *Tidal Phenomena* (Vol. 66). Berlin, Heidelberg: Springer-Verlag https://doi.org/10.1007/BFb0011453

Williams, S. D. P. (2003). The effect of coloured noise on the uncertainties of rates estimated from geodetic time series. *Journal of Geodesy*, *76*(9–10), 483–494. https://doi.org/10.1007/s00190-002-0283-4

Williams, S. D. P., Baker, T. F., & Jeffries, G. (2001). Absolute gravity measurements at UK tide gauges. *Geophysical Research Letters*, *28*(12), 2317–2320. https://doi.org/10.1029/2000GL012438

Williams-Jones, G., & Rymer, H. (2002). Detecting volcanic eruption precursors: A new method using gravity and deformation measurements. *Journal of Volcanology and Geothermal Research*, *113*(3–4), 379–389. https://doi.org/10.1016/S0377-0273(01)00272-4

Williams-Jones, G., Rymer, H., Mauri, G., Gottsmann, J., Poland, M., & Carbone, D. (2008). Toward continuous 4D microgravity monitoring of volcanoes. *Geophysics*, *73*(6), WA19–WA28. https://doi.org/10.1190/1.2981185

Wilson, C. R., Scanlon, B., Sharp, J., Longuevergne, L., & Wu, H. (2012). Field test of the superconducting gravimeter as a hydrologic sensor. *Ground Water*, *50*(3), 442–449. https://doi.org/10.1111/j.1745-6584.2011.00864.x

Woodhouse, J. H., & Deuss, A. (2015). Theory and observations—Earth's free oscillations. In *Treatise on Geophysics* (pp. 79–115). Amsterdam: Elsevier. https://doi.org/10.1016/B978-0-444-53802-4.00002-6

Wöppelmann, G., & Marcos, M. (2016). Vertical land motion as a key to understanding sea level change and variability. *Reviews of Geophysics*, *54*(1), 64–92. https://doi.org/10.1002/2015RG000502

Wouters, B., Bonin, J. A., Chambers, D. P., Riva, R. E. M., Sasgen, I., & Wahr, J. (2014). GRACE, time-varying gravity, Earth system dynamics and climate change. *Reports on Progress in Physics*, *77*(11), 116801. https://doi.org/10.1088/0034-4885/77/11/116801

Wright, T. J., Sigmundsson, F., Pagli, C., Belachew, M., Hamling, I. J., Brandsdóttir, B., … Calais, E. (2012). Geophysical constraints on the dynamics of spreading centres from rifting episodes on land. *Nature Geoscience*, *5*(4), 242–250. https://doi.org/10.1038/ngeo1428

Wu, K., Li, G., Hu, H., & Wang, L. (2017). Active low-frequency vertical vibration isolation system for precision measurements. *Chinese Journal of Mechanical Engineering*, *30*(1), 164–169. https://doi.org/10.3901/CJME.2016.0428.062

Wu, X., Heflin, M. B., Schotman, H., Vermeersen, B., Dong, D., Gross, R. S., … Owen, S. E. (2010). Simultaneous estimation of global present-day water transport and glacial isostatic adjustment. *Nature Geoscience*, *3*(9), 642–646. https://doi.org/10.1038/ngeo938

Xu, J., Sun, H., & Ducarme, B. (2004). A global experimental model for gravity tides of the Earth. *Journal of Geodynamics*, *38*(3–5), 293–306. https://doi.org/10.1016/j.jog.2004.07.003

Xu, S., Wang, P., & Yao, Q. (2013). Analysis of tidal effects on measurement accuracy of HLS. In *Proceedings of IPAC2013* (pp. 2989–2991). Shanghai. Retrieved from http://accelconf.web.cern.ch/accelconf/ipac2013/papers/wepme027.pdf

Zerbini, S., Matonti, F., Raicich, F., Richter, B., & van Dam, T. (2004). Observing and assessing nontidal ocean loading using ocean, continuous GPS and gravity data in the Adriatic area. *Geophysical Research Letters*, *31*, L23609. https://doi.org/10.1029/2004GL021185

Zerbini, S., Richter, B., Rocca, F., van Dam, T., & Matonti, F. (2007). A combination of space and terrestrial geodetic techniques to monitor land subsidence: Case study, the southeastern Po Plain, Italy. *Journal of Geophysical Research*, *112*, B05401. https://doi.org/10.1029/2006JB004338

Zhan, F., Zhu, Y., Ning, J., Zhou, J., Liang, W., & Xu, Y. (2011). Gravity changes before large earthquakes in China: 1998–2005. *Geo-Spatial Information Science*, *14*(1), 1–9. https://doi.org/10.1007/s11806-011-0440-0

Zhou, M.-K., Duan, X.-C., Chen, L.-L., Luo, Q., Xu, Y.-Y., & Hu, Z.-K. (2015). Micro-Gal level gravity measurements with cold atom interferometry. *Chinese Physics B*, *24*(5), 050401. https://doi.org/10.1088/1674-1056/24/5/050401

Ziegler, Y., Hinderer, J., Rogister, Y., & Rosat, S. (2016). Estimation of the gravimetric pole tide by stacking long time-series of GGP superconducting gravimeters. *Geophysical Journal International*, *205*(1), 77–88. https://doi.org/10.1093/gji/ggw007

Zürn, W. (1997). Earth tide observations and interpretation. In H. Wilhelm, W. Zürn, & H.-G. Wenzel (Eds.), *Tidal Phenomena* (Vol. 66, pp. 77–94). Berlin/Heidelberg: Springer-Verlag. https://doi.org/10.1007/BFb0011458

Zürn, W., Exß, J., Steffen, H., Kroner, C., Jahr, T., & Westerhaus, M. (2007). On reduction of long-period horizontal seismic noise using local barometric pressure. *Geophysical Journal International*, *171*(2), 780–796. https://doi.org/10.1111/j.1365-246X.2007.03553.x

Zürn, W., Laske, G., Widmer-Schnidrig, R., & Gilbert, F. (2000). Observation of Coriolis coupled modes below 1 mHz. *Geophysical Journal International*, *143*(1), 113–118.

Zürn, W., & Meurers, B. (2009). Clear evidence for the sign-reversal of the pressure admittance to gravity near 3 mHz. *Journal of Geodynamics*, *48*(3–5), 371–377. https://doi.org/10.1016/j.jog.2009.09.040

Zürn, W., Richter, B., Rydelek, P. A., & Neuberg, J. (1987). Comment: Detection of inertial gravity oscillations in the Earth's core with a superconducting gravimeter at Brussels. *Physics of the Earth and Planetary Interiors*, *49*(1–2), 176–178. https://doi.org/10.1016/0031-9201(87)90140-3

Zürn, W., & Widmer, R. (1995). On noise reduction in vertical seismic records below 2 mHz using local barometric pressure. *Geophysical Research Letters*, *22*(24), 3537–3540. https://doi.org/10.1029/95GL03369